An evaluation of a microchannel reactor for the production of hydrogen from formic acid

IM Ndlovu

orcid.org 0000-0003-3521-2524

Dissertation submitted in fulfilment of the requirements for the degree *Master of Engineering in Chemical Engineering* at the North-West University

Supervisor:	Prof. Raymond C. Everson
Co-supervisor:	Dr. Steven Chiuta
Co-supervisor:	Prof. Hein W.J.P. Neomagus
Assistant supervisor:	Dr. Henrietta Langmi
Assistant supervisor:	Dr. Jianwei Ren
Assistant supervisor:	Dr. Dmitri G. Bessarabov

Graduation: May 2018

Student number: 25839527

DECLARATION

I, **Isabella Mandimpa Ndlovu**, declare herewith that the dissertation entitled: "**An evaluation of a microchannel reactor for the production of hydrogen from formic acid**", submitted in fulfilment of the requirements for the degree Masters in Chemical Engineering, is my own work, except where acknowledged in the text, and has not been submitted to any other tertiary institution in whole or in part.

Signed at North-West University (Potchefstroom Campus)

Isabella Ndlovu

ACKNOWLEDGEMENTS

My utmost gratitude to God the Almighty ,God the Father, God the Omnipotence, God the Omnipresence and God the Omniscience. As promised, He instructed me in the way I should go and through him I leaped over a wall. As I write, I sing my forever song of the year by Sifiso Ngcwane (R.I.P) "Ingakho ngicula", for I cannot possibly visualize a perfect journey without God.

I am most grateful to my team of study leaders: Professor Raymond C Everson, Dr Steven Chiuta, Dr Dmitri Bessarabov, Dr Henrietta Langmi,Dr Jianwei Ren and Professor Hein Neomagus. As I look back, I feel blessed to have walked amongst giants who stretched me to my potentials. Raymond, thank you for directing the project in this direction, I learnt a lot and I truly could not have been a better engineer. Most importantly your supervising technique was a rare combination of patience and encouragement .Steven, thank you for believing it could be done; I could not have done it without you. I am also thankful to Dmitri for the support he gave me throughout this project, right from the access to the research facility at HySA Infrastructure in NWU, thank you for the opportunity. My appreciation also goes out to DST HySA Infrastructure and CSIR for the financial support. I will always remember CSIR as the builder that laid the first foundation of my career. As I write this dissertation I remember a man, not part of this dissertation, but who will always be part of my research career; cheers to Dave Rogers!

This work would not have been a success without a few of my colleagues from NWU and CSIR, HySA Infrastructure; Phillimon Modisha , thank you for the 'ferrule days' the experimental setup would not have been so perfect without you. To Francois Stander and Nicolaas Engelbrecht, thank you for taking time to help me with the CFD model, I wouldn't have learnt so much without you; my gratitude also goes out to Tshiamo Segakweng for the help in catalyst characterization, I would also like to thank the guys of the NWU workshop, Ted and Jan for their continuous support.

My most heartfelt gratitude goes out to my family (Sphamandla and Olwethu) for their warm love, support and understanding throughout this journey. To Olwethu, thank you for being such an angel, you kept me smiling throughout these years, like your name Nonkanyiso, you were just my brightness. This list will never be complete without the greatest parents (Micah and Patricia) in the whole world. Thank you for always believing in me more than I have ever believed in myself. Last but not least, I dedicate this dissertation to my grandparents (Rosea and Isaac Tenika); I am because you were thank you!

ABSTRACT

This dissertation evaluates the performance of a microchannel reactor for the decomposition of vaporised formic acid as a promising technology for the production of hydrogen for proton exchange membrane fuel cell applications. Accordingly, a combined experimental and modelling approach was used to evaluate the microchannel reactor coated with a gold supported on alumina (1.15 wt. % Au/Al_2O_3) catalyst. For the experimental evaluation, two phase of experiments were carried out where pure formic acid (99.99 %) and dilute formic acid (50 vol. %) were taken as the feed to the reactor respectively. The first phase of the experimental evaluation involved measuring key performance parameters such as, formic acid conversion, formic acid residual concentration, selectivity to hydrogen and hydrogen yield at different temperatures of 250 – 350°C and formic acid (99.99 %) vapour flowrates of 12 – 48ml/min. Overall, the reactor performed well in decomposing pure formic acid (99.99 %), achieving conversions (98 to 99 %) close to equilibrium at 350 ^oC and all studied vapour formic acid flowrates of 12 – 48 ml/min. At all studied temperatures however, both dehydrogenation ($HCOOH \rightarrow H_2 + CO_2$) and dehydration ($HCOOH \rightarrow H_2O + CO$) reactions occurred and the dehydrogenation reaction was found to be dominant. The dehydration reaction was mostly favoured at high temperatures and carbon monoxide concentrations ranged between 4 – 15 % while the corresponding selectivity towards H_2 production ranged between 0.7 and 0.88. Effort was made to improve the H_2 yields in the second phase of the experiments through decomposing a mixture of formic acid and water (50/50 vol. %) thereby promoting the occurrence of the forward water gas shift reaction. Under these conditions, carbon monoxide concentrations decreased to a range of 2 – 7 % while selectivity towards hydrogen production increased to a range of 0.84 – 0.94. Overall, for both pure FA (99.99 %) and dilute FA (50 vol.%), the best microchannel reactor performance was achieved at a reactor operating temperature of 350 ^oC and FA vapour flowrate of 48 ml/min (17.1 $Nml.gcat^{-1}.h^{-1}$). At these conditions, H_2 production rate (11.8 $NL.g_{cat}^{-1}.h^{-1}$) was maximised with pure FA (99.99 %) while selectivity (0.81) and H_2 yield (80) were maximised with dilute FA (50 vol.%). Overall, the reactor was found stable at a continuous period of 144 hours after running for approximately 1 200 hours. A computational fluid dynamic model was developed for concentrated formic acid (99.99 %) experiments aimed at describing reaction-coupled transport phenomena relating to velocity, mass and temperature profiles within the microchannel reactor. Kinetic rate expressions that best described the experimental results were successfully estimated using a model-based parameter optimisation and refinement on Comsol Multiphysics™ 4.3b. Validation of the model against the experimental results showed that the developed model was an acceptable fit to the

experimental conversions and hydrogen yields especially at temperatures higher than 250 ^{o}C. Overall, this dissertation highlights the first steps in the development and use of microchannel reactors in promoting formic acid as a future hydrogen storage medium for portable and distributed fuel cell applications.

Keywords: Formic acid decomposition, Hydrogen production, Dehydrogenation, Dehydration, Microchannel reactor, Reactor evaluation, Au/Al_2O_3 catalyst, Computational fluid dynamic (CFD) modelling, Kinetic parameter estimation, Comsol Multiphysics.

TABLE OF CONTENTS

LIST OF TABLES

LIST OF FIGURES

NOMENCLATURE

Symbols

a_i	Stoichiometric coefficient of species *i*
B	Line broadening at half intensity
Cp_i	Component fluid heat capacity, J kg^{-1} K^{-1}
Cp	Fluid heat capacity, J $kg^{-1}K^{-1}$
Cf	Forchheimer drag coefficient
D_{ij}	Binary diffusivity of component *i* in *j*, $m^2 s^{-1}$
$D_{ij,eff}$	Effective diffusivity of component *i* in *j* m^2 s^{-1}
E_1	Activation energy of reaction 1, kJ mol^{-1}
E_2	Activation energy of reaction 2, kJ mol^{-1}
$F_{mix, out}$	Outlet flowrate of a bubbler, ml min^{-1}
$F_{N2, in}$	Bubbler inlet flowrate of nitrogen, ml min^{-1}
$H_{2, yield}$	Hydrogen yield
ΔH_r .	Enthalpy of reaction J mol^{-1}
K	Permeability m^2
k_i	Thermal conductivity of component, W m K^{-1}
k	Thermal conductivity of a fluid, W m K^{-1}
k_{eff}	Effective thermal conductivity, W m K^{-1}
k_s	Thermal conductivity of a catalyst, W m K^{-1}
K_s	Dimensionless shape factor
k_1	Rate constant of formic acid adsorption
k_2	Rate constant of intermediate decomposition
$k0, _1$	Pre-exponential factor of reaction 1
$k0, _2$	Pre-exponential factor of reaction 2
l	Catalyst crystallite size, µm
M_i	Molecular weight of component *i*, kg mol^{-1}
M_j	Molecular weight of component *j*, kg mol^{-1}
n_ic_i	Group contribution value m s K kg
$n_{FA, in}$	Molar feed rate of FA , $mol.h^{-1}$
p	Partial pressure of formic acid
P_{HCOOH}	Partial pressure of formic acid, Pa
P	Pressure vector
P_o	Operating pressure, Pa
$\langle P \rangle$	Fluid pressure in porous region, Pa
$P_{FA,V}$	Equilibrium pressure of FA in a bubbler, Pa
P_{local}	Local pressure in a bubbler headspace, Pa
P_{N2}	Partial pressure of N_2 in a bubbler, Pa
r	Rate of dehydrogenation
r_1	Rate of reaction 1 , mol m^{-3} s^{-1}
r_2	Rate of reaction 2 , mol m^{-3} s^{-1}
R	Reaction rate, mol kg^{-1} s^{-1}
R_g	Universal gas coefficient, Pa m^3 mol^{-1} K^{-1}
S	Selectivity to H_2 and CO_2 production
T	Operating temperature*, K*
$\langle T \rangle$	Fluid temperature in porous region, K
T_r	Reduced temperature, K
T_c	Critical temperature, K
T_{inlet}	Reactant inlet temperature to the reactor, K
$T_{initial}$	Reactor initial temperature, K
T_{wall}	Reactor wall temperature, K
v_i	Atomic diffusion volume of component *i* cm^3 mol^{-1}
v_i	Atomic diffusion volume of component *j* cm^3 mol^{-1}
v_{inlet}	Inlet velocity of the feed to the reactor,m s^{-1}
$v_{initial}$	Initial velocity in the reactor,m s^{-1}
V	Fluid velocity vector
$\langle V \rangle$	Fluid velocity in porous region, m s^{-1}
$v_{x,y,z}$	Fluid velocity component in x,y,z direction , m s^{-1}
w_i	Mass fraction of component *i* in a mixture
$\langle wi \rangle$	Mass fraction of component *i* in the porous

	region
$w_{i\ inlet}$	Mass fraction of *i* in reactor feed
$w_{i\ initial}$	Initial mass fraction of *i* in the reactor
x_i	Molar fraction of species *i*
x_{outlet}	Molar fraction of component in the reactor outlet
x_{FA}	Mole fraction of formic acid out of bubbler
X_{FA}	Conversion of formic acid, %
x_{N2}	Mole fraction of nitrogen out of bubbler
y_{co2}	Mole fraction of CO_2 out of the reactor
y_{co}	Mole fraction of CO out of the reactor
y_{FA}	Mole fraction of FA out of the reactor

Greek symbols

μ	Viscosity of a fluid Pa.s
μ_B	Brinkman viscosity, Pa.s
μ_{FA}	Viscosity of gaseous FA at low pressures, Pa.s
ε	Porosity of a porous medium.
λ	X-ray wavelength
θ	Bragg angle
θ_i	Coverage by the intermediate
ρ	Density of a fluid, kg m^{-3}
ρ_s	Density of a catalyst, kg m^{-3}

Abbreviations

AFM	Atomic force microscopy
BASF	Badishe Anilin-und Soda-Fabrik
BET	Brunauer, Emmet, and Teller
CFD	Computational fluid dynamics
DFAFC	Direct formic acid fuel cells
DMFC	Direct methanol fuel cells
DST	Department of science and technology
EDS	Energy –Dispersive X-ray Spectroscopy
FA	Formic acid
FID	Flame detector
FT	Fisher Tropsh
GC	Gas chromatography
GTL	Gas-to-liquid
HID	Hydrogen induction detector
LHSV	Liquid hourly space velocity
MCFCs	Molten carbonate fuel cells
MOFs	Metal organic frameworks
MSR	Methanol steam reforming
PAFC	Phosphoric acid fuel cells
PARDISO	Parallel sparse direct linear solver
PEMFC	Proton Exchange membrane fuel cells
PVA	Polyvinyl alcohol
WGS	Water gas shift reaction
TCD	Thermal conductivity detector
TOF	Turn over frequency
SEM	Scanning electron microscopy
XRD	X-ray powder diffraction

CHAPTER 1: INTRODUCTION

This Chapter presents an overview of the dissertation. First, the background is presented in Section 1.1 to set the scene and put the dissertation into perspective. Secondly, the project motivation and problem statement are formulated in Section 1.2 to highlight the research gaps. Thereafter, the research aim and objectives are outlined in relation to the background and problem statement. The chapter concludes in Section 1.5 with an outline of the full dissertation where a brief description of all chapters is presented.

1.1 BACKGROUND

The progressive depletion of fossil fuel reserves, rise in energy demand as well as the need to reduce greenhouse gases have recently led to a worldwide search for an alternative energy source. Accordingly, hydrogen (H_2) is currently receiving attention as an alternative energy carrier due to its high energy density of 142 MJ/kg (Boddien, *et al*., 2013). For instance, when compared to gasoline, 1 kg of H_2 has approximately the same energy content as one gallon (2.83 kg) of gasoline (Zhao & Burke, 2015). Overall, H_2 can be used in fuel cells to generate electric power at near-zero pollution levels. Various types of fuel cells such as, alkaline fuel cells, molten carbonate fuel cells (MCFCs), phosphoric acid fuel cells (PAFC) and proton exchange membrane fuel cells (PEMFCs) are therefore being researched worldwide. Although fuel cells have gained significant interest for various stationary and non-stationary applications, they are still far from being established. The main challenge facing the H_2 fuel cell economy is the lack of sustainable supply and storage infrastructure that can adequately deliver H_2 for fuel cell applications. This challenge is attributed to H_2's low volumetric energy density. As such, current research is focused on developing practical solutions to these storage challenges.

Currently, near-term options and techniques for storing H_2 include compressed H_2 (700 bar), liquefied H_2 (-253˚C) and solid metal hydrides (Boddien, *et al*., 2013). Liquefied and compressed H_2 techniques, however, suffer from high costs, loss of H_2 and safety issues. Metal hydrides on the other hand currently do not reach the target gravimetric H_2 storage capacity (Klerke, *et al*., 2008). In addition to conventional systems, storage materials such as zeolites, metal organic frameworks (MOFs) and porous organic polymers are being developed. These porous materials currently require operational temperatures around -196 ºC. It is therefore clear that lack of

adequate H_2 storage systems to supply H_2 for PEMFC still remains a gap in H_2 fuel cell technology.

1.2 MOTIVATION AND PROBLEM STATEMENT

As a promising solution, liquid chemical compounds (ammonia, methanol, ethanol, formic acid (FA) etc.) have recently gained attention as H_2 storage media. This is mostly because they are liquid at standard conditions and easy to transport. More particularly, FA is a promising H_2 carrier with an acceptable H_2 content of 4.4 wt. % (Zhou, *et al*., 2010; Loges, *et al*., 2010; Yoo, *et al*., 2014). In pure form, FA's energy content (2086 $Wh.l^{-1}$) is five times higher than that of commercially available lithium ion batteries (Boddien, *et al*., 2013), which promote its suitability for small scale applications of H_2 such as in portable devices. In addition, FA is a suitable H_2 carrier because it is relatively non-toxic and non-flammable (Zhou, *et al*., 2010; Zhu, *et al*., 2014). Furthermore, the release of H_2 from FA can be attained at lower temperatures (ambient) compared to its release from other liquid carriers such as methanol (Loges, *et al*., 2010). Table 1.1 summarises the safety properties of FA in comparison to those of other common liquid chemical carriers.

Table 1.1: Comparison of different liquid chemical carrier properties (Sigma-Adrich, 2011)

Parameter	Formic acid	Methanol	Ethanol	Ammonia
H_2 content (wt. %)	4.4	12.5	13	17.7
Hazard codes	C	F,T	F	T,C,N
Risk statements (R-phase)	R10,R35	R11,R23/24/25,R39/23/24/25	R11	R10,R23,R34,R50
Boiling point (ºC)	101	64.7	78	-33
Explosion limits (Upper-lower vol. %)	18-57	6-36	3.3-19	15-25
Flash point (ºC)	48	9.7	14	132

The above safety and risk information was obtained from relevant material safety data sheets which can be accessed from commercial suppliers ,where F-Highly flammable, T-Toxic, C-corrosive, and N-Dangerous to the environment,R10-Flammable,R35-Causes severe burns, R11-Highly flammable, R23/24/25-Toxic by inhalation, in contact with skin and if swallowed, R39/23/24/25- Danger of very serious irreversible effects through inhalation, in contact with skin and if swallowed,R34-Causes burns,R50-Very toxic to aquatic organisms.

As shown in Table 1.1, FA is easy to handle and transport as it is less hazardous compared to other carriers as methanol and ammonia. In addition to the safety properties in Table 1.1, FA is a readily available energy source that can be obtained from renewable resources such as wet biomass (Wolfel, *et al*., 2011). It can also be produced from a carbon neutral cycle during the hydrogenation of carbon dioxide (CO_2) (Wesselbaum, *et al*., 2012). Moreover, BASF currently produces around 255,000 metric tons of formic acid per year in Germany and China (BASF, 2012). This generally means that the use of FA as a H_2 storage method can easily make use of the readily available transportation infrastructure.

Despite the interesting properties of FA, its decomposition has only been intensively studied as a model reaction for catalyst selection (Fukuda, *et al*., 1969; Tamaru, 1958; Iglesia & Boudart, 1983). It is only in recent times that FA decomposition has received increasing attention as a potential H_2 storage medium. Without exception, the emphasis on selective catalyst development has been the sole theme in recent studies concerning FA decomposition for H_2 production (Soylomosi, *et al*., 2011; Gazsi, *et al*., 2011; Bulushev, *et al*., 2010; Zhang , *et al*., 2013). However, the advancement of FA decomposition for portable and distributed H_2 production also needs to consider appropriate reactor infrastructure.

Thus far, microchannel reactors have been identified in numerous studies as a transformative technology that inherently satisfies the strict requirements (i.e. high conversion with small catalyst volume) for portable and distributed H_2 generation (Men, *et al*., 2007; Peela, *et al*., 2011; Aartun, *et al*., 2005; Chiuta, *et al*., 2014; Chiuta, *et al*., 2015; Paunovic, *et al*., 2015; D'Angelo , *et al*., 2014; Echave, *et al*., 2013; DeSouza, *et al*., 2013). These reactors have large surface to volume ratios which lead to short diffusion lengths, resulting in good heat and mass transfer effects (Atkinson & McDaniel, 2010; Lerou, *et al.*, 2010; Kolb & Hessel, 2004). It is therefore these important aspects that have elevated microchannel reactors for distributed fuel cell applications.

There is however currently no experimental work reporting on the use of microchannel reactors for the production of H_2 from FA. Moreover, mathematical modelling to understand and decipher the operational insights of FA decomposition within the microchannel reactors has not been reported yet. For application in FA decomposition however, it is more favourable to decompose vaporised FA, as large pressure losses and clogging of the microchannel reactor may occur in liquid phase reactions (Guangwen, *et al*., 2008). Against this background, this dissertation combines the advantages of an active heterogeneous catalyst (1.15 wt. % Au/Al_2O_3) with that of a microchannel reactor in decomposing vaporised FA for H_2 production. The choice of the catalyst was based on its availability and activity towards FA decomposition as reported in literature. For

instance, Ojeda & Iglesia, (2009) studied the decomposition of FA on a 0.61 wt. % Au /Al_2O_3 and reported the catalyst to be active at near ambient conditions. In addition, Gazsi, *et al*., (2011) further reported that Au/Al_2O_3 catalyst was active and resistant to CO poisoning due to the low adsorption strength of CO on Au surface (Zhou, *et al*., 2008). This characteristic of the catalyst will therefore be advantageous for the long term operation of the microchannel reactor.

1.3 RESEARCH AIM AND OBJECTIVES

Against the outlined background, the research aim and objectives were outlined in Section 1.3.1 and 1.3.2 to give the reader an understanding of the overall goal of the study.

1.3.1 Aim

In alignment with the current trend in hydrogen storage, this study experimentally evaluates the performance of a microchannel reactor for the production of hydrogen from vaporised formic acid using a gold supported on alumina catalyst. In addition, the study aims at developing and validating a computational fluid dynamic model of the microchannel reactor.

1.3.2 Objectives

The specific objectives of the study are as outlined below;

- To specify reactor design parameters and demonstrate the use of a microchannel reactor for the production of hydrogen from vaporised formic acid using a commercial gold supported on alumina (1.15 wt. % Au/Al_2O_3) catalyst. The final microchannel catalyst layer is also characterised to understand the catalyst properties.
- To experimentally evaluate the performance of a microchannel reactor by determining the best operating conditions that result in high conversions, hydrogen production rate and formic acid throughput. Two sets of experiments are carried out where pure formic acid (99.99 %) and dilute formic acid (50 vol. %) are used as the feed to the reactor respectively.
- To develop a computational fluid dynamic model that describes reaction-coupled transport profiles within the microchannel reactor. The model is developed for pure formic acid (99.99 %) and COMSOL Multiphysics 4.3b is used for this purpose.

- To validate the developed model against the experimental results such as, formic acid conversion and hydrogen yield.

1.4 SUMMARY OF RELEVANCE OF STUDY

In South Africa (SA), the Department of Science and Technology (DST) developed a national strategy which was branded Hydrogen South Africa (HySA).This strategy was developed to guide innovation along the value chain of H_2 and fuel cell technologies. HySA consists of three Centres of Competence namely; HySA Infrastructure, HySA Catalysis and HySA Systems. Under HySA Infrastructure, South Africa has joined worldwide researchers in developing different H_2 storage methods. This project therefore falls under HySA Infrastructure's research thrust on chemical carriers as H_2 storage methods. The benefits are outlined below;

- The study aims to provide SA with options to meet its medium term energy supply requirements on safe, clean, affordable and reliable H_2 energy supply. This is mainly because FA is relatively non-toxic, affordable, safe to handle and use, and can be obtained from renewable resources such as biomass (Wesselbaum, *et al*., 2012).
- The research makes use of Au/Al_2O_3 as the catalyst for decomposing FA. The use of Au may therefore promote use of local resources as the catalyst is supplied by Mintek (SA).

1.5 DISSERTATION OUTLINE

Chapter 1 presents an overview of the dissertation through an outline of the project background, motivation and problem statement. This chapter mainly highlights the project's aim and objectives to give the reader the overall goal of the project.

Chapter 2 presents a literature review, summarised in three main sections. The chapter starts off with a brief discussion of the concept of FA production and decomposition for H_2 production. This section is then followed up with a detailed discussion of the current status of FA decomposition for H_2 production. It is in this section that the gaps existing in the field of H_2 production from FA are identified. Thereafter the literature chapter identifies microchannel reactors as the appropriate units for H_2 fuel cell applications. In this section, microchannel reactor advantages, challenges, modelling and mechanical design are presented.

Chapter 3 presents the experimental methodology followed in evaluating the microchannel reactor. The chapter starts off with a brief description of the microchannel reactor fabrication

process and results of the catalyst layer characterisation. Thereafter, a full description of the experimental apparatus and equipment used in this dissertation is given. The last section of this chapter presents a step by step procedure of the experimental work carried out. It is in this section that key parameters used to evaluate the reactor are outlined and discussed.

Chapter 4 presents the experimental results where, a microchannel reactor is evaluated using key parameters such as FA conversions, selectivity towards H_2 formation, H_2 yield and H_2 production rate. The first section of the chapter presents results on the decomposition of pure FA (99.99 %) while the second section presents results on the decomposition of a FA/H_2O mixture (50/50 vol. %). The last two sections present the results of the reactor stability study and the recommended best reactor operating conditions respectively. Overall the experimental results are discussed and analysed with reference to available literature in this chapter.

Chapter 5 presents the microchannel reactor modelling for the decomposition of pure FA (99.99 5). The chapter starts off with a presentation of the model development procedure where equations and assumptions are discussed. Thereafter, results of the model are presented and validated by comparing the model results to those obtained from experiments. The chapter concludes with a presentation of the transport profiles within the studied microchannel reactor as obtained from the developed model.

Chapter 6 concludes the dissertation with a summary of the key findings as well as recommendations based on the experimental results and model validation.

CHAPTER 2: LITERATURE REVIEW

This chapter presents a review of the literature relevant for the overall accomplishment of the project. The literature starts off in Section 2.1 with a brief discussion on the concept of FA for H_2 production to give the reader an overview of the subject. Under this section, a description of the mechanism of FA production and decomposition is given. Section 2.2 presents the current status of FA decomposition for H_2 production where the gaps that exist in promoting FA as a H_2 carrier are outlined. The last section (Section 2.3) discusses microchannel reactors as a potential solution for efficient H_2 production from FA. Advantages and challenges facing microchannel reactor technology are given. Lastly, the various methods of fabricating and constructing microchannel reactors are discussed to prepare the reader for the chapters that follow.

2.1 CONCEPT OF FORMIC ACID PRODUCTION AND DECOMPOSITION

Formic acid has historically been considered an undesirable intermediate product of different industrial processes such as, the hydrothermal oxidation of organic compounds (Akiya & Savage, 1998) as well as the second generation bio refinery processes (Bulushev, *et al*., 2010). Today however, this chemical compound finds increasing use as a food preservative and antibacterial agent in livestock feed (Bull, 2010). As the global call for renewable energy sources increases, FA is also receiving a renewed attention as a H_2 storage medium. In alignment with the current H_2 storage requirements, FA can reversibly store and release H_2 on demand based on a carbon neutral storage cycle shown in Figure 2.1.

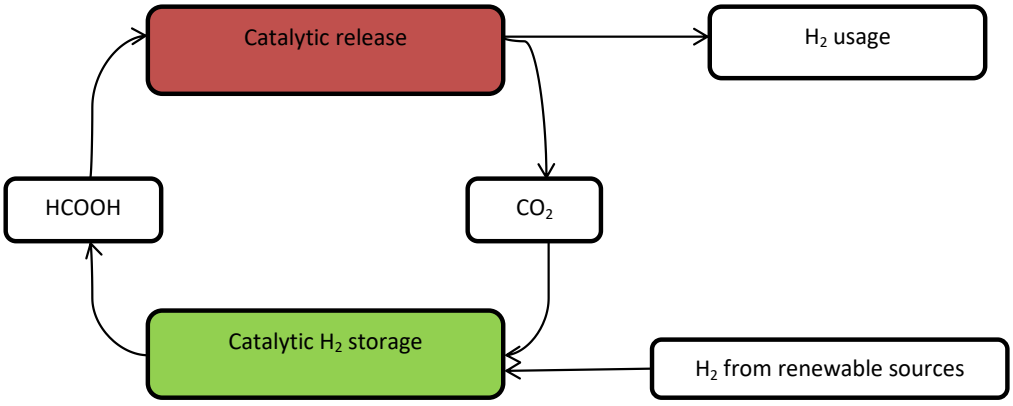

Figure 2.1: A carbon neutral cycle for the storage and production of H_2 from FA (Loges, *et al*., 2010)

In the first part of the cycle, carbon dioxide (CO_2) is converted to FA either electrochemically (Benson, *et al*., 2009) or through catalytic hydrogenation (Leitner, 1995; Jessop, *et al*., 2004). On the other side of the cycle, H_2 is released either in direct FA fuel cells (DFAFC) or by decomposition into CO_2 and H_2 that can be used in PEMFCs. The three parts of the cycle are briefly discussed in Sections 2.1.1 to 2.1.3 respectively.

2.1.1 Formic acid production

Formic acid is widely produced by Badishe Anilin-und Soda-Fabrik (BASF) in Germany and China at a rate of approximately 255 000 metric tons per year (BASF, 2012). The process of producing FA has since evolved with time due to the rise in FA demand as a preservative for food. For instance, FA was historically produced from the reaction of sulfuric acid and formamide with ammonium sulfate as a by-product. The separation of FA from ammonium sulfate was however, found to be hazardous and as such, a better process was needed. As the demand for ammonium sulfate reduced, a new process for producing FA was developed with no by-product. The current process at BASF produces FA from the hydrolysis of methyl formate with water and the typical process is shown in Figure 2.2.

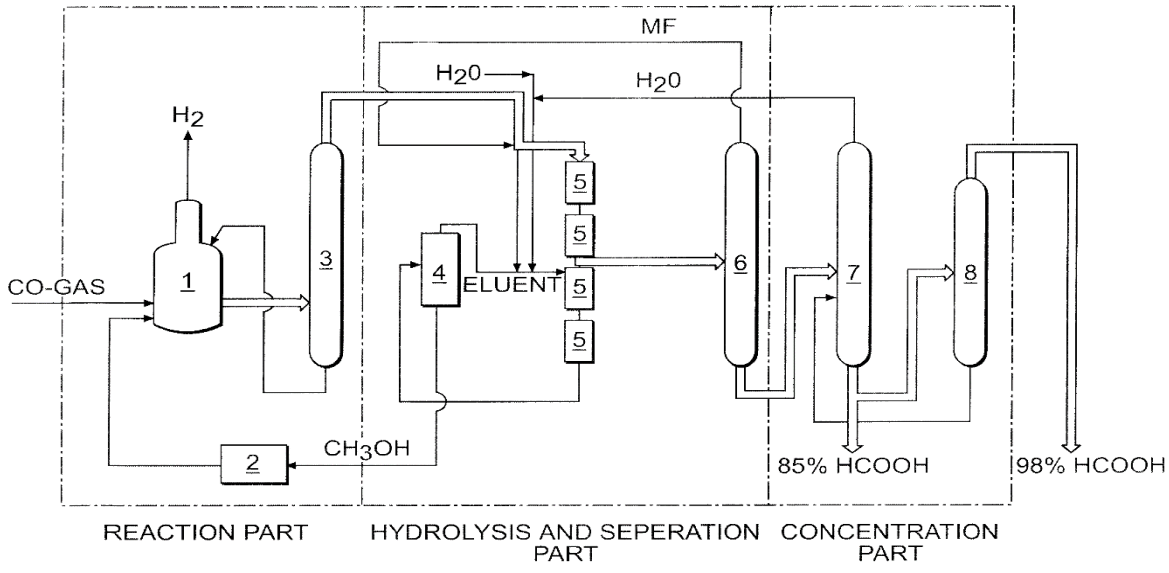

Figure 2.2: Process of producing FA from the hydrolysis of methly formate *(*Kari, *et al*., 1998)

As shown in Figure 2.2 the overall process consists of three main sections namely; the reaction section, the hydrolysis and separation section and the concentrations section. Methanol is

produced as a by-product of the hydrolysis section and this is then separated from FA and recycled to the reaction section to produce methyl formate in the presence of carbon monoxide (Kari, *et al*., 1998). The produced FA from the separators is finally concentrated in the concentrator section. Overall, carbon monoxide (CO) and water (H_2O) are the main inputs of this process.

As the call to reduce the amount of CO_2 in the atmosphere increases however, the production of FA from CO_2 is under consideration as an alternative process (Figure 2.1). This process generally involves the hydrogenation of CO_2 over a suitable catalyst. This process is however difficult due to the high kinetic and thermodynamic stability of CO_2 which means that the reaction occurs slowly and is not spontaneous (Moret, Dyson, & Laurenczy, 2014). An excellent review by De Vries & Elsevier, (2007) shows that the catalytic hydrogenation of CO_2 has been successfully demonstrated using homogeneous catalysts of ruthenium (Ru) and rhodium (Rh). In most of these studies however, hydrogenation was performed in the presence of amine bases since the reaction is thermodynamically unfavourable in the absence of a base. Overall, current research is focused on improving the catalytic production of FA from CO_2 without the use of bases. Successful production of FA from CO_2 will therefore be attractive especially for the purpose of using FA for H_2 storage.

2.1.2 Formic acid for use in direct formic acid fuel cells

Direct formic acid fuel cells are types of PEMFC where FA fuel is directly fed to a fuel cell before any form of decomposition or reforming. In a DFAFC, FA is directly oxidised to CO_2 according to an overall FA oxidation reaction at the anode (2.1). At the cathode, oxygen reduction occurs through a 4-electron reaction usually facilitated by a platinum based catalyst (2.2).

$$HCO_2H \rightarrow CO_2 + 2H^+ + 2e^- \quad \text{.....2.1 (Anode)}$$

$$\frac{1}{2}O_2 + 2H^+ + 2e^- \rightarrow H_2O \quad \text{.....2.2 (Cathode)}$$

Direct FA fuel cells have so far been reported as a better option to the commonly used direct methanol fuel cells (DMFCs) (Baik, *et al*., 2011; Cai, *et al*., 2013; Moreno-Zuria, *et al*., 2014; Cai, *et al*., 2012). This is mostly due to the high kinetic rate of FA oxidation in comparison to that of methanol (Cai, *et al*., 2012). Moreover, FA exhibits smaller crossover flux than methanol which in

turn allows for the use of highly concentrated FA. Direct formic acid fuel cells can therefore achieve high power densities adequate to power small scale devices.

The process of using FA in DFAFCs is however still faced with challenges. For instance, FA oxidation can proceed via a CO intermediate which can poison the platinum anode catalyst. In this regard, research in DFAFC is focused on improving the anode catalyst (Al-Akraa, *et al*., 2015; Cai, *et al*., 2012). Overall, most catalysts for this technology still suffer from gradual deactivation with time which suggests that this process is not yet economically efficient. Apart from this challenge, DFAFCs experience crossover challenges where FA diffuses from anode, through the membrane to the cathode side. Under this condition, FA can react directly with O_2 resulting in the production of unwanted heat that can reduce the overall fuel efficiency of the system (Lycke & Blair, 2009). Most of the challenges facing DFAFC are however not normally associated with the traditional PEMFC systems (Lycke & Blair, 2009). It is in this regard that current studies are giving more focus on the decomposition of FA to produce H_2 for application in PEMFC rather than its use in DFAFCs.

2.1.3 Formic acid decomposition

Contrary to the well-established FA production via the hydrolysis of methyl formate, the catalytic H_2 release from FA is far from being established. The study of FA decomposition process gained attention early in 1910 due to the nature of its reaction mechanism. One of the early studies was performed by Sabatier and Mailhe (1912) where it was shown that FA decomposes on metal surfaces according to the dehydrogenation and dehydration reaction pathways outlined below (Mars, *et al.*, 1963).

$$HCO_2\,H(g) \rightarrow CO_{2(g)} + H_{2(g)} \qquad \Delta H^0 = -38.88\,kJ/mol \quad \text{.....2.3 (Dehydrogenation)}$$

$$HCO_2\,H(g) \rightarrow CO_{(g)} + H_2O_{(g)} \qquad \Delta H^0 = 10.25\,kJ/mol \quad \text{.....2.4 (Dehydration)}$$

Following on this study, early research identified the fundamental decomposition processes that FA undergoes at the metal surfaces. An excellent review by Mars, *et al*., (1963) and Columbia & Thiel, (1994) showed that FA decomposes in two main steps. In the first step, the molecular acid reacts with the metal surface to produce a surface intermediate. The intermediate may then decompose in the second step to produce CO, CO_2, water (H_2O), H_2, O and carbon (C). This intermediate has thus far been identified as an adsorbed formate (HCOO) (Noto, *et al*., 1967;

Fukuda, *et al*., 1969; Tamaru, 1958; Johnson, *et al*., 2010; Yoo, *et al*., 2014). Overall, the selectivity to either of the reaction pathways is temperature dependent. For instance, dehydrogenation is favoured at low temperatures while dehydration is favoured at high temperatures. Moreover, the catalyst type also influences the selectivity of the FA decomposition process and a detailed discussion is given in Section 2.2.1.

In addition to the dehydrogenation and dehydration pathways, there are other possible reactions that can occur as a result of FA decomposition. The most reported of these reactions is the forward water gas shift (WGS) reaction.

$$H_2\,O_{(g)} + CO_{(g)} \leftrightarrow CO_{2(g)} + H_{2(g)} \qquad \Delta H^0 = -41.1 kJ/mol \text{ .....2.5} \quad \text{(WGS)}$$

The WGS is in equilibrium and occurs as a link between the two parallel reactions where reaction products of dehydration react to form reaction products of dehydrogenation. The WGS reaction intermediates are generally the same as those for FA decomposition (Byron, *et al*., 2010; Mellor, *et al*., 1997) and as such, the creation of formate has been identified as the rate determining step in the WGS reaction. Similar to the dehydration and dehydrogenation processes, the occurrence of the WGS reaction is also dependent on the catalyst type. Moreover, studies in FA decomposition have reported that the presence of water in the feed promotes the occurrence of the WGS reaction (Soylomosi, *et al*., 2011; Bulushev, *et al*., 2010; Gazsi, *et al*., 2011). This in turn improves the selectivity towards the dehydrogenation reaction while suppressing the dehydration reaction. Water was also historically tested as a chemical reaction medium at elevated temperatures (320-500 ºC) and pressures (178 – 303 atm) (Blake & Hinshelwood, 1960; Blake, *et al*., 1971; Yu & Savage, 1998). In some of these studies, it was reported that water can act as a catalyst in the decomposition of FA following the dehydrogenation route.

2.2 CURRENT STATUS OF FORMIC ACID DECOMPOSITION FOR HYDROGEN PRODUCTION

The historical focus on FA decomposition has been on the fundamental reaction mechanism and not on its potential as a H_2 carrier. It is only recently that the focus has shifted to its use as a H_2 storage medium. The release of H_2 from FA however does not proceed spontaneously due to the high activation energy associated with the reaction. It is in this regard that current studies in promoting FA as a H_2 carrier are focussing on developing catalysts for the decomposition process. Moreover, everything else equal, the selectivity towards either dehydrogenation or dehydration is dependent on the catalyst type. Developing catalysts that are selective toward H_2 production has

therefore been the sole study in promoting FA as a H_2 carrier. This is mainly because CO poisons catalysts used in fuel cells and as such, for H_2 production, the dehydration reaction needs to be suppressed.

2.2.1 Catalysts for formic acid decomposition

The study of the catalytic decomposition of FA was first performed by Mailhe and Sabatier, (1912) on different metals and oxides. In this study, the selectivity of the catalysts was investigated and oxides were reported to favour the dehydration process while metals promoted the occurrence of the dehydrogenation route. A closer analysis of the catalytic behaviour of metals and metal alloys (iron, nickel, copper, palladium, silver, platinum, gold, copper-gold, and silver-gold) was also carried out from 1936 by Rienacker and colleagues (Mars, *et al*., 1963). Overall, these studies mainly focused on determining the effect of metal alloying on the rate of the catalytic reactions. Another early study was carried out on nickel (Ni) and copper (Cu) metals and the selectivity towards H_2 formation was found to be 0.75-0.83 for Ni and Ni-rich catalysts and 0.95-0.98 for Cu and Cu-rich catalysts (Iglesia & Boudart, 1983; Iglesia & Boudart, 1983). In these early studies however, the decomposition reaction was only used as a model for catalyst selection and testing and no focus was placed on H_2 production.

With respect to H_2 production, noticeable advances have been made in selective decomposition of FA with the use homogeneous catalysts (Boddien, *et al*., 2009; Fellay, *et al*., 2008; Fellay, *et al*., 2009; Himeda, 2009; Boddien, *et al*., 2010; Boddien, *et al*., 2011; Boddien, *et al*., 2010). For instance, different Ru-phosphine complexes for FA decomposition were developed achieving a turn over frequency (TOF) of 3630 hour $^{-1}$ from FA-amines at temperatures close to ambient (Boddien, *et al*., 2008). In addition, Fellay, *et al*., (2008) and Fellay, *et al*., (2009) designed a Ru-TPPTS catalyst that could release H_2 and CO_2 from an aqueous solution of FA-sodium formate (SF) at temperatures of 70 – 120 ^{o}C. More recently, Boddien, *et al*., (2011) developed iron catalysts that can release H_2 from FA at 80 ^{o}C. Overall, the most successful catalysts for decomposing FA have mostly been homogeneous catalysts of ruthenium (Ru) and rhodium (Rh) (Loges, *et al*., 2010). Homogeneous catalysts are however not easy to separate and recycle especially in conventional packed bed reactors. Due to this challenge, heterogeneous catalysts which are easy to re-use are being developed.

In contrary to the advances in homogeneous catalysis, the heterogeneous catalysis of FA decomposition is still a subject for research. The most studied heterogeneous catalysts for decomposing FA are those from transition metals such as Pt, Pd, Ni, Rh, iridium (Ir) and Rh.

Overall, the activity of these metals was reported to follow the sequence Ir > Pt > Pd > Ru > Rh on vaporised FA (Soylomosi, *et al*., 2011) and Pd > Rh > Pt > gold (Au) > silver (Ag) on liquid FA (Tedsree, *et al*., 2011). It should however be noted that these catalysts were of different metal dispersion and as such, the results reported by these studies might not reflect the actual catalytic properties of these metals.

Although transition metals such as Pd have shown higher activity in decomposing FA than other metals, these catalysts deactivate quickly as they are more prone to CO poisoning. Accordingly, many researchers have tried to achieve better selectivity towards dehydrogenation by adding secondary metals to the commonly used Pd catalysts. For instance, Zhou, *et al*., (2008) reported that the addition of Ag, Au and other Cu group metals to Pd tend to retain the activity of Pd and make it more CO resistant. A year later, Ojeda & Iglesia (2009) studied the decomposition of FA on Au/Al_2O_3 and reported that finely dispersed Au nano-particles catalysed the decomposition better than Pt clusters at temperatures ranging from 343 to 383 K. The decomposition of formic acid on Au catalysts was also studied by Gazsi, *et al*., (2011) on different supports. It was reported in this study that Au/SiO_2 was the best catalyst for the decomposition process in terms of selectivity and activity. Following on these studies, bimetallic and tri-metallic catalysts of Pd, Au and Ag have since been studied intensively at near ambient temperatures. Table 2.1 is a summary of active bi- and tri-metallic heterogeneous catalysts developed thus far.

Table 2.1: Bi- and tri-metallic heterogeneous catalysts for FA decomposition for the production of H_2

Catalyst	Feed	Temp (˚C)	CO production	TOF (h^{-1})	Reference
$Ag_{12}Pd_{58}$	Aqueous	50	No	382	(Zhang , *et al*., 2013)
Ag@Pd/C	Aqueous	20	No	192	(Tedsree, *et al*., 2011)
$CO_{0.30}Au_{0.35}Pd_{0.35}$	Aqueous	25	No	80	(Wang, *et al*., 2014)
PdAu/C-CeO_2	Aqueous HCOONa	92	145ppm	113.5	(Zhou, *et al*., 2008)
PdAu@Au/C	Aqueous HCOONa	92	30ppm	21.4	Huang, *et al*., 2010)
Pd-S-SiO_2	Aqueous	85	No	719	Zhao, *et al*., 2011)
AuPd@ED-MIL-101	Aqueous HCOONa	90	Yes	106	Gu, *et al*.,2011

Most of these catalysts studies have shown that the selectivity towards H_2 production is highly dependent on the operating temperature. In addition, the nature of the feed also has a significant

effect on the selectivity and activity of the catalyst. Although these catalysts have been intensively studied, commercialisation of these catalysts has not been achieved yet. Generally, the nature of the reactor feed, operating temperature and catalyst type will be an important variable in evaluating the performance of microchannel reactors in FA decomposition for H_2 production.

2.2.2 Kinetics of formic acid decomposition

Despite intensive studies in catalyst development, reaction kinetics remains relatively scarce in FA decomposition for H_2 pro`duction. Understanding of the reaction kinetics is especially important for reactor design and optimisation purposes of any reaction. One of the early studies on the kinetics of FA decomposition was performed by Hinshelwood and Tropley in 1923 (Mars, *et al*., 1963). It was reported in these studies that the rate of dehydrogenation reaction can be described by zero order kinetics at pressures in the order of 1 atm and/or low operating temperatures (< 500 K). At lower pressures (< 1 atm) and/or high temperatures (> 500 K) however, first order kinetics can describe the dehydrogenation kinetics. The reaction phenomena were related to the adsorption of a reaction intermediate following simple Langmuir kinetics. The reaction scheme in Equation 2.6 (Mars, *et al*., 1963) describes the irreversible adsorption of FA on metal surfaces and the irreversible decomposition of the intermediate species according to the dehydrogenation reaction.

$$HCOOH_{(g)} \overset{k_1}{\rightarrow} adsorbed\ intermediate \overset{k_2}{\rightarrow} CO_{2(g)} + H_{2(g)} \quad \text{.....2.6}$$

At steady state, the rate constants (k_1 and k_2) can be related to FA pressure as shown in Equation 2.7 (Mars, *et al*., 1963)

$$k_1 p(1 - \theta_i) = k_2 \theta_i \quad \text{..... 2.7}$$

And from equation 2.7, $\theta_i = \frac{k_1 p}{k_2 + k_1 p}$

The rate of reaction, *r* can then be described according to Equation 2.8 (Mars, *et al*., 1963)

$$r = k_2 \theta_i \text{..... 2.8}$$

So that $\frac{1}{r} = \frac{1}{k_2} + \frac{1}{k_1 p}$

At pressures approaching 1 atm, the surface is completely covered with intermediate species as such θ_i = 1 and the reaction becomes zero order with respect to the FA pressure.

$$r = k_2 \quad \text{..... 2.9}$$

The activation energy measured in this case is the energy of the decomposition of the FA intermediate. At pressures lower than 1 atm, on the other hand, 1-θ_i = 1 and as such the reaction rate is first order with respect to FA pressure (Mars, *et al*., 1963).

$$r = k_1 p \quad \text{..... 2.10}$$

Following up on the study by Hinshelwood and Tropley (1923), most studies in catalyst development have reported that the decomposition of vaporised FA follows zero order kinetics with respect to FA pressure. For instance, Ojeda and Iglesia (2009) studied the decomposition of FA on Au/Al_2O_3 catalyst and reported zero order kinetics at 1 atm and 353 K. The activation energy in this regime was reported to be 52+/-2 kJ/mol. Zero order kinetics were also reported for Ir,Pt,Rh,Pd and Ru catalysts with activation energies in the range of 70 +/-3 kJ/mol at atmospheric pressure and 473 K (Soylomosi, *et al*., 2011). Furthermore, Gazsi and colleagues (2011), reported zero order kinetics at 473 K on Au catalysts of different supports with activation energies ranging between 58 and 60 kJ/mol. Activation energies in this range were also reported for Pd/C, Au/C and Au/TiO_2 catalysts in the zero order regimes (Bulushev, *et al*., 2010). Higher activation energies between 84 and 138 kJ/mol have, however, been reported for bi-metallic catalysts of Pd at 365 K and 1 atm (Zhou, *et al*., 2008). These high activation energies might be due to highly concentrated FA that was decomposed in this particular study in comparison to other studies.

Although a few studies exist on the kinetics of FA decomposition at low temperatures, kinetics at high temperatures remains scarce. To maximise FA throughput, FA conversions and H_2 production, high temperatures may be required and kinetics at high temperatures become important. The decomposition of FA at high temperatures may however result in the occurrence of the unwanted dehydration reaction and as such, it becomes important to understand kinetics of the dehydration reaction. The historical study of the dehydration reaction focused on understanding the activities of the oxide catalysts and as such, only a few studies reported on the kinetics of this reaction. A review by Mars, et al., (1963) shows that conflicting kinetics has been reported for the dehydration reaction. For instance, the reaction has been reported to follow first and zero order on silica (SiO_2) catalyst by different authors respectively.

In recent studies, kinetics of the dehydration reaction was rarely reported as dehydrogenation was exclusively favoured considering the low operating temperatures (298 to 473 K). One of the few studies that reported on the kinetics of the dehydration reaction was carried out by Sun, *et*

al., (1988) at high operating temperatures (350 to 800 K) using a Ru (001) catalyst. The occurrence of both dehydration and dehydrogenation reactions was witnessed with dehydrogenation being dominant. Arrhenius kinetic plot results showed that two distinct kinetic regimes existed at the operated temperature range. In Regime 1, zero order kinetics was reported at a temperature range of 360 to 400 K while in Regime 2, first order kinetics was reported at temperatures above 500 K for both dehydrogenation and dehydration (Table 2.2). Overall, the gradual change from zero order to first order with increase in temperature as reported by Sun, *et al*., (1988) was in accordance with literature studies.

Table 2.2 : Kinetic parameters for the decomposition of FA on Ru (001) catalyst (Sun, *et al*., 1988)**.**

	Regime 1	**Regime 2**
Temperature range	360 to 400 K	Above 500K
Reaction order	zero	First
Activation energy	16.0+/-0.3kcal/mol (dehydrogenation) 15.0+/-1.0kcal/mol (dehydration)	-1.3+/-0.2kcal/mol (dehydrogenation) -0.2+/-0.3kcal/mol (dehydration)

The negative activation energies reported in regime 2 however, indicate a complex reaction mechanism where the rate of reaction decreases with an increase in temperature.

Another study carried out at high operating temperatures of 275 to 400 ^{o}C and atmospheric pressure (1 atm) was performed by Patermarakis, (2003) on pure alumina (γ-Al_2O_3) and magnesium oxide (MgO) doped Al_2O_3 catalysts. In this study, both dehydration and dehydrogenation reactions occurred and zero order kinetics was reported. The selectivity and Arrhenius kinetic parameters differed for the two catalysts (pure γ-Al_2O_3 and MgO doped Al_2O_3) although activation energies were similar. Table 2.3 shows the kinetic parameters reported in this study for both catalysts at a time interval of 3.5 to 8.5 hours.

Table 2.3: Arrhenius kinetic parameters for the decomposition of FA on Al_2O_3 and MgO doped Al_2O_3 catalysts (Patermarakis, 2003)

Parameter	Al_2O_3 catalyst	Al_2O_3 + MgO catalyst
Reaction order	Zero	Zero
Activation energy	E_1= 87.4 kJ/mol (dehydrogenation) E_2=129.7 kJ/mol (dehydration)	E_1= 87.9 kJ/mol (dehydrogenation) E_2= 125.1 kJ/mol (dehydration)
Pre-exponential factor	ln $k_{o,1}(mol\ s^{-1}\ g^{-1}) = 8.4$ (dehydrogenation ln $k_{o,2}(mol\ s^{-1}\ g^{-1}) = 15.0$ (dehydration)	ln $k_{o,1}(mol\ s^{-1}\ g^{-1}) = 8.0$ (dehydrogenation) ln $k_{o,2}\ (mol\ s^{-1}\ g^{-1}) = 14.1$ (dehydration)

Overall, kinetics for FA decomposition at high temperatures (<500 K) is scarce and more research is required especially for the purpose of maximising FA throughput and H_2 production in most reactors.

2.2.3 Reactors for formic acid decomposition

Although reaction kinetics still remains a gap in FA decomposition for H_2 production, there is also a lack of literature reporting on reactor development for FA decomposition. For use in PEMFCs, FA is first decomposed in a suitable reformer to produce H_2. Historically, the non-catalytic decomposition of FA was mostly carried out in plug flow tubular reactor systems as described by Thornton and Savage (1990). In catalytic decomposition however, fixed bed and packed bed reactors have been used. For instance, Hyde and Poliakoff (2004) used a packed bed to decompose FA over a Pd catalyst. In addition to this study, Bulushev, *et al*., (2010) also carried out the decomposition reaction in a packed bed reactor over a Pt catalyst. In these conventional reactors however, smooth material flow tend to be obstructed by the packed bed which leads to undesirable pressure drops and clogging of the reactor tube (Javaid *et al*., 2013). In addition, large temperature gradients exist within these large reactors and the extent of most reactions may be reduced.

To overcome challenges of packed bed reactors, a micro tubular reactor of less than 0.5 mm inner diameter was studied (Javaid *et al*., 2013). Palladium and palladium oxide (PdO) were used as the catalysts for the reaction and these were coated on the reactor walls. In this study, it was reported that the reactor continuously decomposed aqueous FA in a much shorter residence time compared to conventional reactors. It was also concluded that the reactor offered large surface to volume ratio, good mixing and heat transfer properties that enhanced reaction rate. The effect of pressure, residence time, addition of sodium formate and temperature on the performance of

the reactor were investigated. Unlike in non-catalytic reactions, pressure had no significant effect on the FA conversion while sodium formate was found to increase the conversion. The micro tubular reactor generally achieved more than 99% FA conversion at 300ºC.

In addition to these reactors, Neah Power Systems recently demonstrated a reformer that allows onsite generation of H_2 using FA (Millikin, 2014). In this reformer, FA decomposes to produce H_2 which is then passed through a preferential oxidation (PrOx) reactor to remove CO. Hydrogen is then passed to a fuel cell stack to produce electric power while anode gases are vented to the atmosphere (Millikin, 2014). Table 2.4 shows the capability of this reformer technology.

Table 2.4: Capability of Neah Power Systems demonstration reformers for FA decomposition (Millikin, 2014)

Power (W)	Size of reformer Unit (cc)	Fuel flowrate (ml/min)	Fuel vol,20hrs (L)	Energy Density* (Wh/L)	Energy Density* (Wh/kg)
5	5	0.16	0.19	508	417
10	10	0.32	0.38	508	417
50	50	1.61	1.93	505	415
100	120	3.2	3.84	505	415

Although FA has been successfully decomposed to produce H_2 in most of these reformers, most of the conventional reactors are not compact enough to adequately deliver H_2 for small scale applications like PEMFC. Accordingly, most studies on the production of H_2 from liquid chemical carriers have reported microchannel reactors as suitable processing units. Section 2.3 presents recent studies in promoting microchannel reactors as suitable units for H_2 production for PEMFC.

2.3 MICROCHANNEL REACTOR TECHNOLOGY

Most studies focusing on the production of H_2 from liquid chemical carriers have highlighted microchannel reactors as suitable processing units. For instance, microchannel reactors have been studied in the steam reforming of methanol (MSR) to produce H_2, noting that methanol is by far the most used source of H_2 for fuel cells (Mei, *et al*., 2014; Park, *et al*., 2005). Most studies in MSR highlighted the effect of design parameters (channel length, width, height etc.) on the conversion rate (Du, *et al*., 2012). It was reported in these studies that an increase in microchannel reactor length result in increased conversion rate due to an increased reaction surface area. Apart from studies in MSR, the performance of microchannel reactors was also evaluated for the

production of H_2 from ethanol (Men, *et al*., 2007; Peela, *et al*., 2011), propane (Aartun, et al., 2005), ammonia (Chiuta, *et al*., 2014; Chiuta, *et al*., 2015), hydrogen peroxide (Paunovic, *et al*., 2015) and sorbitol (D'Angelo, *et al*., 2014). Most of these studies concluded that microchannel reformers performed exceptionally well to warrant consideration in H_2 supply to fuel cell systems. This is mainly due to the numerous advantages of microchannel reactors in comparison to conventional systems.

Microchannel reactors are basically compact reactors with channel diameters in the millimetre range. These reactors have large surface-to-volume ratios that result in high heat and mass transfer efficiencies (Atkinson & McDaniel, 2010). Their small sizes enable safe operation, especially with highly reactive and hazardous products (Mohammad, *et al*., 2013). In addition to these advantages, the compact design results in rapid response times which is an advantage in process control of most heterogeneous reactions (Mohammad, *et al*., 2013). Moreover, microchannel reactors are also easier to design and scale up compared to conventional reactors. This is mainly because a single channel is designed and reactor scale up is achieved by increasing the number of the designed channel while keeping the hydrodynamics constant (Robota, *et al*., 2014).

2.3.1 Industrial application of microchannel reactors

In addition to laboratory scale studies, microchannel reactors' abilities in process intensification have been demonstrated at a large scale level in the gas-to-liquid (GTL) Fischer-Tropsch (FT) process. The FT process was historically carried out in large fixed-bed or slurry-bed reactors. Recently however, Velocys developed a small scale GTL technology based on microchannel reactors (Brophy, 2004). This current reactor technology has the ability to accelerate reactions 10 – 15 fold compared to conventional reactors (Atkinson & McDaniel, 2010). Figure 2.3 shows the Velocys microchannel reactor size relative to a conventional plant for the equivalent production process.

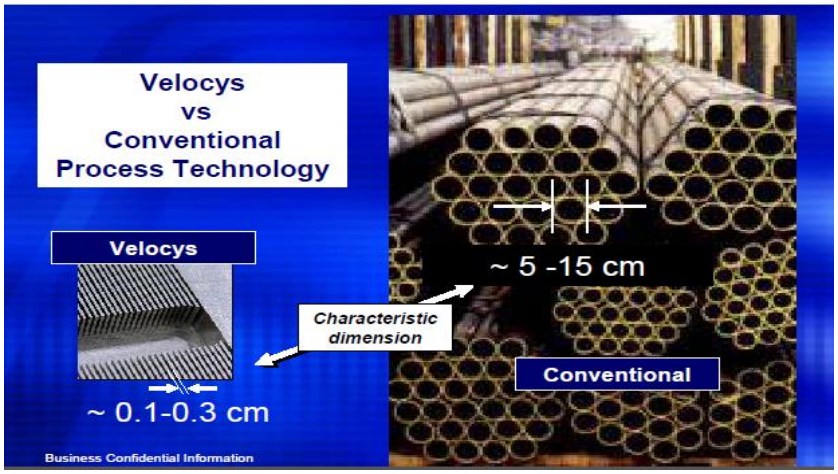

Figure 2.3 Comparison of a microchannel reactor and a conventional reactor by size for an equivalent production (Brophy, 2004)

The enormous advantages demonstrated by the Velocys microchannel technology warrants consideration of this reactor type in process and reactor advancement. Although this reactor has not been applied specifically for the production of H_2 from FA, consideration of this reactor will improve the energy and economic efficiency of the process.

2.3.2 Challenges in microchannel reactor technology

Although heterogeneous microchannel reactors have numerous advantages, their applications are still limited due to their design. For instance, these reactors have been more successful in gaseous reactions than in liquid phase reactions. This is mainly because pressure loss is large and clogging may occur in heterogeneous liquid phase reactions (Guangwen, *et al*., 2008). In liquid reactions that result in gaseous products, gases may adhere to the surface of the catalyst. Consequently, this may inhibit the contact between the catalyst and the raw material which then affects the reaction rate (Ryu, *et al*., 2013). It is in this regard that the application of such reactors in FA decomposition will be more favourable with vaporised FA.

Design parameters such as the manifold shape also affect the performance of most microchannel reactors. Depending on the manifold shape, a lack of flow uniformity can occur especially in parallel channels (Quiram, *et al*., 2007). This non-uniform flow distribution can then result in non-uniform heat transfer which can lead to lower reactor performance (Commenge, *et al*., 2002). Moreover, as the residence time affects the conversion; the conversion may therefore vary among microchannels due to non-uniform flowrates (Mohammad , *et al*., 2013; Commenge, *et al*., 2002). Reactor modelling is generally fundamental in solving most of the design challenges facing

microchannel reactors. It is therefore of paramount importance that the general modelling approaches be understood to help with design and optimisation of reactors. In addition to these design challenges, microchannel reactors are also prone to fouling caused by difficulties in cleaning the equipment (Worz, *et al*., 2001). Overall, it can be concluded that there still exist gaps in microchannel reactor technology; however, its advantages outweigh disadvantages.

2.3.3 Microchannel reactor modelling approach

Modelling, design and optimisation of most reactors require intensive understanding of transport phenomena. The subject of transport phenomena is made up of three main related fields namely; fluid dynamics, heat transfer and mass transfer (Bird, *et al*., 2002). Fluid dynamics describes the transport of momentum, heat transfer deals with the transport of energy while mass transfer on the other hand involves the transport of mass of chemical species. These three fields can easily be described by relevant mathematical equations. Microchannel reactor modelling then involves solving the reactor design equations to obtain transport profiles. In the past few years, different approaches (one dimensional (1D), two dimensional (2D) and three dimensional (3D)) for microchannel reactor modelling have been developed. Unlike in most conventional reactors, a single channel is normally modelled while scale up is achieved by increasing the number of the designed channel. In Section 2.3.3.1 to 2.3.3.3, different microchannel reactor modelling approaches are discussed with focus on studies in H_2 production.

2.3.3.1 One dimensional approach

One dimensional models are the simplest to develop as they require less computational power (Holladay & Wang, 2015). These models mostly assume plug flow behaviour where flow in microchannels is defined as a well-mixed plug of fluid. Accordingly, bulk convective mass and energy transport are only considered in the direction of fluid flow. This assumption however neglects radial diffusion assuming it is fast enough to maintain uniform profiles across the reaction channels (Parak, 2011). Most 1D models are therefore not adequate for describing transport profiles in most catalyst coated microchannel reactors where reactions are mostly mass transfer limited. Due to these shortcomings, only few studies have followed this approach in H_2 production. For instance, Kawamura, *et al*., (2006) used this approach to optimise the heat and mass transfer in their design of a methanol reformer for PEMFCs. In general, this approach is mostly suitable in describing transport profiles in homogeneous reactions rather than heterogeneous reactions.

2.3.3.2 Two dimensional approach

The most followed approach in modelling of microchannel reactors for H_2 production is the 2D approach. The 2D models provide more accurate predictions and more complicated designs compared to 1D models (Holladay & Wang, 2015). With this approach, velocity, temperature and mass profiles are assumed to be relevant in two directions. One of the earliest two dimensional models was developed by Karim, *et al*., (2005). In this study, the performance of a wall coated microchannel reactor was compared with that of a conventional packed bed reactor. This model was generally used to study the effect of reactor design parameters such as size and catalyst layer on the overall performance of the reactor. Karakaya & Avci, (2011) also used this approach to study the effect of microchannel reactor geometry and material configuration on temperature distribution and H_2 yield (Karakaya & Avci, 2011). In this study, the finite element method was used to solve for transport phenomena profiles on Comsol Multiphysics. It was reported in this study that the H_2 yield increased with an increase in microchannel reactor side length.

2.3.3.3 Three dimensional approach

The 3D approach is more powerful and allows for more accurate designs than the 2D approach**.** This approach mainly solves the profiles in all possible directions (x, y, z) considered. Commege, *et al*., (2002) followed this approach in determining the effect of the geometrical characteristic of microchannel structures on the flow distribution. In their study, Fluent software package was used as the computational fluid dynamics (CFD) tool. The results from this model were used to optimise the reactor design for maximum flow uniformity. Following up on this study, Mei, *et al*., (2013) used the same software package to study flow uniformity. It was reported that longer microchannels with a higher aspect ratio and small side length in the manifolds were beneficial for attaining uniform flow distribution. Another 3D study on flow uniformity was performed using Comsol Multiphysics (Mohammad , *et al*., 2013). In this study, the effect of microchannel width, depth, and channel spacing on flow distribution and pressure drop were investigated. In H_2 production, Chiuta, *et al*., (2014) developed a 3D model using Comsol Multiphysics for the production of H_2 from ammonia. In this study, an understanding of reaction-coupled transport phenomena within the microchannel reactor was developed.

In general, multidimensional approaches lead to a system of partial differential equations that can easily be solved using CFD software packages such as FLUENT, FEMLAB and COMSOL Multiphysics.

2.3.4 A review of microchannel reactor fabrication methods

The main advantage of microchannel reactors lies in their compact design and as such, it is important to understand their mechanical design. Microchannel reactors relevant to this dissertation consist of two plates (bottom and cover) stacked together face to face and enclosed in a case. The bottom plate consists of a network of micro-sized channels in which reactions take place. The material of construction of these plates is an important aspect of the design as it determines the thermal efficiency of the reactor. Materials of construction therefore account for heat transfer, reactor operating temperature and the thermodynamics of the chemical species. In cases where high operating temperatures are required, materials of construction are then limited to silicon, aluminium, stainless steel and high temperatures ceramics (Mitsos & Barton, 2009). In the aspect of chemical species, the materials of construction need to be corrosion resistant (Brand, *et al*., 2006). Due to these requirements, microchannel reactor plates are mainly made from stainless steel. This material has good mechanical stability and can withstand high operating temperatures (Nageswara & Kunzru, 2007; Kolb & Hessel, 2004).

Section 2.3.4.1 to 2.3.4.4 presents general techniques for the construction of microchannel reactors relevant to this dissertation. A typical microchannel reactor design relevant to this dissertation is shown in Figure 2.4.

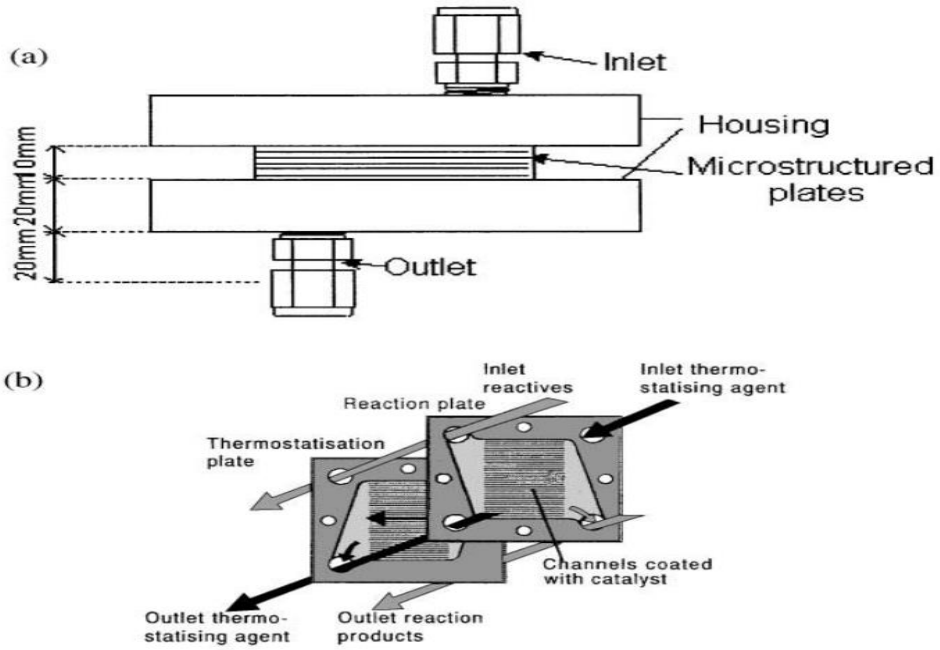

Figure 2.4: Basic configurations of a microchannel reactor (Rouge , *et al*., 2001)

2.3.4.1 Microstructuring

Typically, microstructuring is the first stage in fabricating a microchannel reactor. During this stage, microchannels are manufactured on the reactor bottom plate according to different techniques. General techniques for fabricating microchannels include micromachining, dry etching, micromolding, wet chemical etching, micro electro-discharge machining and laser ablation (Nageswara & Kunzru, 2007). Among these, micromachining and wet chemical etching are the most common. Wet chemical etching is however, more attractive than micromachining as it is flexible and cheaper.

The wet chemical etching process utilises liquid chemicals to dissolve substrate materials as required (Avinash, *et al*., n.d.; MEMS, n.d.). The solution used to dissolve the material is referred to as an etchant and it is generally selective, as such; substrates of different materials will require different chemicals. In microchannel reactors relevant to this study, an iron chloride solution is mostly used as an etchant (Hessel, *et al*., 2005). Acids such as hydrochloric acid can also be added to the iron chloride solution to increase the solubility of ferrous ions in the etchant solution as these tend to increase and become insoluble as etching proceeds (Nageswara & Kunzru, 2007). The chloride solution can however, deactivate the catalyst during the catalyst coating stage. This drawback is minimised by the calcination of reactor plates in air to reduce the chlorine content (Zapf, *et al*., 2003). The calcination of reactor plates also result in the formation of an oxide layer on reactor walls which in turn improves the adherence of the catalyst coating.

Typically, etching is performed to accomplish a certain pattern on the surface of the plate and as such, a mask is used to cover the portions of the plate surface that do not require etching. The masking material has to be resistant to the etchant solution or preferably etch at a slower rate than the substrate material (MEMS, n.d.). A photo-resist polymer is therefore mostly used for masking. Overall, the wet chemical etching technique does not lead to the formation of raised edges as experienced in micro machining (Nageswara & Kunzru, 2007). On the other hand, materials such as noble metals are stable against most of the etching processes and as such, machining can be advantageous (Brandner, 2008). For both methods however, microchannels are connected leaving spacious compartments (manifolds) for reactants and products at the inlet and outlet of the reactor. This is mainly done to allow for a uniform distribution of components as they enter and exit the reactor.

2.3.4.2 Catalyst coating

Unlike in conventional packed-bed reactors, catalysts in microchannel reactors relevant to this study are mostly chemically bound to the channel walls. Different methods for coating the reactor channels include anodic oxidation, sol-gel process, washcoating, electrophoretic deposition and chemical vapor deposition (Haas-Santo, *et al*., 2002; Hwang, *et al*., 2007). Among these, the most prominent method for coating readily made catalysts (commercial catalysts) is washcoating. According to this method, a suspension of the catalyst (washcoat) to be coated is first prepared from a mixture of the catalyst, binders, acid and solvent such as water (Meille, 2006). A good washcoat is achieved with catalysts of particle sizes in the range between 2–5 µm. Small catalyst particle sizes generally result in more adherent coatings compared to catalysts of lager particle sizes (Agrafiotis & Tsetsekou, 2000).

In addition to catalyst particle sizes, the addition of acids such as nitic acid also results in much uniform washcoats. Furthermore, the use of binders improves the stability of the suspension while improving the loading and adhesion of the catalyst (Mitra & Kunzru, 2008). This is mainly because, binders tend to pack between the spaces of the catalyst particles and improve the contact of the catalyst particles. One of the most commonly used binders when preparing washcoats for deposition in stainless steel microchannel is a Poly vinyl alcohol (PVA) (Zapf, *et al*., 2006). Hwang, *et al*., (2007) studied the effect of adding a PVA binder in alumina sols and reported that the PVA resulted in better adhesion of the alumina layer due to a decreased rate of water evaporation. At the end of the wash coating process, binders are usually decomposed and removed during the calcination stage (Section 2.3.4.3) of the reactor plates (Zapf, *et al*., 2006). These binders therefore have no effect on the activity of the catalyst as applied. Overall, the wash coating procedure result in ease catalyst deposition and is widely used in microchannel reactor technology.

2.3.4.3 Temperature treatment

The stage that follows catalyst deposition is the drying and calcination stage where reactor plates are treated in air at high temperatures. The drying procedure is mainly carried out either through microwave and room temperature drying or oven drying at 100 ˚C (Mitsos & Barton, 2009). This stage is usually performed to achieve homogeneity of the active metals on the catalyst carrier. On the other hand, calcination of the coated channels result in the complete decomposition of

organic additives such as binders added during the wash coating stage (Mitsos & Barton, 2009). This stage therefore ensures that only the catalyst is left on the channel walls.

2.3.4.4 Reactor bonding and packaging

The final stage of microchannel reactor construction is the plate sealing or microchannel reactor bonding stage. At this stage, the top and bottom plates are sealed face-to-face and the technique used is determined by the temperature stability of the catalyst. The methods for bonding include electron beam welding, brazing, sintering, laser welding and diffusion bonding (Mitsos & Barton, 2009). Laser welding has been reported to be advantageous as it has limited energy input hence it protects the catalyst from damage. In spite of the method used, bonding is performed in a way that achieves regularly shaped channels throughout the reactor. After the bonding, the stacked microchannel reactor is packaged in such a way that it can be connected to other equipment such as heat exchangers and inlet tubing. Generally, packaging is done ensuring no leaks exist in the system. The overall procedures result in devices that can withstand pressures up to 100 MPa for stainless steel microchannel reactors (Mitsos & Barton, 2009).

CHAPTER 3: EXPERIMENTAL

In this chapter, the experimental equipment, apparatus, as well as the methodology followed in evaluating the microchannel reactor is presented. The chapter starts off in Section 3.1 with a summary of the reactor specifications where emphasis is placed on the reactor construction and dimensions. Thereafter, the microchannel catalyst layer is characterised to give an understanding of the catalyst properties. Following on, Section 3.3 presents a detailed description of the equipment used in decomposing FA, where, the experimental flow diagram is described and the purpose of each piece of equipment is discussed. The experimental evaluation procedure is then described in Section 3.4. The parameters used to evaluate the microchannel reactor are outlined and discussed in this section. A step-by-step operation of the assembled experimental apparatus and equipment is also given with emphasis on the reactor daily start-up and shut-down, as well as data collection. Mathematical tools used to analyse the collected data are also presented in this section. In summary, this chapter presents a detailed procedure undertaken to accomplish the aim and objectives of this dissertation.

3.1 MICROCHANNEL REACTOR FABRICATION

The microchannel reactor used in this study was similar to that studied by Chiuta, *et al*., (2014). The reactor was constructed in collaboration with Fraunhofer (ICT-IMM) in Germany according to a wet chemical etching method as described in Chapter 2, Section 2.3.4.1. Generally, 80 microchannels were constructed on a 2 mm stainless steel plate with a 250 µm gap (fin) between them. In addition, right-angled triangle manifolds were manufactured at the inlet and outlet of the plates for uniform distribution of reactants. A commercial 1.15 wt. % Au/Al_2O_3 catalyst obtained from Minkek (South Africa) was supplied to ICT- IMM in the form of 2 mm extrudates (pellets). As per the manufacturer's catalyst technical data, the average Au crystallite size was 2 – 3 nm. This catalyst was then coated on manufactured microchannel walls according to the wash coating method as described in Chapter 2, Section 2.3.4.2. According to this procedure, the catalyst pellets were first milled into a fine catalyst powder of an average particle size of 75 nm (Appendix B). Thereafter, a catalyst washcoat was prepared and deposited onto the manufactured microchannels after which channels were dried and calcined accordingly. The complete microchannel reactor comprised of a heating block accompanied by two heating cartridges (watlow FIREROD) for reactor temperature control purposes. Thermocouples were integrated onto these heating cartridges for temperature measurements. Table 3.1 shows the full

specifications of the microchannel reactor while Figure 3.1 shows the complete manufactured reactor as used in this dissertation.

Table 3.1: Microchannel reactor target specifications for the production of H_2 from FA

Parameter	Specification
Catalyst	1.15 wt.% Au/Al_2O_3 (Mintek)
Number of channels	80
Channel length per plate	50 mm
Channel width per plate	450 µm
Channel height per plate	150 µm
Catalyst layer	40 µm (92 mg)
Material of construction	SS 314 (German classification 1.4841)
Maximum working temperatures	800 ºC
Working fluid	Formic acid (99.99 %) Formic acid/water (50/50 vol.%)
Flow rate range	0-20 ml/s
Inlet and outlet	1/8'' SS tubing, laser welded

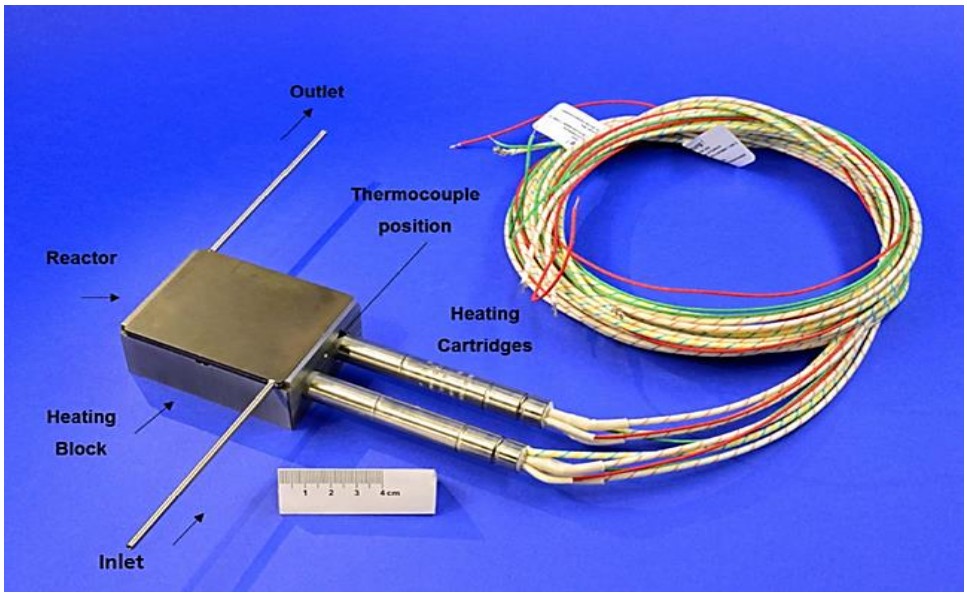

Figure 3. 1: Depiction of the constructed reactor with laser welded inlet and outlet tubings as well as the corresponding heating block and heating cartridge

3.2 MICROCHANNEL REACTOR PLATE CHARACTERISATION

The final catalyst coated microchannel plate was characterised to give a better understanding of the catalyst properties. Characterisation was carried out in collaboration with the National Centre

for Nano-Structured Materials at CSIR using X-ray Powder Diffraction (XRD) and Scanning Electron Microscopy (SEM) techniques. Sections 3.2.1 and 3.2.2 present the catalyst characterisation results. Characterisation results of the original catalyst powder and catalyst washcoat are also presented in Appendix B

3.2.1 X-ray Powder Diffraction

In order to determine the crystalline phases of the reactor catalyst layer, the catalyst was characterised by XRD technique. The XRD patterns were obtained at ambient conditions using a PANalytical X'Pert Pro powder diffractometer as described by Dyosiba, *et al*., 2016. Figure 3.2 shows the XRD peaks.

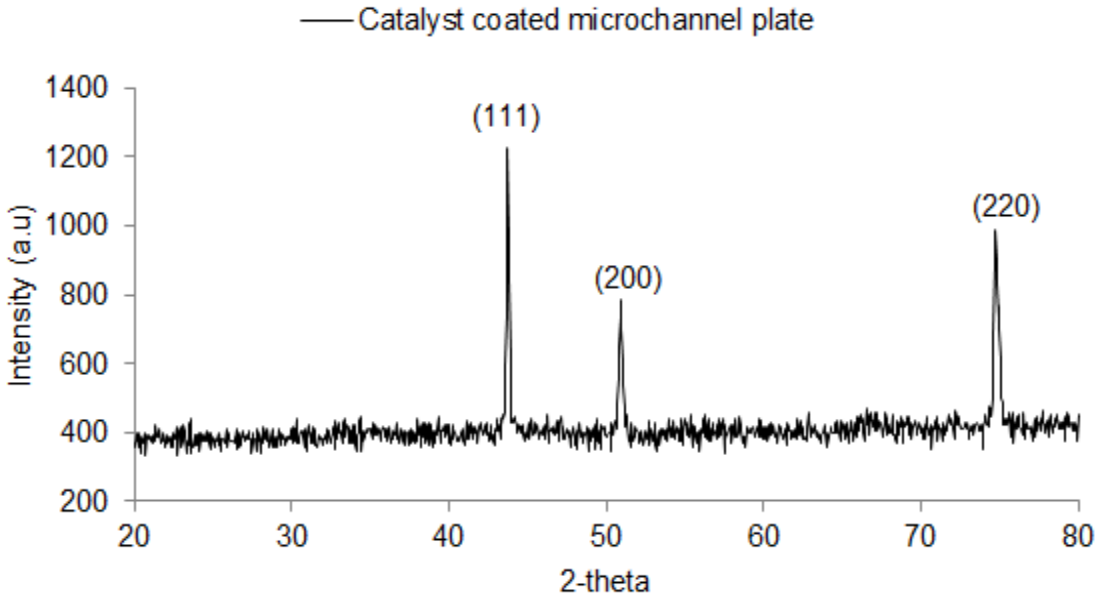

Figure 3. 2: XRD pattern of the catalyst coated microchannel plate.

The microchannel plate showed the presence of Au (111), Au (200) and Au (220) peaks at 2-theta values of 43 º, 50 º and 73 º respectively. These phases were indexed in Figure 3.2 in accordance with literature (Lee, *et al*., 2008). The (220) phase was however measured at higher 2-theta values indicating a possible decrease in lattice parameter after the wash coating, drying and calcination procedures employed. The shift to higher 2-thetha values may also indicate strong characteristic peaks of stainless steel crystalline structure (Kuo, *et al*., 2007). This would be expected as stainless steel (314) was used as the material of construction for the reactor plate. Moreover, the catalyst layer was very thin (40 µm) in comparison to the stainless steel plate making it possible for the XRD pattern to represent that of the stainless steel plate.

3.2.2 Energy-Dispersive X-ray Spectroscopy

The catalyst coated microchannel plate was further analysed by use of an Auriga Cobra Focused-Ion Beam Scanning Electron Microscope (FIB-SEM) equipped with Energy-Dispersive X-ray Spectroscopy (EDS). The SEM-EDS mapping of the catalyst coated plate was aimed at providing a spatial distribution of the elements on the microchannel. Figure 3.3 shows the SEM micrograms as well as the EDS mapping of the microchannel reactor.

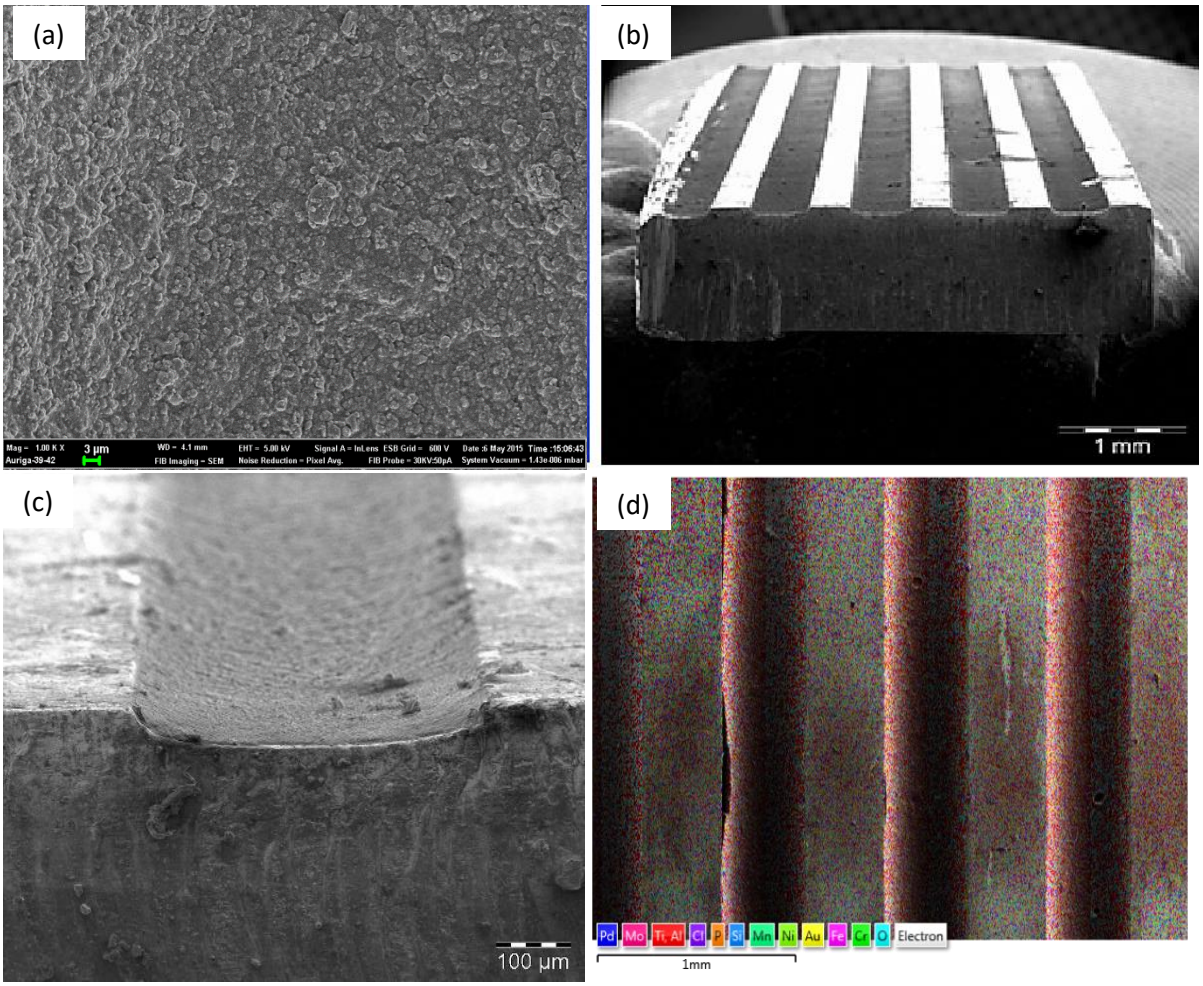

Figure 3. 3: SEM image showing (a) the microchannel plate surface,(b) the reactor channels and fin , (c) a single reactor channel catalyst layer and (d) the elemental mapping of the microchannel reactor plate .

The SEM image in Figure 3.3 a shows a uniform distribution of the catalyst particles across the microchannel plate. The catalyst particles were also well dispersed as the image showed no particles clumped together. The EDS mapping of the microchannel (Figure 3.3 d) showed the

presence of aluminium as the main element across the reactor. This was expected as alumina was used as the support for the Au catalyst. Accordingly, oxygen was also detected across the channel as well as Au. In addition to the elements making up the catalyst, the microchannel plate also showed the presence of elements such as chromium (Cr), iron (Fe), Manganese (Mn), silicon (Si), phosphorous (P), nickel (Ni) and chlorine (Cl). These elements were mainly from the stainless steel material used in constructing the reactor plate. A typical elemental composition of stainless steel (314) material is shown in Table B.1 of Appendix B. The catalytic effects of these elements on the decomposition process are however currently unknown and as such, for future purposes, it is recommended that an uncoated reactor be manufactured for the purpose of performing blank tests.

The presence of the Cl element can be attributed to the use of an iron chloride solution during the chemical etching process (Chapter 2, Section 2.3.4.1). The chloride content is however normally reduced during the calcination process and, as such, only residues were detected by SEM. It can therefore be concluded that the microchannel plate was made up of the stainless steel material and the catalyst as coated.

3.3 EXPERIMENTAL APPARATUS

Experimental apparatus and equipment were assembled consisting of the feed preparation, reaction and product analysis sections. Figure 3.4 is a process flow diagram showing the three main sections and these were discussed in Sections 3.3.1 to 3.3.3.

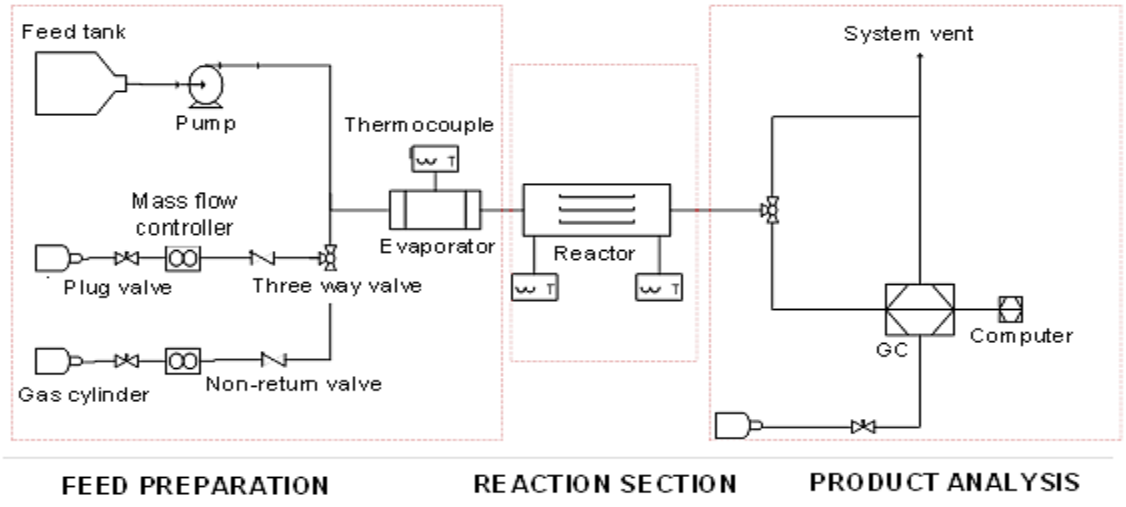

Figure 3. 4 : An experimental flow diagram for the production of hydrogen from formic acid.

3.3.1 Feed preparation

The feed preparation section consisted of a syringe pump (NE-1000 series) capable of holding a single 50 ml syringe. At its minimum rate of 0.001 ml/min, the pump could achieve a continuous 800 h run. At a maximum flowrate of 0.1 ml/min, the syringe capacity was adequate for a 6 h continuous run. Overall, the pump capacity was sufficient for the reactor operating conditions studied in this dissertation. The feed section also comprised N_2 (99.99 %) and H_2 (99.99 %) gas cylinders regulated by respective pressure regulators and Brooks SLA5850 thermal mass flow controllers. Furthermore, the feed section included an evaporator heated by a heating cartridge (HI-TECH elements) with a maximum temperature output of 450 ^oC. The evaporator temperature was regulated by a temperature controller and the temperature was monitored by a K-type thermocouple inserted at one end of the cartridge. In the evaporator, the reactants were vaporized prior to being fed into the reaction section (Section 3.3.2).

3.3.2 Reaction section

The reaction section consisted of a microchannel reactor (Section 3.1) where vaporised FA was decomposed to produce H_2. The microchannel reactor was heated to required operating temperatures by a heating block heated by two cartridge heaters (watlow FIREROD) with integrated thermocouples. The cartridge temperature was controlled by relevant temperature controllers. In addition to the heating cartridge thermocouples, two more thermocouples were inserted on opposite ends of the heating block to measure the reactor wall temperature. To prevent heat losses from the reactor to the surroundings, the reactor was insulated. Generally, FA was decomposed in this section and the products were then analysed in the product analysis section (Section 3.3.3).

3.3.3 Product analysis

The products of the reaction section were analysed using a SRI 8610C gas chromatography (GC). This GC was equipped with two TCDs, one HID, one FID, two molecular Sieve 13X (MS13X) columns (1.8 m) and one HayeSep D column (1.8 m). Hydrogen volume fractions were determined from the MS 13X channel connected in parallel to the other two columns and argon (Ar) was used as the carrier gas. Carbon dioxide and unconverted FA were then analysed from the channel consisting of the HayeSep D column connected in series with the second MS 13X and Helium (He) was used as the carrier gas. Initial experiments showed the presence of CO in

the product stream as such, this component was also analysed from the HayeSep D column. These three sections were therefore assembled to give an experimental arrangement shown in Figure 3.5.

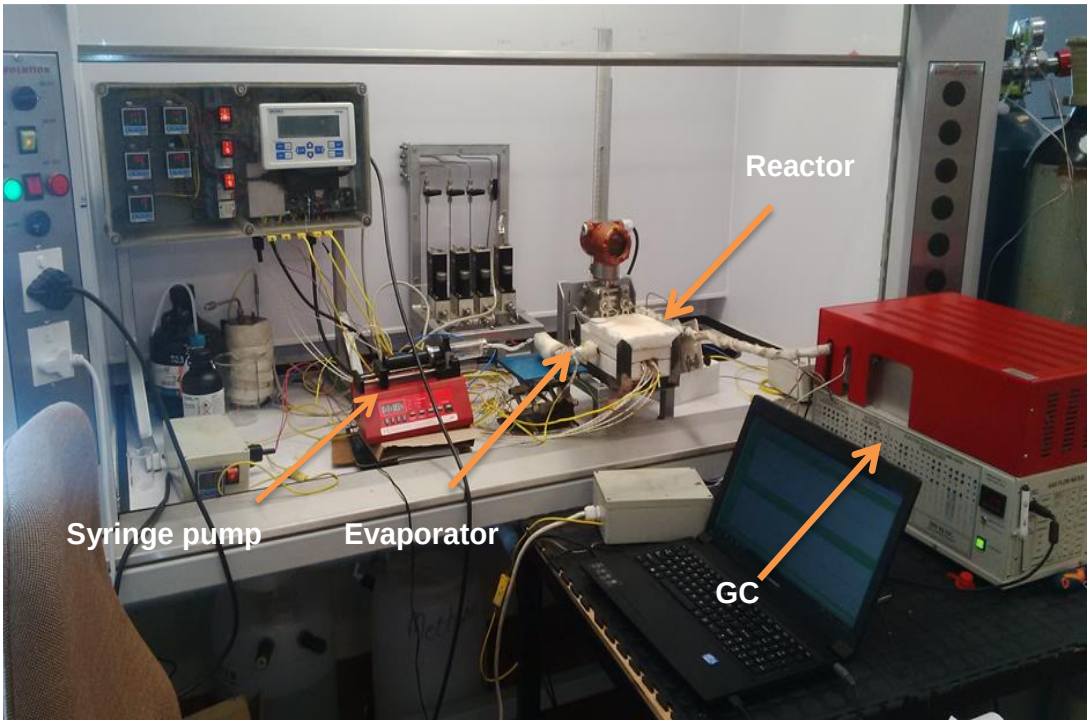

Figure 3. 5: An assembled experimental apparatus and equipment for the performance evaluation of a microchannel for the production of H_2 from FA.

As shown in Figure 3.5, the lines connecting the three sections of the experimental setup were maintained at 150 ^oC using heating tapes (HI-TECH Elements). This was done to prevent condensation of FA at any point in the system. These lines were further thermally-insulated and the temperature was controlled and monitored by relevant controllers and thermocouples, respectively. Section 3.4 presents the experimental procedure for FA decomposition using the assembled experimental apparatus and equipment.

3.4 EXPERIMENTAL PROCEDURE

The experimental procedure followed three main steps, namely the leak tests, GC calibration and FA decomposition. Sections 3.4.1 to 3.4.3 discuss these steps, respectively.

3.4.1 Leak test

A leak test was performed on the assembled system before the start of the experiment. This was done to ensure the safe, efficient, and reliable operation of the evaluation setup. Prior to performing the leak test, the system was purged with N_2 to sweep air out of the system. Thereafter, the reactor was pressurised and soap water was used to check for any leaks before leaving the reactor at 6 bar for 2 hours. During these 2 hours, the reactor pressure was monitored to ensure there was no pressure loss. On completion of the leak test, the reactor system was depressurised back to atmospheric conditions (0.88 bar).

3.4.2 Calibration of Gas Chromatography

Prior to start of the evaluation process, the GC was calibrated for H_2, CO_2, CO and FA. Initial experiments and calculated equilibrium mole fractions were used as a guide in determining the suitable standards for calibration. Figure 3.6 shows the calculated equilibrium mole fractions according to the dehydrogenation and dehydration reactions at relevant temperatures.

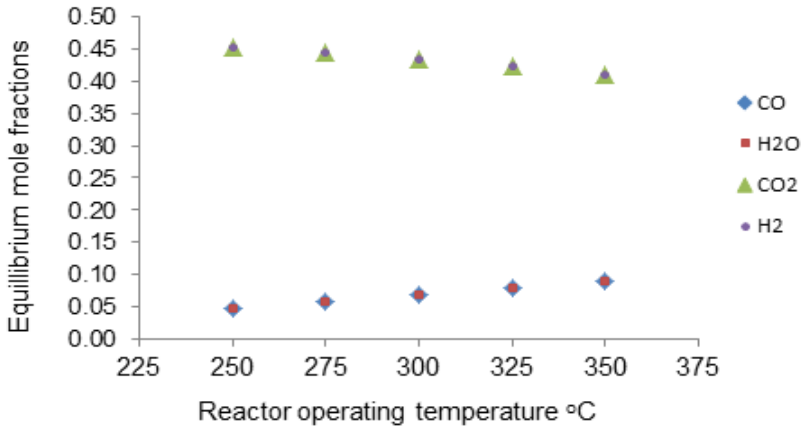

Figure 3. 6 : Calculated equilibrium mole fractions for the decomposition of FA (99.99%) according to the dehydrogenation and dehydration reactions

The equilibrium mole fractions as well as initial experiments were therefore used to estimate the highest concentrations of calibration standards.

3.4.2.1 Hydrogen, carbon monoxide and carbon dioxide calibration standards

Three standards of known concentrations of H_2, CO and CO_2 (10 to 80%) were purchased from Afrox. Calibrations were performed at atmospheric pressure (0.88 bar) and this pressure was maintained during the entire experimental investigation. For each standard, calibration runs were

repeated three times and an average of the three concentrations was taken. The corresponding calibration curves are shown in Appendix C.

In addition to these standards, calibration standards for FA were prepared as described in section 3.4.2.2.

3.4.2.2 Formic acid calibration standards

Formic acid calibration standards were prepared using a stainless steel N_2 bubble humidifier which was connected to the GC. The bubble humidifier walls were heated by an encapsulated heating tape (thermolyne silicone rubber) with a maximum application temperature of 260 ^oC. The bubble humidifier temperature was regulated by a temperature controller similar to that used in the evaporation section. The wall and inside temperatures were then measured by K-type thermocouples (3 mm). The bubble humidifier was further insulated to prevent heat losses, as shown in Figure 3.7.

For standard preparation, the bubble humidifier was partially filled with FA (99.99%) and heated to required FA temperatures (25, 50 and 75 ^oC). At each FA temperature, N_2 (99.99 %) was bubbled through at a constant flow rate of 40 ml/min. The resulting FA/N_2 mixture was fed to the GC for calibration purposes. The line connecting the bubble humidifier outlet to the GC was maintained at 2 ^oC above the bubble humidifier set temperature to avoid condensation. The GC calibration conditions were maintained throughout the entire experimental work.

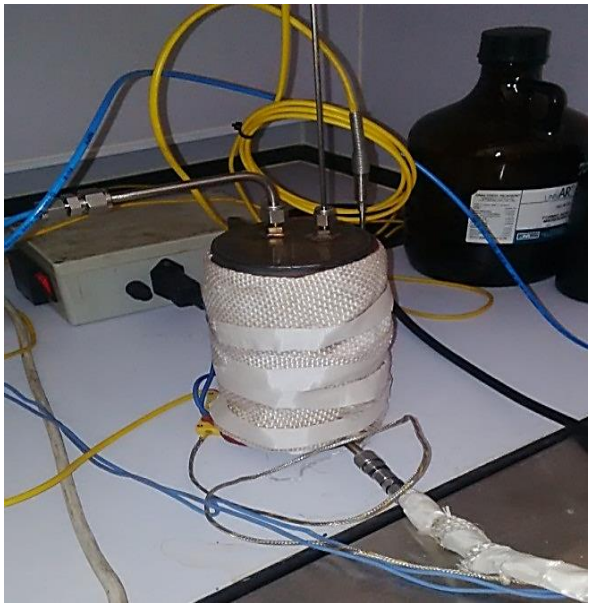

Figure 3. 7: A nitrogen bubble humidifier for FA calibration.

The temperature of FA in the bubble humidifier determined the extent of N_2 saturation with FA in accordance with the vapour pressure of FA at different temperatures. The concentration of FA in the outlet of the bubble humidifier was therefore calculated according to equation 3.1 and 3.2 (Dopkin, n.d.). In accordance with this equation, only the vapour phase was assumed to leave the bubble humidifier at any given point in time. In addition, the outlet gas was assumed to have the same composition as the gas in the empty space above the FA surface in the bubble humidifier.

$$\frac{x_{FA}}{x_{N2}} = \frac{P_{FA,V}}{P_{N2}} = \frac{P_{FA,V}}{P_{local} - P_{FA,V}} \quad \text{..... 3.1}$$

The flowrate of the stream coming out of the bubble humidifier was then calculated according to equation 3.2.

$$F_{mix,out} = F_{N2,in} \frac{P_{FA,V}}{P_{local} - P_{FA,V}} \quad \text{.....3.2}$$

The calculated equilibrium concentrations were therefore found to be 7, 20 and 51 % at a FA bubble humidifier temperatures of 25, 50 and 75 ^{o}C respectively. The corresponding calibration curve is shown in Appendix C. Figure 3.8 illustrates the parameters used in equation 3.1 and 3.2 to calculate FA concentrations.

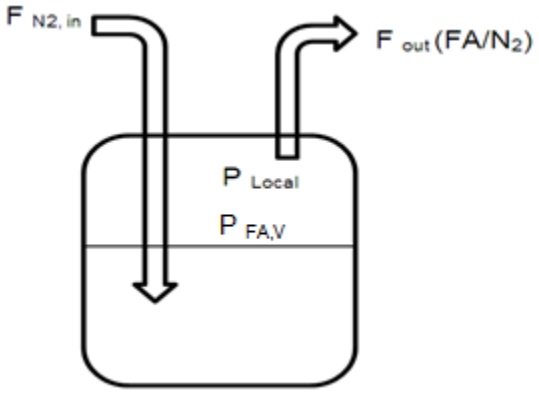

Figure 3. 8: Illustration of parameters used to calculate the FA/N_2 equilibrium mole fractions from the bubble humidifier

A FA mass balance experiment was performed to validate the calculated bubble humidifier outlet concentrations. The N_2/FA mixture was condensed using glycol at 3 ^{o}C and the time taken to collect a specific liquid FA sample was noted. The liquid sample was then weighed to determine the actual concentration of the bubble humidifier outlet stream. Table 3.2 shows the experimental and calculated (equation 3.2) FA equilibrium concentrations at a N_2 flowrate of 40 ml/min.

Table 3. 2: Experimental and calculated FA concentrations from the bubble humidifier.

Temperature (°C)	N_2 volume flow (ml/min)	FA volume fraction (experimental)	FA volume fraction (calculated)
75	40	0.50	0.51
50	40	0.18	0.20
25	40	0.06	0.07

3.4.2.3 Component retention times

The component retention times determined the frequency of data collection during the experimental work. Figure 3.9 shows the retention times of components as obtained from the GC.

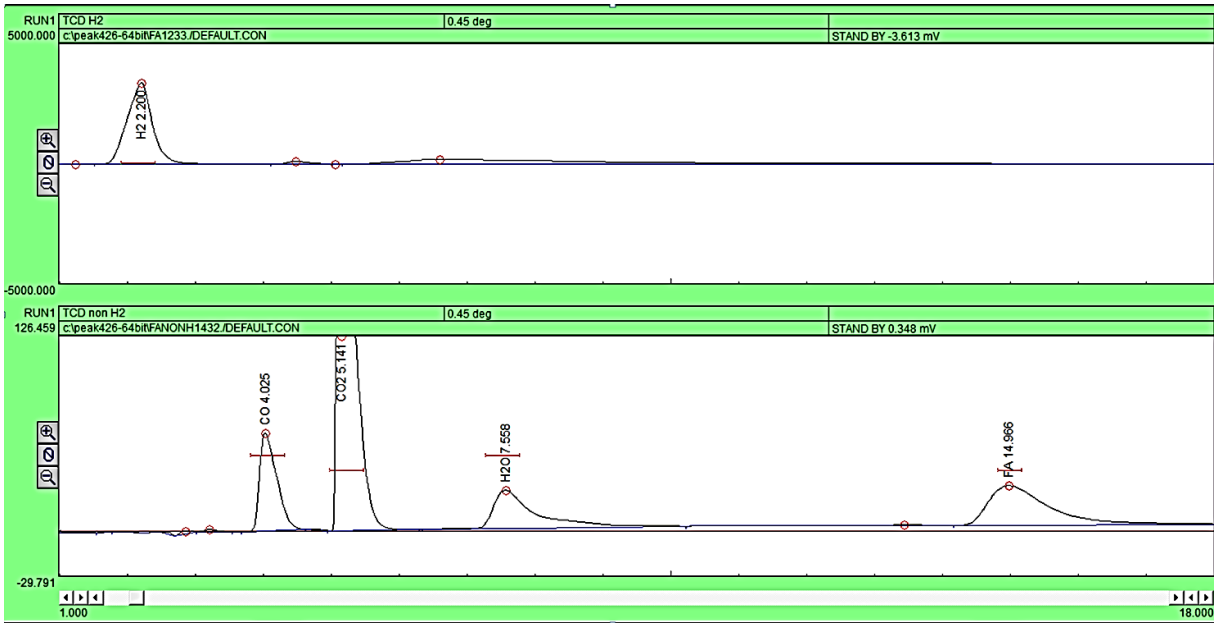

Figure 3. 9: Depiction of the components' retention times as obtained from the GC.

As shown in Figure 3.9, the retention times were found to be 2.2, 4.0, 5.1, 7.6 and 14.9 minutes for H_2, CO, CO_2, H_2O and FA, respectively. The retention times would however vary depending on calibration parameters such as pressure, carrier gas flowrate and GC oven temperature. Based on the FA retention time, data from the GC was collected within 30 minutes intervals. Calibrations for H_2O were not performed in this study and as such; H_2O concentrations were taken as equivalent to CO concentrations in accordance with the reaction stoichiometry of the dehydration reaction.

3.4.3 Formic acid decomposition

This section presents the procedure undertaken to decompose FA in a microchannel reactor starting off with the day to day operation of the reactor through to the data collection and analysis.

3.4.3.1 Catalyst reduction

Prior to start of the decomposition process, the catalyst was reduced in H_2 (50 ml/min) at 400 ^oC for 2 hours (Gazsi, Bansagi, & Solymosi, 2011). The reactor temperature was then adjusted to room temperature under N_2 (99.99 %, 50 ml/min) flow.

3.4.3.2 Reactor start-up and shutdown

The reactor was started-up and shut-down under N_2 flow (50 ml/min) to prevent catalyst deactivation. Nitrogen also served as a means for sweeping air out of the reactor at start-up. In addition, the GC columns were baked at 240 ^oC for 1 hour to drive off any moisture in the columns prior to experiments.

3.4.3.3 Performance evaluation

Two sets of experiments were performed to evaluate the performance of a microchannel reactor. In the first experiments, vaporised pure FA (99.99 %) was decomposed while in the second phase, vaporised FA/H_2O (50/50 vol. %) mixture was decomposed. In both sets of experiments, the microchannel reactor was evaluated by investigating the effect of reactor operating conditions on FA decomposition. Specifically, the effect of reactor temperature (250 – 350 ^oC) and vapour inlet flowrate (12 – 48 ml/min) on key parameters such as FA conversion, selectivity towards dehydrogenation and H_2 yield were investigated at atmospheric pressure (0.88 bar). In this dissertation, the reactor operating temperature was taken as the average of the two thermocouple readings inserted on the side of the heating block. The vapour inlet flowrate on the other hand was calculated as the liquid mass flowrate (from syringe pump flowrates) divided by the density of the reactant at the evaporator temperature (200 ^oC). The temperature and vapour flowrate range were chosen based on preliminary experimental results which gave minimum and maximum conversions close to 50 % and equilibrium, respectively.

Table 3.3 is a summary of the experimental runs for each set of experiment.

Table 3. 3: Summary of experimental planning

Experimental Number	Vapour flowrate (ml/min)	Temperature (°C)
1 to 5	12	250,275,300,325 and 350
6 to 10	24	250,275,300,325 and 350
10 to 15	36	250,275,300,325 and 350
15 to 20	48	250,275,300,325 and 350

Overall, the reactor operating temperature determines the extent of FA conversion and the amount of H_2 produced which makes it a suitable parameter for evaluating the microchannel reactor. The flowrate on the other hand defines the contact time between the catalyst surface and reactants which in turn determines the extent of reaction. These two variables were therefore suitable for the experimental evaluation of the microchannel reactor.

3.4.3.4 Data collection

Overall, all experiments were conducted one variable at a time while keeping the other variable constant. A single run was performed for a continuous period of 6 hours where data was collected within a 20 – 30 min interval. Twelve data points were therefore recorded during the 6 h period (Appendix E), and these were averaged to give a single data point.

3.4.3.5 Reproducibility

The reproducibility of the experimental results was investigated by repeating the experimental runs on different days. Section 4.1.5 shows the reproducibility test results and these were reproducible within a standard error of +/- 2 % for conversions and +/- 0.02 for selectivity values.

3.4.3.6 Reactor stability

Upon completion of the two sets of experiments, a performance durability and stability test was conducted on the reactor. This was performed over a period of 144 h continuous operation at a vapour FA flowrate of 36 ml/min and reactor operating temperature of 325 °C. Section 4.3 shows the reactor stability test results.

3.4.4 Performance evaluation parameters

The reactor performance key parameters were calculated from the experimental data according to equation 3.3 to 3.5

- **FA conversion**

The percentage FA conversions were calculated considering the amount of FA consumed according to the dehydrogenation and dehydration reactions. As CO and CO_2 were the only carbon components produced during the decomposition experiments, the sum of moles of these components were taken as equivalent to moles of FA consumed. Equation 3.3 was therefore used to calculate the percentage conversion of FA as the ratio of the sum of CO_2 and CO concentrations to the sum of CO_2, CO and FA concentrations in the product.

$$X_{FA} = \frac{y_{CO2}+y_{CO}}{y_{CO2}+y_{CO}+y_{FA}} \times 100 \quad \text{.....3.3}$$

- **Carbon dioxide and hydrogen selectivity**

The CO_2 selectivity of Au/Al_2O_3 catalyst was calculated as the ratio of CO_2 concentration to that of the sum of CO and CO_2 concentrations in the product (Bulushev, *et al*., 2010; Gazsi, *et al*., 2011). Overall, the CO_2 selectivity in this study can be defined as the fraction of the moles of FA consumed that forms CO_2. According to the stoichiometry of the dehydrogenation reaction, the H_2 selectivity is taken as equivalent to the CO_2 selectivity (Bulushev, *et al*., 2010). Equation 3.4 shows the mathematical equation for selectivity as used in this dissertation. Throughout this dissertation, the selectivity is used as a measure of the catalyst's ability to favour the desired dehydrogenation reaction rather than the undesired dehydration reaction.

$$S = \frac{y_{CO2}}{y_{CO2}+y_{CO}} \quad \text{.....3.4}$$

- **Hydrogen yield**

The hydrogen yield was calculated by multiplying the selectivity values by the FA conversion values as shown in equation 3.5 (Bulushev, *et al*., 2010; Gazsi, *et al*., 2011). This parameter represents the percentage FA conversion achieved due to the dehydrogenation reaction resulting in the formation of H_2.

$$H_{2,Yield} = SX_{FA} \quad \text{.....3.5}$$

CHAPTER 4: EXPERIMENTAL RESULTS AND DISCUSSION

This chapter presents the experimental results of this study. The Chapter starts off in Section 4.1 with a presentation of the decomposition of pure FA (99.99 %) results. Under this section, Section 4.1.1 and 4.1.2 presents the effect of reactor operating temperature (250 – 350 ^{o}C) and FA vapour flowrates (12 – 48 ml/min) on FA conversion and residual concentration. As both dehydration and dehydrogenation reactions were observed to occur, the effect of reactor operating conditions on CO formation, H_2 selectivity, and H_2 yield are then presented in Sections 4.1.3 and 4.1.4. Section 4.2 then presents the second phase of the experimental results where the effect of added water (50 vol.%) on FA decomposition is discussed. This section was aimed at improving the H_2 yield by inhibiting the dehydration reaction. Under this section, Sections 4.2.1 to 4.2.3 presents the effect of added H_2O on FA conversion, CO formation, selectivity towards dehydrogenation and H_2 yield. Thereafter, results of the reactor stability test are presented in Section 4.3. Finally, the chapter concludes with a discussion on the recommended reactor operating conditions based on the results of this study. In summary, it is in this chapter that the microchannel reactor is experimentally evaluated.

4.1 DECOMPOSITION OF PURE FORMIC ACID (99.99 %)

Taking into consideration the low H_2 content (4.4 wt. %) of FA, highly concentrated FA (99.99 %) was decomposed to maximise H_2 production. The experiments were carried out following the experimental planning in Table 3.3. Data collection and analysis was carried out as discussed in Chapter 3 of the dissertation and as such, the performance parameters were calculated according to equation 3.3 to 3.5.

4.1.1 Effect of reactor temperature on FA decomposition

Figure 4.1 shows the effect of reactor temperature on FA conversion (Equation 3.3) and FA residual concentration at different FA vapour flowrates. The experimental conversions were plotted together with the equilibrium conversions (calculated in Appendix D) to give a better indication of the performance achieved using the microchannel reactor. The equilibrium conversions were calculated considering the two main parallel reactions (dehydrogenation

(equation 2.3) and dehydration (equation 2.4)). For the reactor operating temperatures investigated in this dissertation (250 – 350 °C), the equilibrium conversions were calculated to be in the range of 99.3 – 99.5 % (Appendix D).

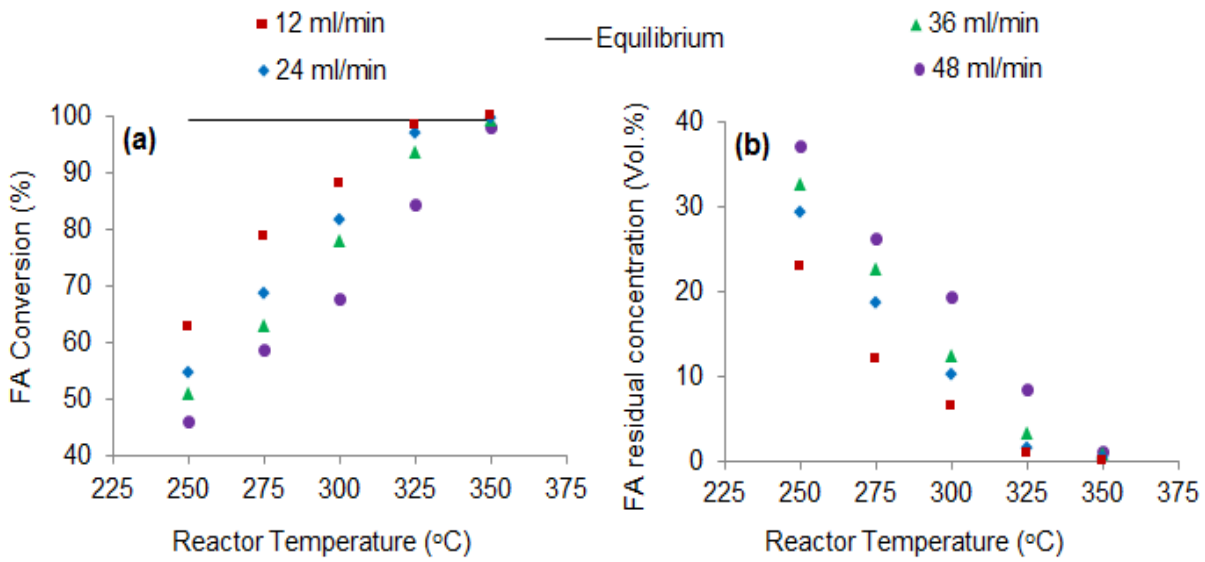

Figure 4. 1: Effect of reactor operating temperature (250 – 350 °C) on (a) FA conversion and (b) FA residual concentration.

As shown in Figure 4.1 (a), FA conversions increased with an increase in reactor operating temperature. Experimental conversions of 98 to 99 % were achieved at the highest operating temperature (350 °C) and all studied FA vapour flowrate of (12 – 48 ml/min). At this temperature, experimental conversions approached equilibrium conversions of 99.5 % (Appendix D). At lower temperatures (250 to 300 °C) however, FA conversions (46 to 63 %) showed a significant deviation from equilibrium conversions. This indicated that equilibrium limitations were mostly experienced at higher temperatures (325 to 350 °C) rather than at low temperatures.

Figure 4.1 (b) shows the change in FA residual concentration with reactor operating temperature. The unconverted FA concentration in the product stream generally decreased with an increase in reaction temperature. At 350 °C however, residual FA peaks were not detected on the GC-TCD. The highest FA product concentration (37 %) was obtained at 250 °C at a FA vapour flowrate of 48 ml/min. Overall; results indicated that reactor temperatures above 300 °C will be most useful for the overall conversion of FA.

There is however, currently no study reporting on the decomposition of FA using microchannel reactors and as such, results were not comparable to those in literature. When comparing these

results to those performed using a similar catalyst however, it is evident that the conversions at high temperatures (325 and 350 ^{o}C) were similar to those reported by (Gazsi, *et al*., 2011). At temperatures below 325 ^{o}C however, conversions found in this study were lower than those reported by Gazsi, *et al*., (2011) using a 1 wt. % Au/Al_2O_3 catalyst in a fixed bed reactor. In their study, Gazsi, *et al*., (2011) decomposed a more dilute FA (7 %) compared to highly concentrated FA (99.99%) used in this study. The lower conversions obtained in this study might therefore be due to the decomposition of concentrated FA. Javaid, *et al*., (2013) studied the decomposition of FA at different concentrations and reported higher conversions with low FA concentrations than highly concentrated FA. Overall, the microchannel reactor performed well in decomposing FA especially at temperatures above 300 ^{o}C allowing for a high throughput of FA.

4.1.2 Effect of flowrate on FA decomposition

Figure 4.2 shows the effect of FA (vapour) inlet flowrate (12 – 48 ml/min) on FA conversion at reactor temperatures of 250 – 350 ^{o}C. The FA vapour flowrates investigated in this study corresponded to gas hourly space velocities (GHSV) of 4.2 – 17.1 $NL.g_{cat}^{-1}.h^{-1}$ respectively.

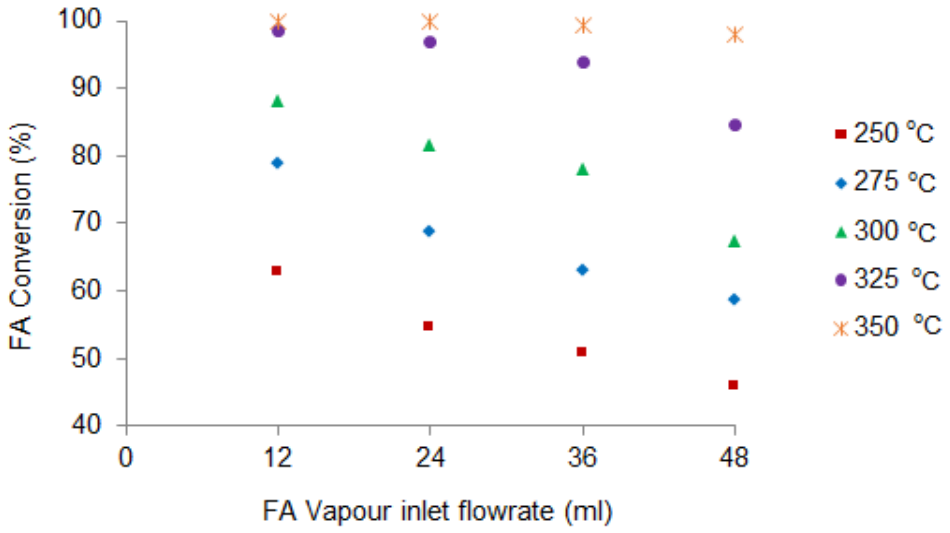

Figure 4. 2: Effect of vapour FA (99.99 %) inlet flowrate on FA conversion

As shown in Figure 4.2, FA conversions decreased with an increase in flowrate at all studied reactor operating temperatures. This is because, at higher FA flowrates, the reactants have lesser contact time with the catalyst layer which in turn results in reduced extent of reactions. Lower flowrates on the other hand offer a higher contact time which explains the high conversions (63 to 99%) obtained at a low flowrate of 12 ml/min (GHSV of 4.2 $NL.g_{cat}^{-1}.h^{-1}$). At 350 ^{o}C however,

FA conversions were found to be independent of FA flowrates. This was a result of thermodynamic limitations experienced at this reactor operating temperature irrespective of the flowrate. These findings, therefore, suggest that the reactor will be more efficient in converting FA with all studied flowrates if operated at 350 ^{o}C. As shown in Figure 4.1 (b), FA product concentrations were also minimal at 350 ^{o}C irrespective of FA flowrates. The highest FA product concentration (37 %) was measured at the highest FA flowrate of 48 ml/min (GHSV of 17.1 NL.gcat^{-1}.h^{-1}) and the lowest operating temperature (250 ^{o}C). Overall, a balance between a high FA conversion and a high FA throughput was achieved in this study at a reactor operating temperature of 350 ^{o}C and FA flowrate of 48 ml/min.

4.1.3 Effect of temperature on selectivity

The Au/Al_2O_3 catalyst used in this study catalysed both the dehydrogenation and dehydration reactions. Accordingly, it was of paramount importance that the effect of operating conditions on dehydrogenation selectivity be investigated. Moreover, as CO has the ability to deactivate catalysts, it is important in any FA decomposition process that the amount of CO produced is known. Accordingly, the extent of CO formation was investigated at the studied reactor operating conditions. Figure 4.3 shows the composition of the reactor product stream as measured on the GC at all studied temperatures and FA flowrates of 12 ml/min and 48 ml/min.

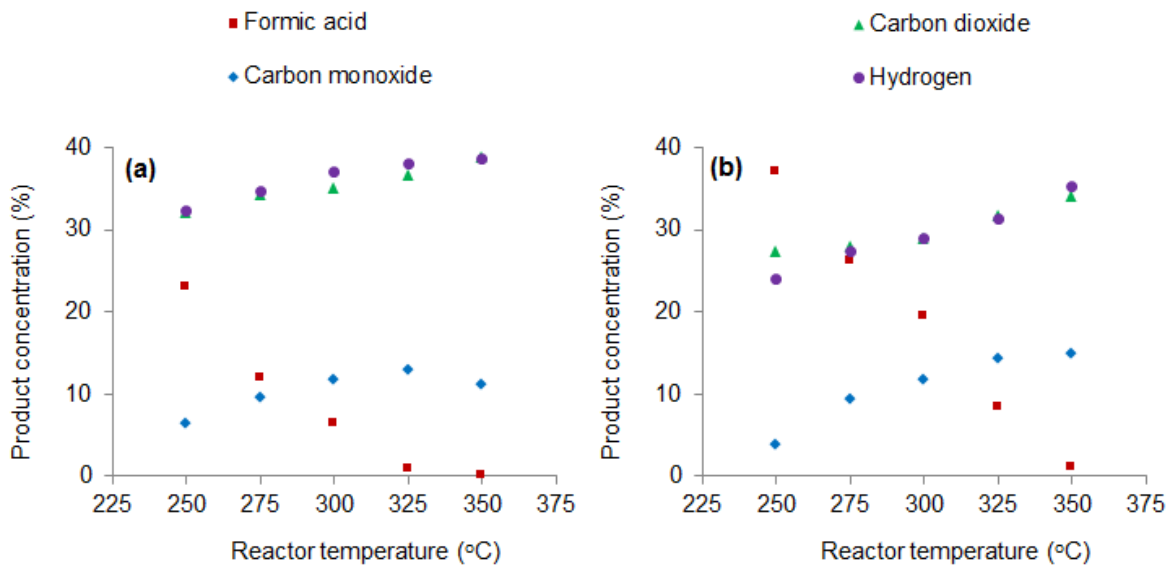

Figure 4. 3: Change in product concentrations with temperature at a FA vapour flowarate of (a) 12 ml and (b) 48 ml/min

As shown in Figure 4.3, the production of H_2 and CO_2 was dominant at all reactor temperatures. Carbon dioxide and H_2 product concentrations were approximately the same at all temperatures and this was in accordance with the 1:1 reaction stoichiometry of the dehydrogenation reaction. Carbon monoxide on the other hand increased from a range of 4 – 5 % at 250 ^oC to a range of 11 – 15 % at 350 ^oC at the studied flowrates. The increase in CO formation with temperature was a result of the endothermic (+10.25 kJ/mol) nature of the dehydration reaction. Generally, dehydration is favored at high temperatures while dehydrogenation (exothermic,-30.88 kJ/mol) is favoured at low temperatures (Mars, *et al*., 1963). Overall, the dehydrogenation reaction was found to be dominant at all studied temperatures showing that the catalyst used in this study was more selective towards dehydrogenation.

Based on the CO and CO_2 product concentrations, the H_2 selectivity was calculated according to equation 3.4. Figure 4.4 shows the effect of reactor operating temperature on selectivity towards H_2 production.

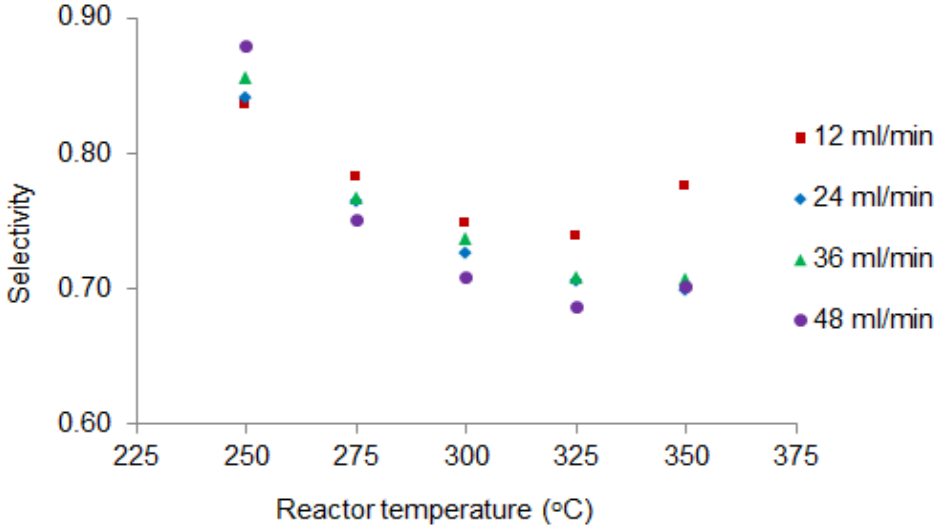

Figure 4. 4: Effect of reactor operating temperature (250 – 350 ^oC) on H_2 selectivity

Accordingly, Figure 4.4 shows a decrease in selectivity with temperature from 250 to 350 ^oC. Selectivity values at these temperatures were found to range between 0.69 and 0.88 at the studied vapour flowrates of 12 – 48 ml/min (GHSV of 4.2 – 17.1 $NL.g_{cat}^{-1}.h^{-1}$). Overall, selectivity values were almost independent of flowrates at most temperatures. This trend might have been an indication that dehydration and dehydrogenation reactions mostly occurred in parallel and the occurrence of the WGS (Equation 2.5) was minimal. The selectivity at a flowrate of 12 ml/min was, however, mostly higher than that at higher flowrates (24 – 48 ml/min) especially at

temperatures above 250 ^{o}C. This could have been an indication that the occurrence of the WGS reaction, although minimal, was more pronounced at the lowest flowrate and high reactor temperatures.

When comparing the results to those by Gazsi and colleagues (2008) on a similar catalyst, the catalyst in this study showed higher selectivity to H_2. The overall difference in results can be attributed to the differences in catalyst pre-treatment methods as well as Au loading. For instance, Mars and colleagues reported that pre-treatment of catalysts at higher temperatures (1000 ^{o}C) can result in dehydration being favoured. The catalyst was however less selective in comparison to that studied by Ojeda and Iglesia (2009). This might be due to the differences in operating temperatures as Ojeda and Iglesia decomposed FA at lower temperatures (383 K) compared to this study. It is generally known that the dehydration reaction is favored at higher temperatures than it is at low temperatures (Mars, et al., 1963).

It can be concluded from the selectivity results that, there is need to purify the gas produced from the microchannel reactor prior to supplying a PEMFC. This is mainly because, the CO concentrations were higher than the maximum allowable (100 ppm) for PEMFC applications (Holladay & Wang, 2015; Zhou, *et al*., 2008). More purification will therefore be required especially at the highest temperatures where selectivity values were the lowest.

4.1.4 Effect of operating conditions on H_2 yield and production rate

To evaluate the efficiency of the microchannel reactor in generating H_2, H_2 yields were calculated according to equation 3.5. Figure 4.5 shows the effect of temperature on H_2 yields at the studied flowrates of 12 to 48 ml/min (GHSV of 4.2 – 17.1 $NL.g_{cat}^{-1}.h^{-1}$).

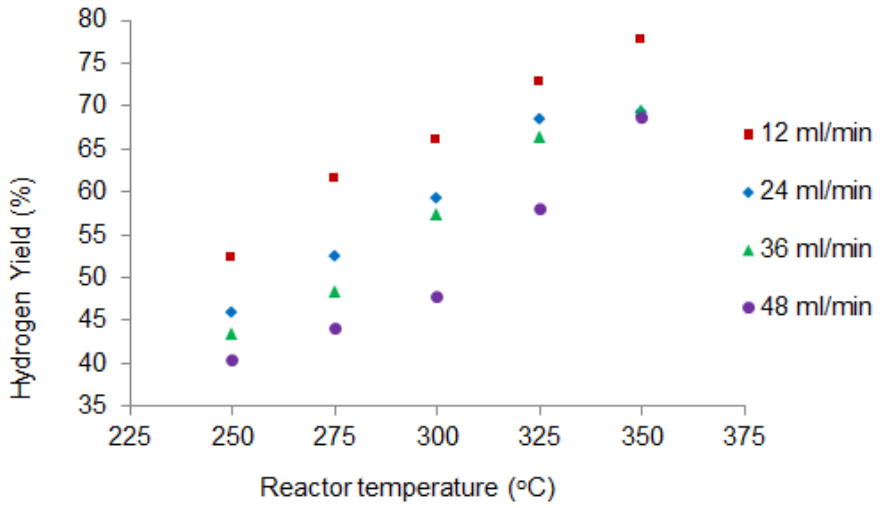

Figure 4. 5: Effect of reaction temperature (250 to 350 °C) on H_2 yield.

As discussed in Section 4.1.3, the selectivity to H_2 production was almost independent of flowrates, as such; H_2 yields were mainly influenced by the conversion at different flowrates. Hydrogen yields were, therefore, higher at high operating temperatures for each flowrates. Based on the H_2 yields calculated, the moles of FA consumed according to the dehydrogenation route were calculated as shown in equation 4.1.

$$moles\ of\ FA\ consumed = \frac{H_{2,yield}}{100} n_{FA,in} \quad \text{..... 4.1}$$

The moles of H_2 produced were then taken as equivalent to the moles of FA consumed by the dehydrogenation reaction in accordance with the reaction stoichiometry. Figure 4.6 shows the change in H_2 production rate with FA flowrate.

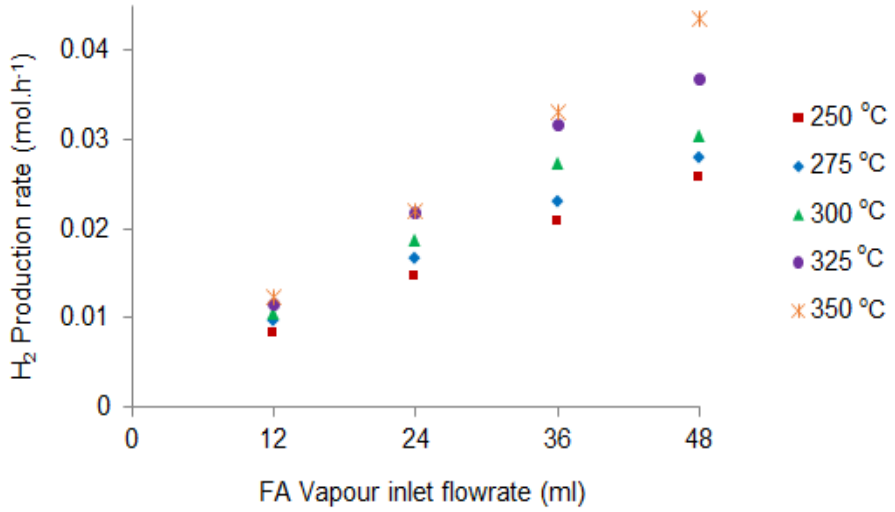

Figure 4. 6: Effect of FA inlet flowrate (12 – 48 ml/min) on H_2 production rate at reactor operating temperatures of 250 to 350 ° C.

As shown in Figure 4.6, the highest H_2 production rate of 0.04 $mol.h^{-1}$ (11.8 $NL.g_{cat}^{-1}.h^{-1}$) was obtained at the highest FA flowrate of 48 ml/min (GHSV of 17.1 $NL.g_{cat}^{-1}.h^{-1}$) and reactor temperature of 350 ° C. The lowest H_2 rate of 0.008 $mol.h^{-1}$ was obtained at the lowest FA flowrate of 12 ml/min (GHSV of 4.2 $NL.g_{cat}^{-1}.h^{-1}$) and a reactor operating temperature of 250 °C. It was concluded from these results that H_2 production rates would be maximised if the reactor is operated at 350 °C at a FA vapour flowrate of 48 ml/min (GHSV of 17.1 $NL.g_{cat}^{-1}.h^{-1}$). At these conditions however, the concentration of CO produced was found to be higher than that produced at low temperatures (250 °C), hence, more purification will be required.

4.1.5 Reproducibility of results

Experiments were repeated on different days to verify the reproducibility of results and also measure the standard error at each data point. Figure 4.7 is a plot of the average conversions measured on different days at three different temperatures (250,300 and 350 °C) and FA flowrates of 12 and 48 ml/min. The uncertainty of the conversion values was described using the standard deviation of the mean (standard error) as shown by the error bars.

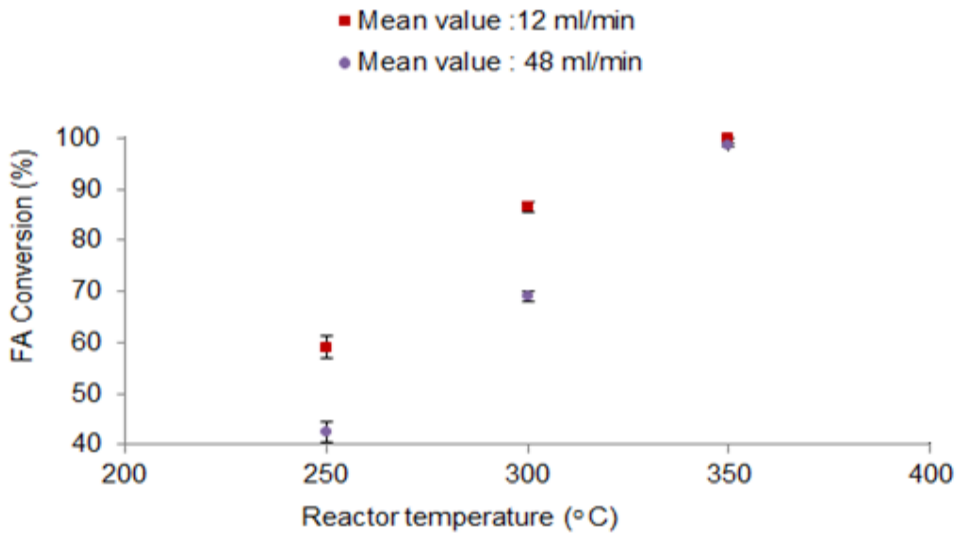

Figure 4. 7: Reproducibility of FA conversions measured at different days at reactor operating temperatures of 250,300 and 350 °C and flowrates of 12 and 48 ml/min

Based on measurements collected over a period of 3 days, the standard error was found to be highest at the lowest reactor temperature of 250 °C. For instance, a standard error of +/- 2.2 % and +/- 1.8 % was measured at 250 °C and FA flowrates of 12 ml/min and 48 ml/min respectively. To further measure the uncertainty of the results, the selectivity values were also measured at different days. The selectivity was found to have the highest standard error of +/- 0.02 and the mean values and error bars are shown in Figure 4.8.

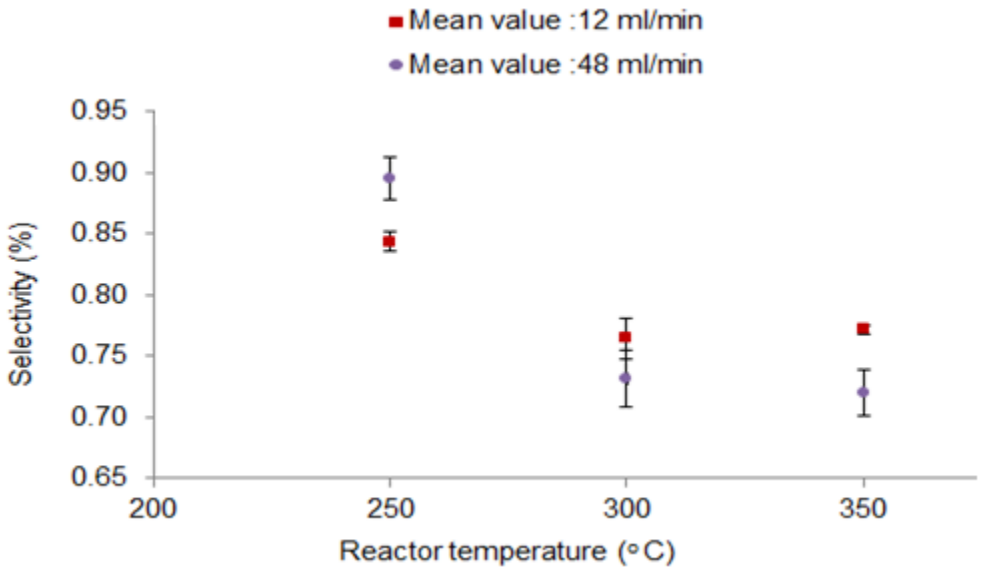

Figure 4. 8: Reproducibility of H_2 selectivity measured at different days at reactor operating temperatures of 250,300 and 350 °C and flowrates of 12 and 48 ml/min

4.2 DECOMPOSITION OF DILUTE FORMIC ACID (50 VOL. %)

Decomposition of FA in water was historically studied under both catalytic and non-catalytic conditions (Chapter 2). In catalytic decomposition, water was added to FA to promote the occurrence of the forward WGS reaction (Equation 2.5) and inhibit the dehydration reaction in an attempt to improve the H_2 yield (Gazsi, *et al*., 2011; Soylomosi, *et al*., 2011; Bulushev, *et al*., 2010). In this section, the effect of added H_2O (50 vol. %) on the decomposition of FA is investigated with the aim of improving the selectivity towards H_2 production. The main purpose of this section was, therefore, to reduce the CO fraction while increasing the H_2 yield. Minimising CO production also minimises the cost of purifying the produced H_2 gas prior to feeding a PEMFC. The choice of the FA/H_2O ratio (50/50 vol.%) investigated in this dissertation was solely based on reported literature (Gazsi, *et al*., 2011; Soylomosi, *et al*., 2011; Bulushev, *et al*., 2010), and the dissertation did not attempt to investigate the effect of different FA/H_2O ratios. Furthermore, the experimental conditions (pressure, temperature and flowrate) investigated in concentrated FA (99.99 %) experiments were maintained in this section.

4.2.1 Effect of water on FA conversion

Figure 4.9 shows the effect of H_2O on FA conversion at reactor temperatures of 250 – 350 ^oC and FA/H_2O vapour flowrates of 12 – 48 ml/min. The experimental results were compared to calculated equilibrium conversions (Appendix D) to give a better evaluation of the reactor's performance under these conditions. The equilibrium conversions in this case were calculated considering the dehydration and the dehydrogenation.

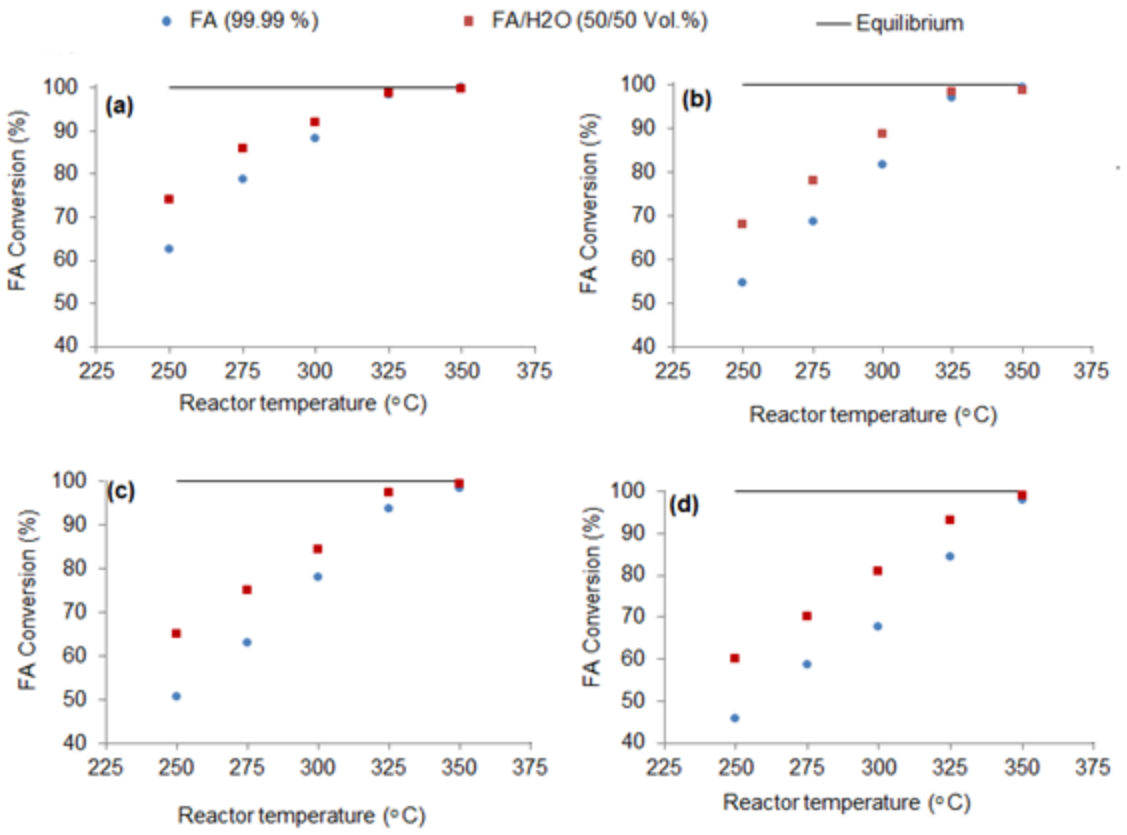

Figure 4. 9: Effect of added H_2O (50 vol. %) on FA (99.99 %) conversion at FA/H_2O (50/50 vol. %) vapour flowrates of (a) 12ml/min, (b) 24 ml/min, (c) 36 ml/min and (d) 48 ml/min

As shown in Figure 4.9, the addition of H_2O resulted in slight increased conversions, especially at temperature of 300 ^oC and below. For instance, the conversion increased from 63 to 74 % at 250 ^oC at an FA/H_2O flowrate of 12 ml/min. At higher temperatures however, both sets of results showed conversions close to equilibrium. Literature studies on the effect of H_2O on FA decomposition reported that the effect of added water on conversion was insignificant (Bulushev, *et al*., 2010; Soylomosi, *et al*., 2011). The general increase in conversion in this study might therefore not be a direct result of added H_2O, but rather, a result of decomposing dilute FA (50 vol. %). For instance, Javaid, *et al*., (2013) studied the effect of FA concentration on conversion at 300 ^oC and reported higher conversions of 99.2 % with dilute FA (0.15 M) while lower conversions of 90 % were reported for concentrated FA (0.6 M).

4.2.2 Effect of water on CO formation and H_2 selectivity

The main aim of decomposing FA/H_2O mixture was to improve the selectivity of the catalyst by lowering the extent of CO formation at the studied reactor operating temperatures. Accordingly, the effect of added water on CO formation was studied and Figure 4.10 shows the results at the various studied flowrates (12 – 48 ml/min).

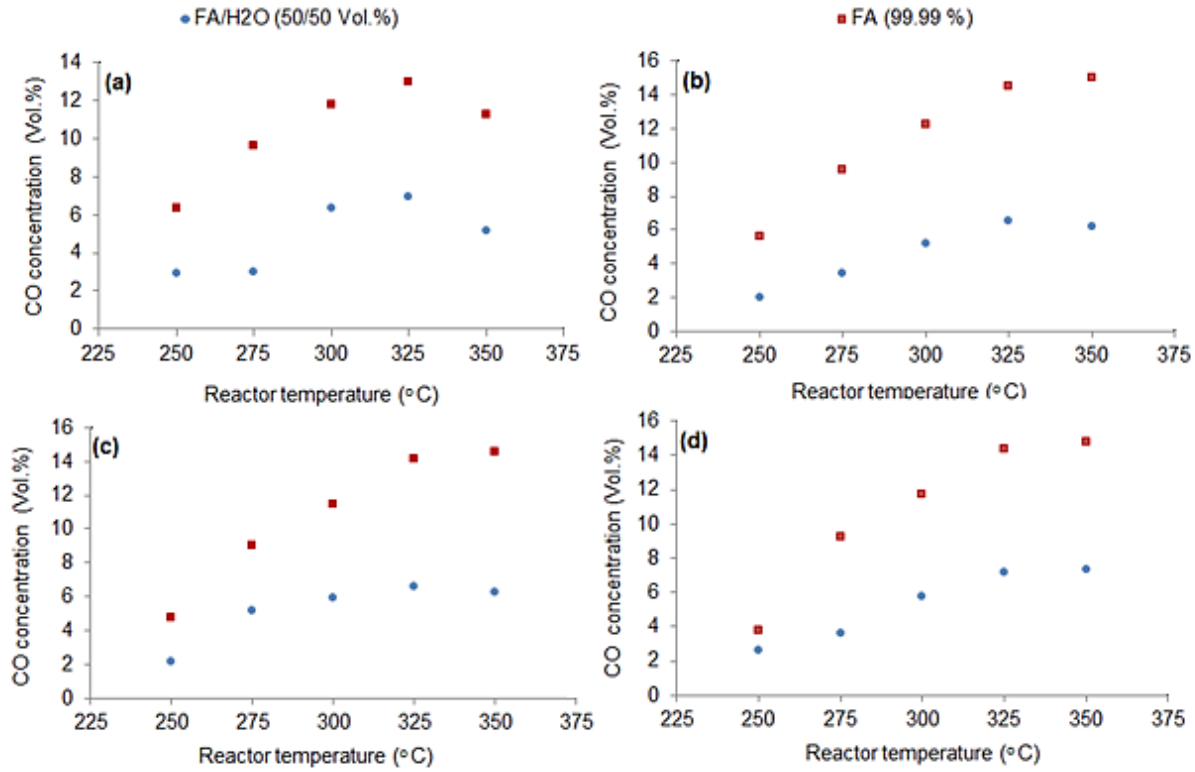

Figure 4. 10: Effect of added H_2O (50 vol. %) on CO formation at FA/H_2O vapour flowrates of (a) 12 ml/min, (b) 24 ml/min, (c) 36 ml/min, and (d) 48 ml/min.

As shown in Figure 4.10, CO concentrations decreased from a range of 4 – 15 % with highly concentrated FA (99.99 %) to a range of 2 – 7 % in the presence of H_2O. These results were in accordance with literature studies on the effect of added H_2O on the selectivity of Au catalysts (Gazsi, *et al*., 2011; Bulushev, *et al*., 2010). Generally, the presence of H_2O in excess promotes the occurrence of the forward WGS reaction which results in the conversion of CO to CO_2. As shown in Figure 4.10, a significant reduction in CO was obtained at high temperatures of 300,325 and 350 ^{o} C. This showed that the conversion of CO through the WGS reaction was more pronounced at high temperatures than it was at low temperatures. A study by Bulushev, et al., (2010) also reported an increase in CO conversions with temperature through the WGS reaction. The corresponding improvement in selectivity towards H_2 production is shown in Figure 4.11.

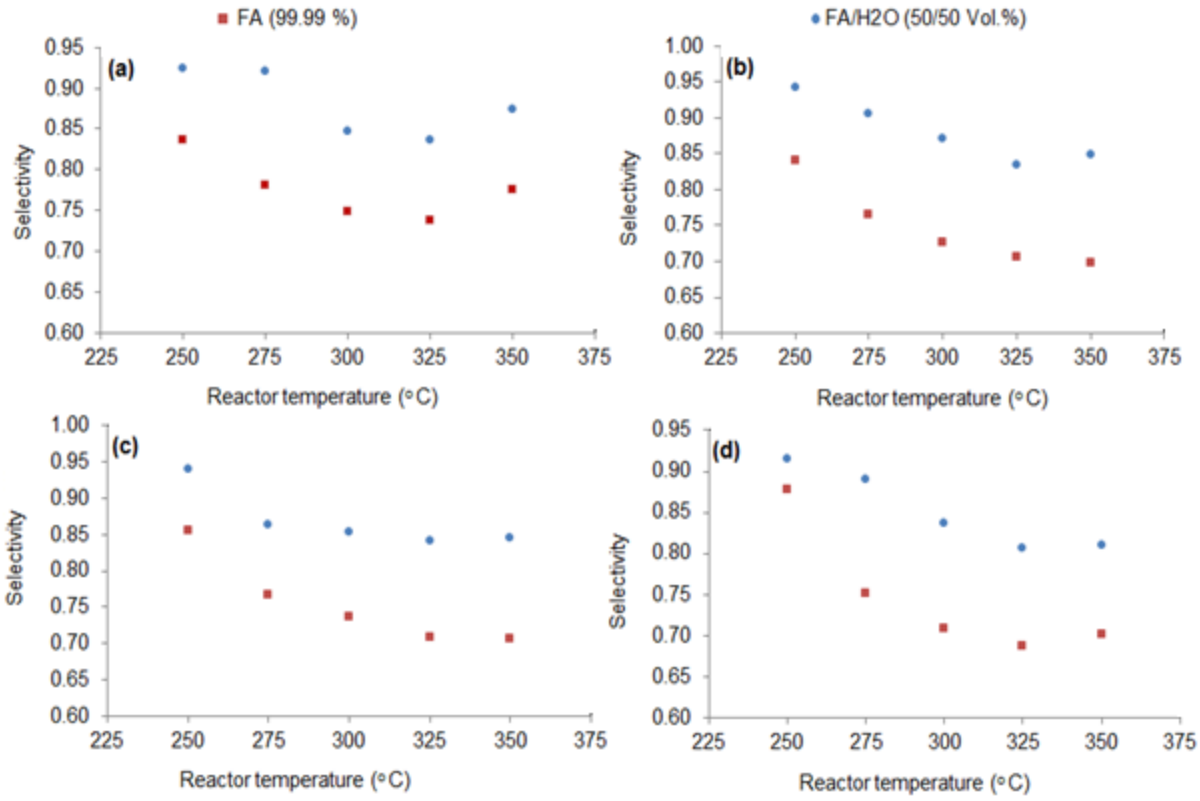

Figure 4. 11: Effect of added H_2O (50 vol. %) on selectivity towards H_2 production at FA/H_2O (50/50 vol.%) vapour flowrates of (a) 12 ml/min , (b) 24 ml/min , (c) 36 ml/min and (d) 48 ml/min

The addition of H_2O resulted in an increase in H_2 selectivity at all FA/H_2O inlet flowrates and reactor operating temperatures. Overall, the selectivity increased from a range of 0.69 – 0.88 with concentrated FA (99.99 %) to a range of 0.84 – 0.92 with added H_2O (50 vol. %). It can be concluded from these results that Au/Al_2O_3 catalysed the WGS reaction, resulting in an increased selectivity towards H_2 production. Although dehydration products were successfully reduced via the WGS, the amount of CO produced was still above the maximum allowable (100 ppm) for PEMFC applications. Consequently, there is still need for a CO removal step prior to supplying H_2 to a PEMFC. Furthermore, decomposing dilute FA (50 vol.%) results in reduced H_2 production rate at the same reactor operating conditions compared to decomposing concentrated FA. On the other hand, lesser purification will be required if dilute FA is decomposed than if pure FA is decomposed. Overall, the addition of water resulted in improved H_2 yields at all studied conditions and Figure 4.12 shows the results.

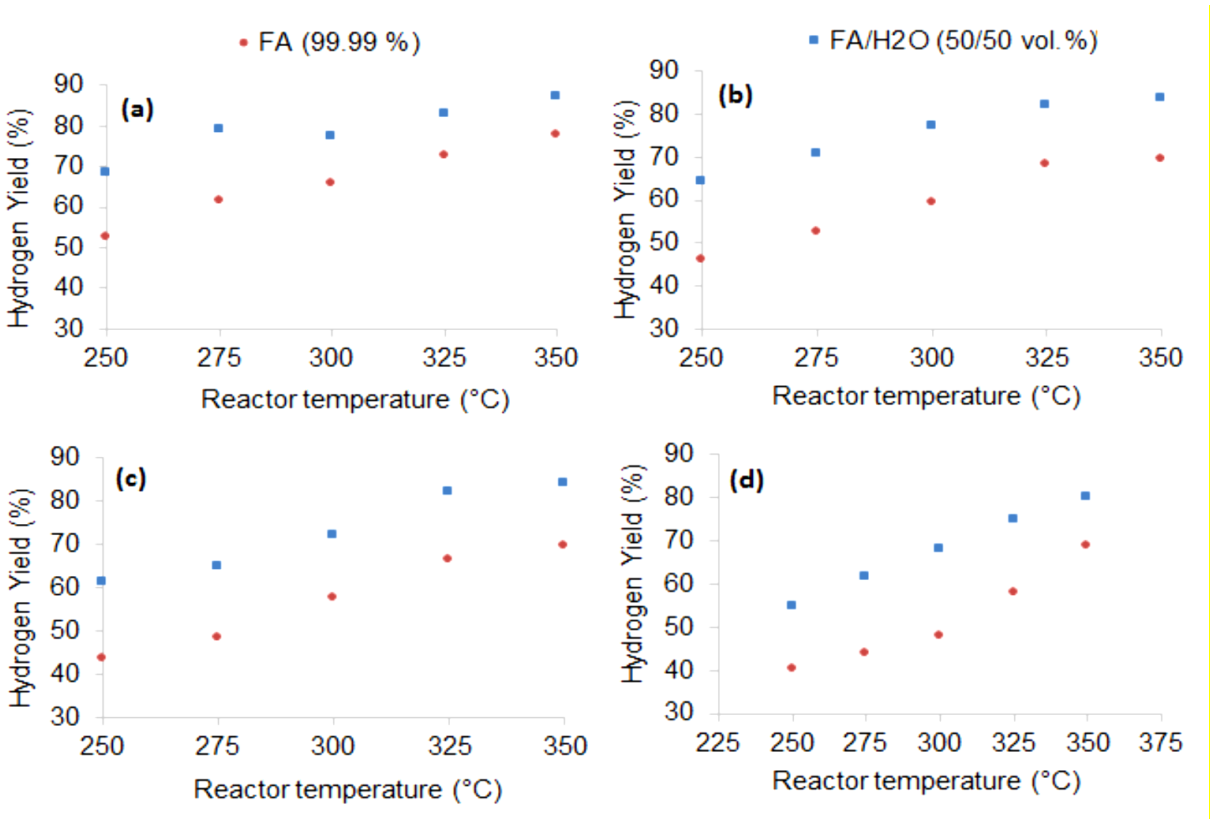

Figure 4. 12: Effect of added H_2O (50 vol. %) on H_2 yields at FA/H_2O (50/50 vol.%) vapour flowrates of (a) 12 ml/min , (b) 24ml/min , (c) 36 ml/min and (d) 48 ml/min

As shown in Figure 4.12, the H_2 yield increased from a range of 40 – 78 % with pure FA to a range of 55 – 87 % with dilute FA. Similar to pure FA decomposition experiments, the highest yield was measured at a reactor temperature of 350 ^oC and feed rate of 48 ml/min. At these conditions, a H_2 production rate of 6.9 $NL.g_{cat}^{-1}.h^{-1}$ was obtained. The addition of water therefore resulted in increased selectivity and H_2 yield; however, H_2 production rates were reduced.

4.3 LONG TERM REACTOR STABILITY TEST

The reactor stability test was performed at the end of all experimental runs. This was performed after the reactor had run for an approximate period of 1 200 h. Twelve experimental runs were successively conducted with concentrated FA (99.99 %) at 325 ^oC and a FA vapour flowrate of 36 ml/min. Data was collected within a 12 hour interval where H_2, CO, CO_2 and HCOOH product concentrations were recorded. In total, the reactor was run continuously for a period of 144 h under the same operating conditions. Figure 4.13 shows the product composition during the entire run.

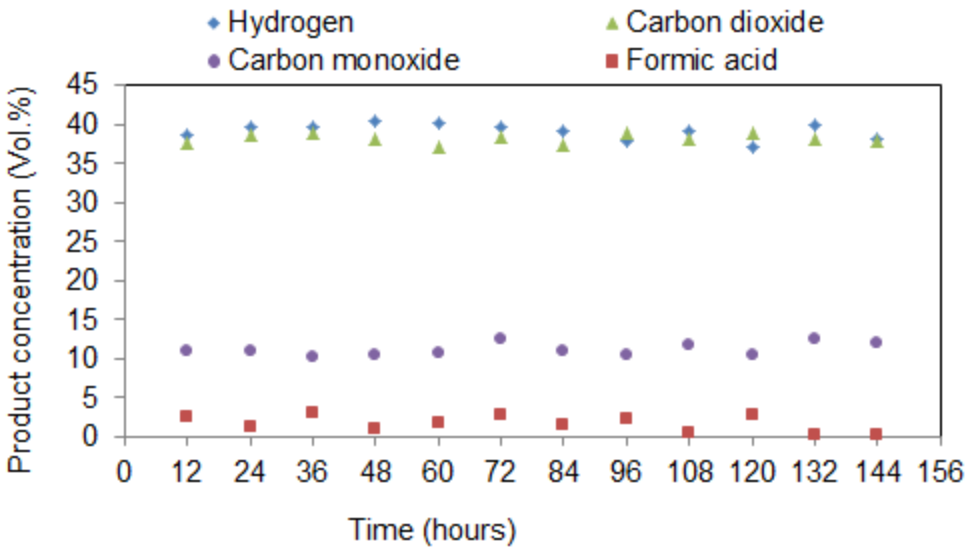

Figure 4. 13: Change in component concentrations with time on stream at a reactor operating temperature of 325 ºC and flowrate of 36 ml/min

As shown in Figure 4.13, CO concentrations remained at approximately 11 % during the entire run while CO_2 and H_2 were approximately 38 %. Overall, the ratio of CO_2 to H_2 remained close to 1 in most cases during the run. The residual FA concentration on the other hand also remained stable at approximately 2 %. The mole fractions were then used to calculate the FA conversion and H_2 selectivity and the results are shown in Figure 4.14

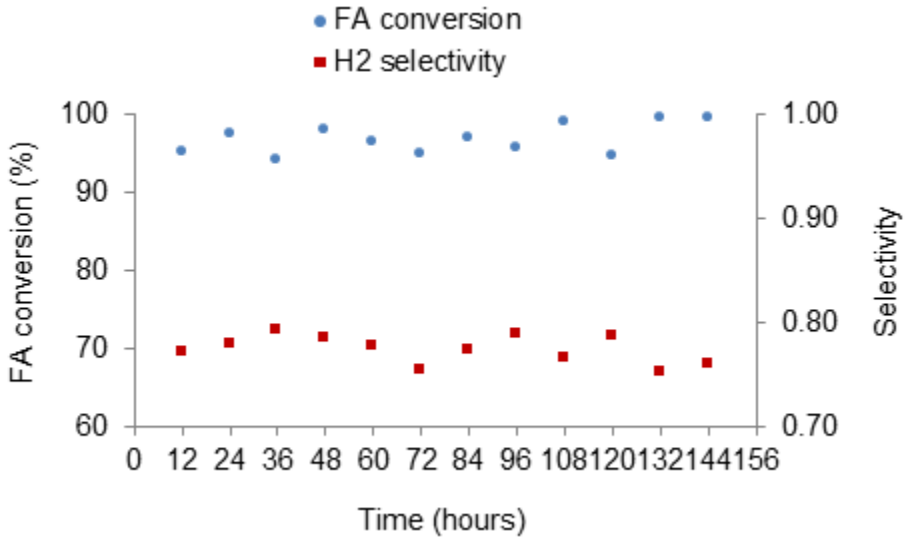

Figure 4. 14: Change in FA conversion and selectivity towards H_2 production with time on stream at a reactor operating temperature of 325 º C and FA flowrate of 36 ml/min

There was generally no significant change in FA conversion and H_2 selectivity at any point during the stability test. The reactor therefore remained stable over a long period of time despite the amount of CO produced during all the runs performed prior to this experiment. The reactor stability was due to the fact that, Au catalysts do not form stable complexes with CO, and therefore the catalyst was not deactivated. These results are consistent with literature as reported for Au and Cu catalysts (Bulushev, *et al*., 2010; Gazsi, *et al*., 2011; Ojeda & Iglesia, 2009). Overall, conversions of approximately 95 % were obtained at the studied reactor operating condition.

4.4 RECOMMENDED OPERATING CONDITIONS FOR FORMIC ACID DECOMPOSITION

In this section, operating conditions that gave the best microchannel reactor performance are summarised based on key performance parameters (Section 3.4.4). The highest hydrogen production rate (0.04 mol/hour) was measured when decomposing pure FA (99.99 %) at a flowrate of 48 ml/min and reactor temperature of 350 ^oC. At these conditions, the FA conversion (98 %) was found to be close to equilibrium conversions of 99.5 % while the residual FA concentration was less than 1 %. At these conditions however, the selectivity towards H_2 production and H_2 yields were minimised due to the concentration of CO produced (15 %) according to the dehydration reaction. Improvement in selectivity was achieved by decomposing a FA/H_2O mixture (50/50 Vol. %) at the same operating conditions of 48 ml/min and 350 ^oC. The CO concentration was generally reduced to 7 % and the corresponding selectivity and H_2 yield increased to 0.81 and 80 % respectively.

Although CO was reduced significantly in the presence of H_2O, a CO removal step would still be required prior to supplying H_2 to a PEMFC as the minimum allowable is 100 ppm (Holladay & Wang, 2015). The cost and energy required to purify 7 % CO is however likely to be lesser than the requirements for purifying 15 % CO as produced when decomposing pure FA. Decomposing dilute FA will therefore be an attractive option when considering minimising CO; however, H_2 production rate is reduced. As the main aim of this study was to produce H_2, concentrated FA (99.99%) was therefore the best feed for maximising FA throughput, FA conversions and H_2 production. It is however recommended that a system analysis be carried out to determine the most important parameter (selectivity or H_2 production rate) suitable for identifying the best performance of the reactor. Table 4.1 summarises the recommended operating conditions of the studied microchannel reactor for both diluted (50/50 Vol. %) and pure FA feed (99.99 %).

Table 4. 1: Recommended operating conditions for the studied microchannel reactor

Parameter	Pure FA (99.99 %) feed	FA/H20 (50/50 Vol.%) feed
Catalyst	1.15 wt. % Au/Al_2O_3 (Mintek)	1.15 wt. % Au/Al_2O_3 (Mintek)
Reaction temperature	350 ^{o} C	350 ^{o} C
Reaction pressure	Atmospheric (0.88 bar)	Atmospheric (0.88 bar)
FA flowrate (vapour)	48 ml/min (17.1 $NL.g_{cat}^{-1}.h^{-1}$)	48 ml/min (8.6 $NL.g_{cat}^{-1}.h^{-1}$)
FA conversion	98 %	>99.99 %
FA residual concentration	< 1 %	<1 %
CO product concentration	15 %	7 %
H_2 Selectivity	0.7	0.81
H_2 Yield	69	80
H_2 production rate	0.04 $mol.h^{-1}$ (11.8 $NL.g_{cat}^{-1}.h^{-1}$)	0.026 $mol.h^{-1}$ (6.9 $NL.g_{cat}^{-1}.h^{-1}$)

In conclusion, the microchannel reactor would be followed up by a CO removal step as shown in Figure 4.15 at both conditions shown in Table 4.1.

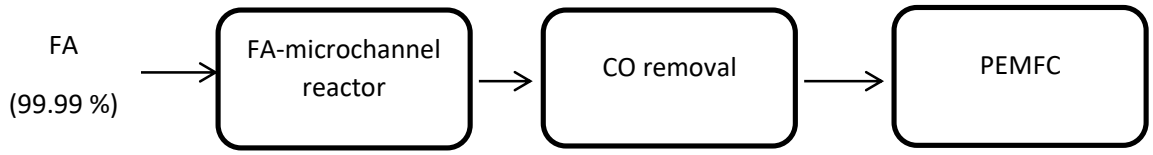

Figure 4. 15: Schematic of the fuel processing system based on the results from this dissertation

Following on the experimental results, the microchannel reactor was further evaluated mathematically in Chapter 5 to give an understanding of the reactor transport profiles.

CHAPTER 5: MODEL RESULTS AND DISCUSSION

In this chapter, a CFD mathematical modelling technique is used to evaluate the microchannel reactor for the production of H_2 from FA on Au/Al_2O_3 catalyst. This chapter was aimed at developing a tool that can be used for future design and optimisation of FA decomposition reactors for H_2 production. The model is developed for the concentrated FA (99.99 %) experiments (Chapter 4) considering both the dehydrogenation and dehydration reaction pathways. The chapter starts off in Section 5.1 where the model development is discussed with emphasis on the geometry, assumptions, governing equations, reaction kinetics and solution procedure. Thereafter, the model results are presented in Section 5.2 starting off with the reaction rate parameters that best fit the experimental results. It is in this section that the model conversions and yields are validated against the experimental results. The chapter closes off in Section 5.3 with a presentation of the transport profiles that exist within the studied microchannel reactor.

5.1 MODEL DEVELOPMENT

The model was simulated using Comsol Multiphysics 4.3.b following a 3D approach as developed by Chiuta, *et al*., (2014). Of importance in this section was identifying the governing equations as well as suitable assumptions and boundary conditions. Reaction kinetics were also important for the purpose of predicting the FA conversions and H_2 formation. This Section therefore presents the relevant parameters considered for the development of the model in this dissertation.

5.1.1 Geometry

A single microchannel (150 µm x 450 µm x 0.05 m) was simulated in this study and this was sufficient considering that all 80 channels making up the reactor were of the same dimensions (Chapter 3). This was also in agreement with literature on microchannel reactor scale up by increasing the number of the designed channels (Atkinson & McDaniel, 2010). Two main computational domains were considered in the channel and these were the free fluid domain and the catalyst layer domain (40µm). The decomposition reaction was considered in the catalyst domain while the bulk movement of reactants was considered in the free-fluid region. In addition, uniform distribution of flow by the manifold was assumed (Chiuta, *et al*., 2014). Finally, only one

quadrant of the single channel was modelled and the symmetry boundary condition (Section 5.1.5) was used to account for the full channel. Figure 5.1 shows a 3D microchannel geometry as simulated using Comsol Multiphysics 4.3b. The geometry was built with 37680 mesh points which were built to emphasise accuracy at the fluid-catalyst boundaries. For instance, the mesh close to the free-fluid-porous media interface and near wall regions was refined to capture the sharp velocity, temperature, and species concentration gradients.

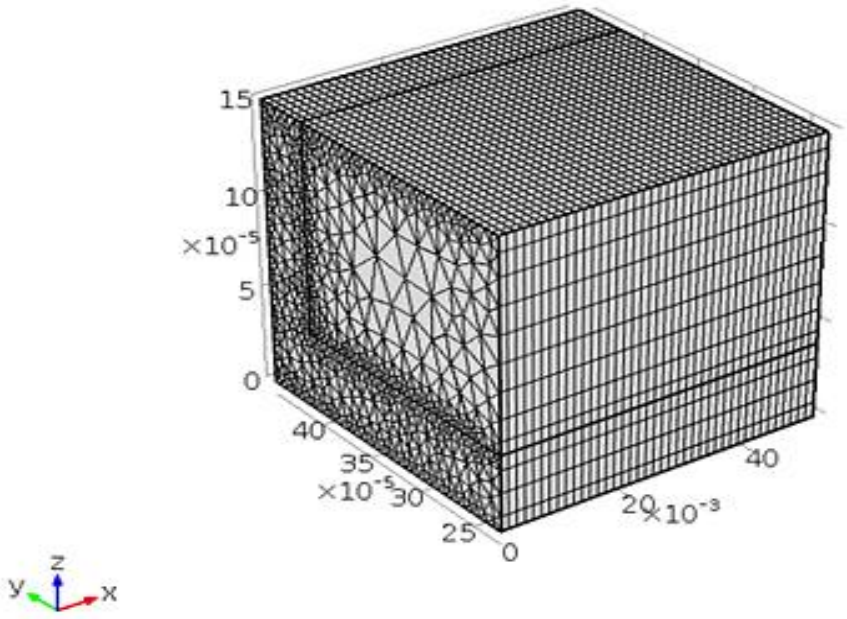

Figure 5. 1: Symmetrical 3D microchannel geometry used in the CFD simulation

5.1.2 Model assumptions

Transport profiles were described using partial differential equations of continuity, momentum, energy, and mass. These were chosen, based on relevant assumptions given and justified in Table 5.1.

Table 5. 1 : Model assumptions

Assumption	Description/explanation
Steady and laminar flow	Reynolds number in most microchannel reactors of this size lies below 500 (Hoebink & Marin 1998).
Weakly compressible flow (Chiuta, *et al*., 2014)	The density was considered to change with temperature and composition of the individual components as the reaction proceeded.
Ideal behaviour	At the reactor operating pressure (atmospheric), the reaction components mostly behave ideally.
Negligible edge effects	Heat transfer between channels was considered negligible.
Negligible homogeneous reactions	The reaction was assumed to occur on the wash coat catalyst layer and reactions in the free fluid region were neglected.
Isotropic wash coat	The physical properties of the catalyst were assumed to be independent of simulation conditions.
Phase thermal equilibrium	The wash coat catalyst and free flow region domains were assumed to be in thermal equilibrium

Based on the above assumptions, the governing equations were chosen as outlined in Section 5.1.3.

5.1.3 Governing equations

Table 5.2 summarises the governing equations used to develop a microchannel reactor model in this dissertation. The model considered transport profiles in three dimensions with heterogeneous reactions occurring in the catalyst wash coat region. In the axial direction, bulk movement of reactants was considered mostly. The axial velocity in this model was described by the momentum balance (Bird, *et al*., 2002). The generic equations of momentum transport were, however, not adequate to describe fluid flow in the catalyst domain, and as such, extension to non-Darcian flow was considered. The Brinkman-Forchheimer-extended Darcy equation (Khaled & Vafai, 2003) was, therefore, used to describe momentum flow in the catalyst region. The mass profiles were described by the Maxwell Stefan equation (Bird, *et al*., 2002) while the temperature profiles were described considering heat transfer by both convection and conduction. In addition,

the chemical reaction source term for these equations was only considered in the porous catalyst region.

Table 5. 2: Governing equations (Chiuta, *et al*., 2014)

Free fluid flow region	Porous catalyst region
Equation of continuity $\nabla.(\rho \boldsymbol{V}) = 0$	Equation of continuity $\nabla.(\varepsilon\rho \boldsymbol{V}) = 0$
Navier-Stokes Equation $\boldsymbol{V}.\nabla(\rho \boldsymbol{V}) = -\nabla.\boldsymbol{P} + \nabla.(\mu \nabla \boldsymbol{V})$	Brinkman-Forchheimer-extended Darcy equation $\boldsymbol{V}.\nabla(\varepsilon\rho \boldsymbol{V}) = -\nabla.\boldsymbol{P} + \nabla.\left(\frac{\mu_B}{\varepsilon}\nabla \boldsymbol{V}\right) - \frac{\mu}{k}\boldsymbol{V} - \frac{\rho\varepsilon Cf}{k}\lvert\boldsymbol{V}\rvert$
Energy balance $\nabla.(\rho Cp \boldsymbol{V}T) = \nabla.(k\nabla T)$	Energy balance $\nabla.(\varepsilon\rho Cp \boldsymbol{V}T) = \nabla.\left(k_{eff}\nabla T\right) + (1-\varepsilon)\Delta H_r \rho_s R$
Maxwell-Stefan equation $\nabla.(\rho w_i \boldsymbol{V}) = \nabla.\left(D_{ij}\nabla w_i\right)$	Maxwell-Stefan equation $\nabla.(\varepsilon\boldsymbol{\rho} w_i \boldsymbol{V}) = \nabla.\left(\varepsilon\rho D_{ij,eff}\nabla w_i\right) + (1-\varepsilon)\sum_{i=1}^{3} a_i M_i \rho_s R$

5.1.4 Mixture physical properties

For the purpose of using the above equations of change in describing reacting flow, physical properties were defined, considering all components involved in the system. The mixture physical properties were described according to Chapman-Enskog theory of molecule kinetics and mixed gas formula (Bird, *et al*., 2002). The individual physical properties (viscosity, thermal conductivity, and heat capacity) on the other hand were obtained from the Korean Thermo-physical Properties Data Bank (CHERIC, n.d.) and Perry chemical engineering handbook (Robert, 1997). Equation 5.1 shows the mixture heat capacity formula, the thermal conductivity and viscosity were also calculated in a similar manner.

- **Heat capacity of a mixture**

$$Cp = \sum_i w_i \frac{Cp_i}{M_i} \quad \text{.....5.1}$$

- **Effective thermal conductivity**

The effective thermal conductivity used in the catalyst region was calculated according to equation 5.2 (Chiuta, *et al*., 2014). This form was used for all other effective properties appearing in the porous media equations.

$$k_{eff} = \varepsilon k + (1-\varepsilon)k_s \quad \text{.....5.2}$$

- **Binary diffusivity at low pressures**

The binary diffusion coefficients were estimated based on the Fuller-Schettler-Giddings (FSG) equation 5.3 (Fuller, *et al*., 1966).

$$D_{ij} = \frac{10^{-3}T^{1.75}\left[\frac{M_i+M_j}{M_iM_j}\right]^{\frac{1}{2}}}{P\left[(\sum v_i)^{\frac{1}{3}}+(\sum v_j)^{\frac{1}{3}}\right]^2} \quad \text{.....5.3}$$

The equivalent effective diffusivity used on the porous media region was calculated according to equation 5.4 (Chiuta, *et al*., 2014).

$$D_{ij,eff} = D_{ij}\varepsilon^{1.5} \quad \text{..... 5.4}$$

- **Density of an ideal gas mixture**

The fluid density was computed assuming ideal gas behaviour of components, and equation 5.5 shows the multicomponent density.

$$\rho = \frac{P_0}{R_gT}\sum_i x_iM_i \quad \text{.....5.5}$$

With the specified governing equations and physical properties, the model was simulated considering the boundary conditions outlined in Section 5.1.5.

5.1.5 Initial and boundary conditions

The free fluid region was considered as the cross sectional area of the channel. At the channel inlet, pure FA was assumed to have an inlet velocity equal to the average across the channel cross section area. At the channel exit; the pressure was specified as the reactor operating pressure. In addition to these specifications, the normal gradients to the flow direction (axial) were set to zero for velocity, species mass fraction and temperature. At the wall-fluid interface, it was assumed that there was no phase-change, no chemical reactions and thus local thermodynamic equilibrium prevailed (Costa *et al*., 2004). The continuity at the wall-fluid interface was taken into account by the Brinkman-Forchheimer-extended-Darcy model. Furthermore, the reactor wall was held at a constant temperature assuming no heat losses to the surroundings. Table 5.3 shows the summarised boundary and inlet conditions as applied in this model.

Table 5. 3: Initial and boundary conditions (Chiuta, *et al*., 2014)

Dirichlet boundary conditions	
Inlet conditions	$v_x = v_{inlet}$, $w_i = w_{i\,inlet}$, $T = T_{inlet} = T_{wall}$
Initial conditions	$v_{initial} = v_{inlet}$, $T_{initial} = T_{inlet}$, $w_{i\,initial} = w_{i\,inlet}$
Neumann Boundary conditions	
Outlet conditions	$\frac{\partial v}{\partial x}_{outlet} = \frac{\partial T}{\partial x}_{outlet} = \frac{\partial w_i}{\partial x}_{outlet} = 0$
Symmetry planes	$\frac{\partial v}{\partial n}_{symmetry} = \frac{\partial T}{\partial n}_{symmetry} = \frac{\partial w_i}{\partial n}_{symmetry} = 0$
Interface	$V = \langle V \rangle \quad P = \langle P \rangle \quad T = \langle T \rangle \quad w_i = \langle w_i \rangle$

5.1.6 Reaction kinetics

Due to the amount of CO measured (2 to 15 %) in the experimental evaluation (Chapter 4), this model considered the occurrence of both dehydrogenation (Equation 2.3) and dehydration (Equation 2.4) reactions. There are, however, currently only a few studies reporting on the reaction rate expressions for both the dehydrogenation and dehydration of FA. Specifically on Au/Al_2O_3 catalyst, the single microkinetic study by Ojeda & Iglesia, (2009) was performed at lower reaction temperatures (383 K) compared to the temperatures studied in this dissertation. Consequently, zero order kinetics were reported with dehydrogenation occurring exclusively, which is contrary to the results of this study.

The few studies reporting on both dehydration and dehydrogenation kinetics of FA at temperatures relevant to this study were, however, performed on different catalysts (Sun, *et al*., 1988; Patermarakis, 2003). Sun, et al., (1988) reported first order kinetics for both reactions on a Ru (001) catalyst at temperatures between 500 K and 800 K. At these same temperatures however, studies on Al_2O_3 and MgO doped Al_2O_3 catalysts reported zero order kinetics for both reactions with activation energies ranging between 87.4 and 129.1 kJ/mol (Patermarakis, 2003). Overall, kinetics of FA decomposition still remains scarce and a summary of the available kinetics was given in Chapter 2. Considering the high operating temperatures (<500 K) in this dissertation, general first order kinetics (Mars, *et al*., 1963) were assumed for dehydrogenation and dehydration.

$$r_1 = k0_{,1}\, exp\left(\frac{-E_2}{R_g T}\right) P_{HCOOH} \quad \text{.....5.6 (Dehydrogenation)}$$

$$r_2 = k0,_2 = exp\left(\frac{-E_2}{R_g T}\right) P_{HCOOH} \quad \text{.....5.7} \quad \text{(Dehydration)}$$

The possible occurrence of the WGS reaction was not considered in this model as it requires a detailed study beyond the scope of this dissertation. This chapter will therefore not attempt to model the decomposition of dilute FA where the WGS (Equation 2.5) reaction was relevant.

5.1.7 Solution procedure

The equations of change were simultaneously solved for the studied reactor operating temperatures (250 – 350 ^{o}C) and vapour flowrates of 12 – 48 ml/min equivalent to inlet velocities of 0.06 – 0.244 m.s^{-1} respectively. The parallel sparse direct linear solver (PARDISO) was used to solve for the different equations with a relative tolerance of 10^{-3}. With the geometry and model setup, kinetic parameters that best fit the experimental results were estimated for both reactions according to a model-based parameter optimisation and refinement on Comsol Multiphysics 4.3 b. Kinetic parameters reported by Patermarakis (2003) on MgO doped Al_2O_3 (Section 2.2.2, Table 2.3.) were used as the initial values for the simulation of dehydrogenation and dehydration. These parameters were then refined to best fit the experimental results presented in Chapter 4. Finally, the developed mathematical model was validated against the experimental results after which transport profiles were plotted.

5.2 RESULTS AND DISCUSSION

This section presents the results of the developed model. In Section 5.2.1; the estimated kinetic parameters that best fit the experimental results are presented and compared to the values reported in literature. The developed model is then validated against the experimental results in Section 5.2.2 after which transport profiles are presented in Section 5.2.3.

5.2.1 Kinetic parameters

Table 5.4 shows the kinetic parameters that were found to best fit the experimental results according to an optimization study based on the Nelder-Mead method. These parameters gave a least squares objective function of 10^{-5} between the experimental and model FA conversions. The table also present the values reported in literature at similar operating conditions, as well as those measured on similar catalysts.

Table 5. 4: Kinetic parameters for FA decomposition

Reaction order	Catalyst	Reaction	ko	Ea (kJ/mol)
First order kinetics (This study)	1.15 wt.% Au/Al_2O_3	Dehydrogenation	2.6×10^5 ($mol.m^{-3}.s^{-1}.pa^{-1}$)	83.5
		Dehydration	5.0×10^5 ($mol.m^{-3}.s^{-1}.pa^{-1}$)	92.4
First order kinetics (Sun, *et al.*, 1988)	Ru (001)	Dehydrogenation	-	-5.4
		Dehydration	-	-0.8
zero order kinetics (Patermarakis, 2003)	MgO doped Al_2O_3	Dehydrogenation	2.98×10^3 ($mol\ g^{-1}\ s^{-1}$)	87.9
		Dehydration	1.33×10^6 ($mol\ g^{-1}\ s^{-1}$)	125.1
zero order kinetics (Ojeda & Iglesia, 2009)	0.61 wt.% Au/Al_2O_3	Dehydrogenation	-	53
		Dehydration	-	-

The best fitting activation energies were found to be lower than the reference values of 87.4 and 125.1 kJ/mol for dehydrogenation and dehydration reactions respectively. These differences might be attributed to the differences in the catalysts used in these studies. Furthermore, Patermarakis, (2003) reported zero order kinetics as opposed to first order kinetics reported in this study. The dehydrogenation activation energy predicted in this study was also found to be higher than the value (52 kJ/mol) reported by Ojeda & Iglesia, (2009) on a 0.61 wt.% Au/Al_2O_3 catalyst. Ojeda & Iglesia, (2009) however decomposed FA at lower temperatures compared to this study and as such, zero order kinetics were also reported. Generally, the results of this study were not comparable to the literature values due to the differences in catalysts used, as well as reactor operating conditions.

The activation energy for dehydrogenation was, however, predicted to be generally lower than that for dehydration. This was mainly because dehydrogenation was found to be dominant in this study. Figure 5.2 shows the rates of reactions along the microchannel length.

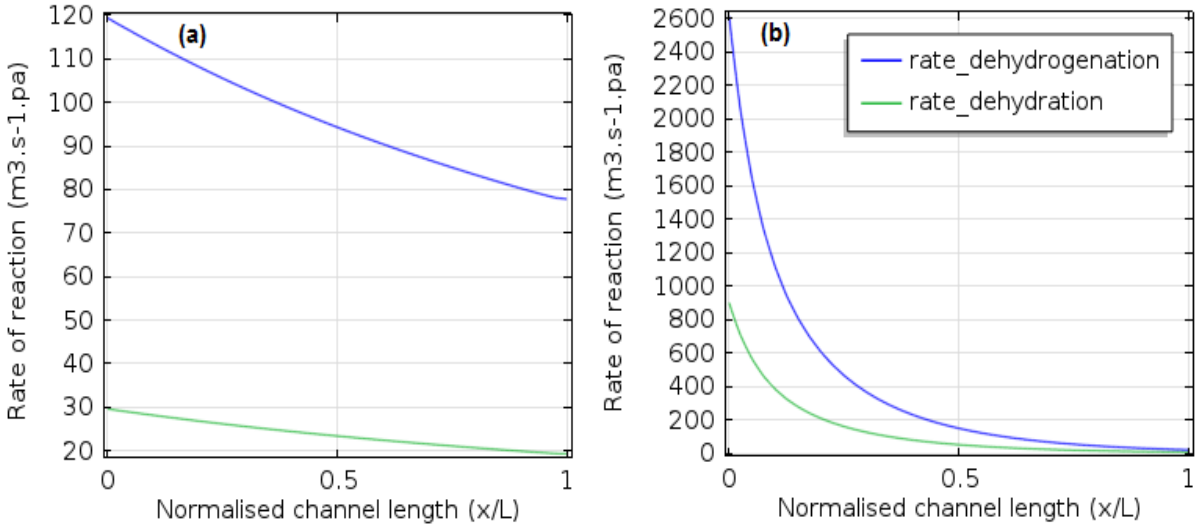

Figure 5. 2: Plot of the rate of dehydrogenation and dehydration along the normalised channel length at an inlet velocity of 0.244 m.s^{-1} (48 ml/min) and reactor temperatures of (a) 250 ^{o}C and (b) 350 ^{o}C.

As shown in Figure 5.2, both dehydrogenation and dehydration reactions were found to decrease along the channel length indicating that the reaction was more intense close to the channel inlet. At 350 ^{o}C however, the rates of reactions reached a constant value earlier in the channel in comparison to that at 250 ^{o}C. This indicated that the reactions reached completion earlier in the reactor at high temperatures resulting in conversions approaching equilibrium. Section 5.2.2 presents the validation of the kinetic model as developed using the above mentioned parameters.

5.2.2 Comparison of model and experimental results

Figure 5.3 shows a plot of the model and experimental FA (99.99 %) conversions at all investigated flowrates (12 – 48 ml/min) and temperatures (250 – 350 ^{o}C).

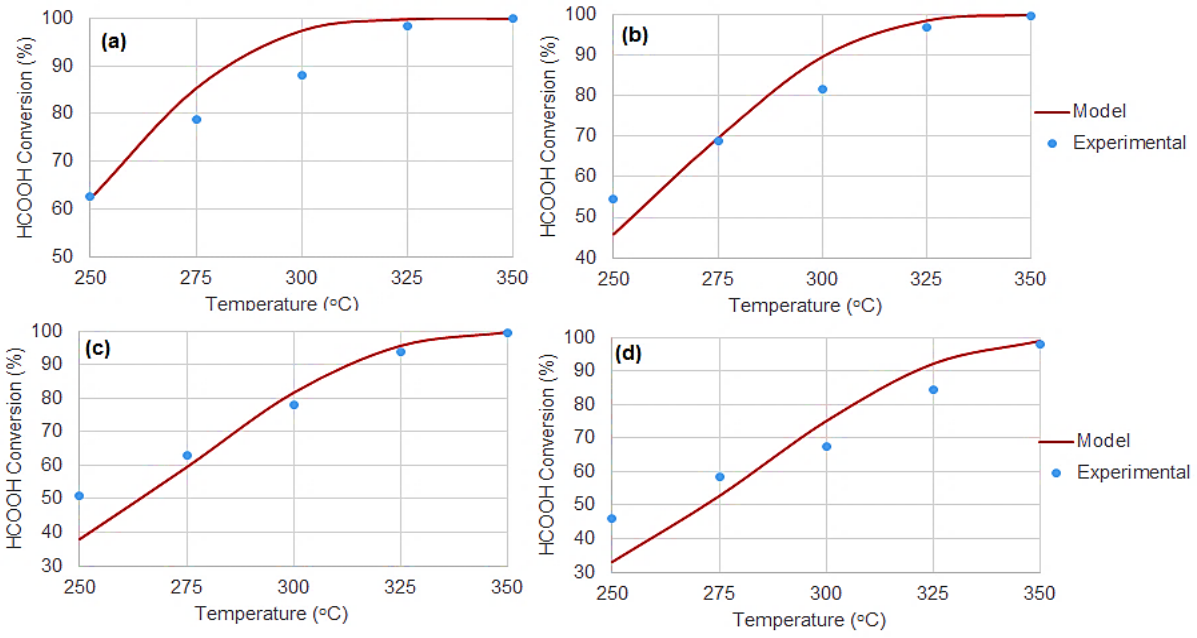

Figure 5. 3: Plot of the model and experimental FA (99.99 %) conversions at reactor temperatures of 250 – 350 °C and FA (99.99 %) vapour flowrates of (a) 12ml/min, (b) 24 ml/min, (c) 36 ml/min, and (d) 48 ml/min.

As shown in Figure 5.3, the model results show a deviation from the experimental results at a reactor temperature of 250 °C. At this temperature, the model generally predicted much lower conversions than those predicted in the experimental work. This deviation might be due to the possibility of zero order kinetics governing the decomposition of FA at lower temperatures. According to Mars, *et al*., (1963), the decomposition of FA can follow either zero order or first order at low and high temperatures, respectively. The gradual change from zero order to first order was also reported by Sun, et al., 1988 on Ru (001) catalyst. In their study, two distinct regimes were reported with zero order kinetics occurring at low temperatures (<500 K) and first order kinetics occurring at temperatures above 500 K. In this study, however, only two low temperature points were studied and these were not adequate for the development of a zero order model. In general, as temperature decreases, reaction mechanisms become more complicated due to side reactions that might obscure the major reactions (Patermarakis, 2003). Due to this reason, contradictory reaction mechanisms have been reported at lower temperatures.

The model was also found to deviate from most of the experimental points at the lowest FA flowrate of 12 ml/min. This behaviour might indicate that the reaction was mostly equilibrium limited rather than reaction controlled as shown by the high conversions achieved at this flowrate. Overall however, the model FA conversions showed an acceptable fit to the experimental results

at temperatures higher than 250 °C and this is shown by parity plots in Figure 5.4. An R^2 value of 0.95 and 0.96 was obtained for FA conversions and FA residual concentrations across all studied conditions, respectively.

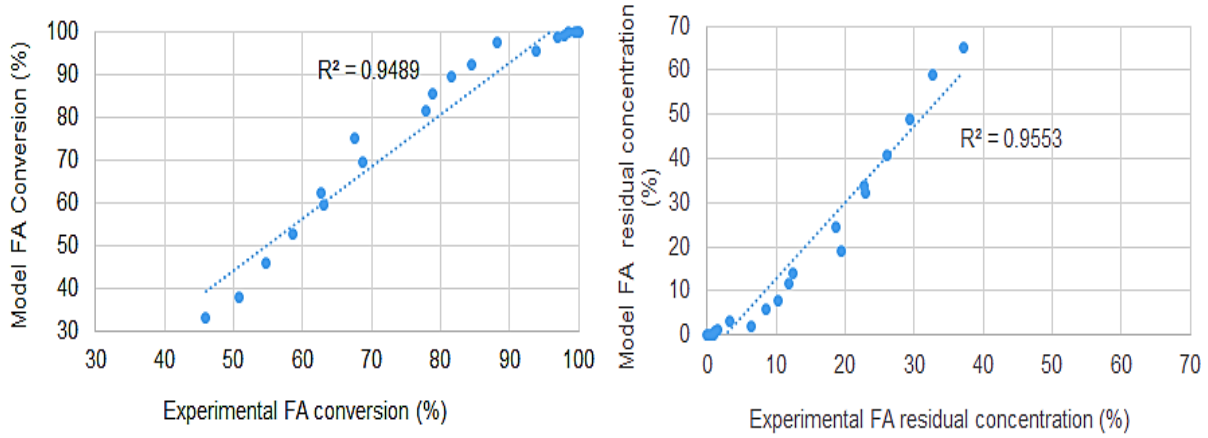

Figure 5. 4: Parity plot of (a) model and experimental FA conversions and (b) model and experimental FA residual concentration at temperatures of 250 – 350°C and flowrates of 12 – 48 ml/min

As shown in Figure 5.4, the experimental and model results show a linear relationship. The R^2 values indicate that the kinetic parameters estimated in this model describes FA conversions and residual concentration especially at temperatures higher than 250 °C. To further validate the model, the experimental and model H_2 yields (equation 3.5) were also plotted as shown in Figure 5.5.

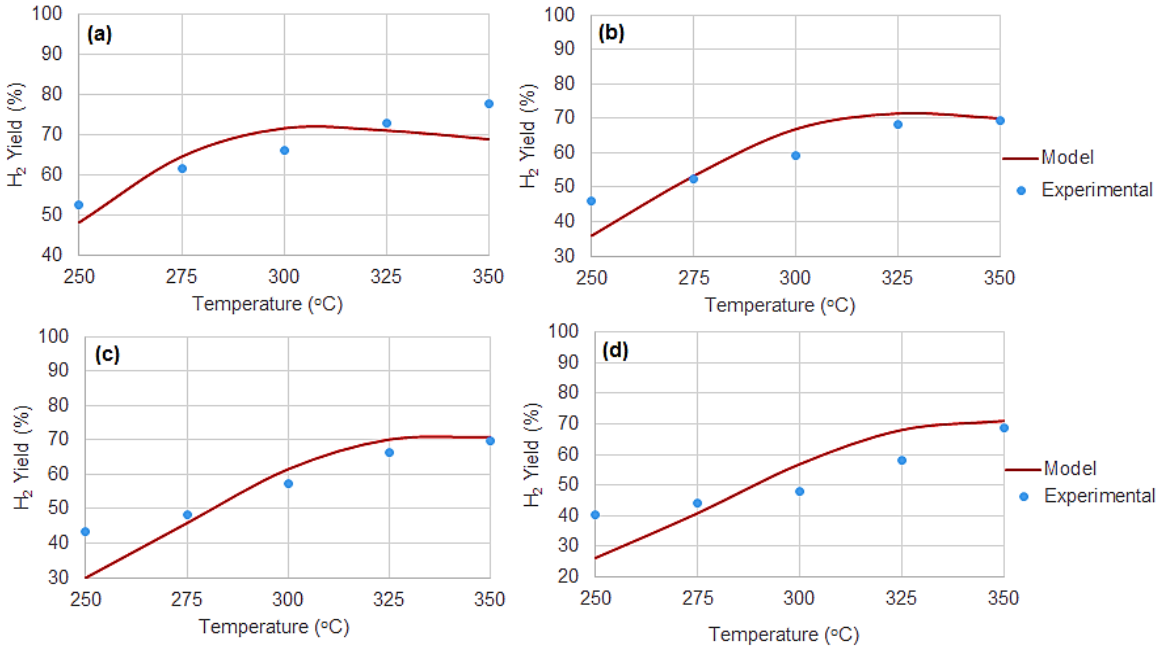

Figure 5. 5: Plot of model and experimental H_2 yield at the studied temperatures (250 – 350 °C) and FA vapour flowrates of (a) 12 ml/min, (b) 24 ml/min, (c) 36 ml/min, and (d) 48 ml/min.

The H_2 yield was found to also deviate at the lowest temperature as this parameter was dependent on FA conversions. Overall, the model H_2 yields were found to fit the experimental yields with an R^2 value of 0.82 (Figure 5.6). This value was found to be lower than that obtained for the conversion and residual FA parity plots. This was mainly because the H_2 yield also depended on the selectivity towards H_2 production. As shown in Chapter 4 (Figure 4.4) however, the change in the selectivity with reactor temperature was not completely linear. Furthermore, although the conversions were only dependent on the dehydrogenation and dehydration reactions, the possible occurrence of the WGS reaction could have had an influence on the selectivity especially at high temperatures. For better fit of the model to experimental yields, it is recommended for future studies that the possible occurrence of the WGS reaction be included in the model.

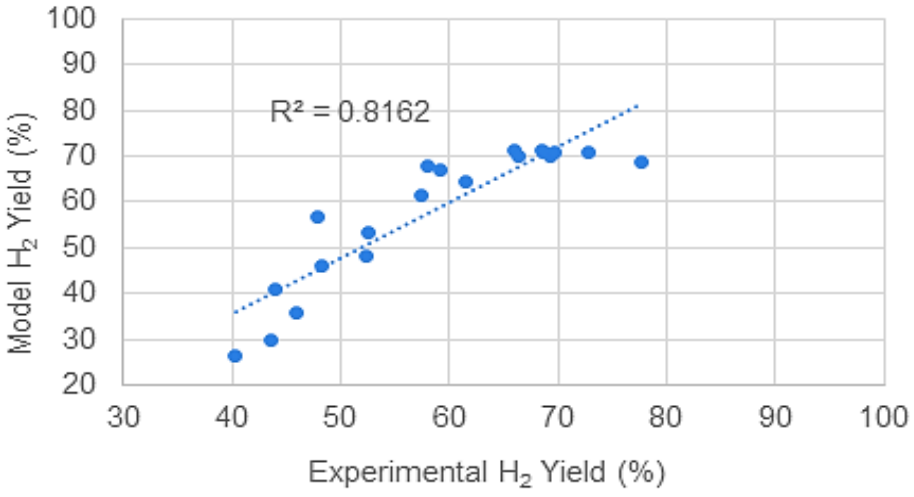

Figure 5. 6: Parity plot of model against experimental H_2 yield across all studied temperatures (250 – 350 ^oC) and flowrates (12 – 48 ml/min)

It can be concluded from the model validation results that the developed model represents the experimental results obtained in this study with deviations at the lowest temperature (250 ^oC). The developed kinetic model can, therefore, describe transport profiles in a microchannel reactor at the studied operating conditions. The respective transport profiles occurring in a microchannel reactor are presented in Section 5.2.3.

5.2.3 Velocity, temperature and concentration profiles

In this section, the velocity, temperature and concentration profiles that exist in a microchannel reactor were presented for the base case conditions shown in Table 5.5. The base conditions present the points of low and high conversions for concentrated FA (99.99 %) experiments at the highest inlet flowrate of 48 ml/min.

Table 5. 5: Base-case simulation conditions.

Geometry	
Microchannel length (m)	0.05 m
Microchannel width (µm)	450
Microchannel height (µm)	150
Catalyst thickness (µm)	40
Washcoat material	
Permeability (m^2)	1 x 10^{-12}
porosity	0.4
Bulk density (kg/m^3)	800
Inlet conditions	
Feed composition	Concentrated FA (99.99 %)
Vapour flowrate (ml/min)	48 (0.244 $m.s^{-1}$,LHSV of 26 $Nml.gcat^{-1}.h^{-1}$)
Temperature (^oC)	250 and 350

5.2.3.1 Velocity profile

Figure 5.7 shows the axial velocity (v_x) profiles along the microchannel reactor in the x-z planes. As shown in Figure 5.7, the axial velocity was found to increase along the channel length at both temperatures. This increase in velocity was due to the expansion of gases as the reaction proceeded according to a 1:2 reaction stoichiometry for both dehydration and dehydrogenation. The velocity profile at 350 ^oC however fully developed earlier in the channel compared to the profile at 250 ^oC. This indicated that the reaction was intense much closer to the channel inlet at higher temperatures than it was at low temperatures.

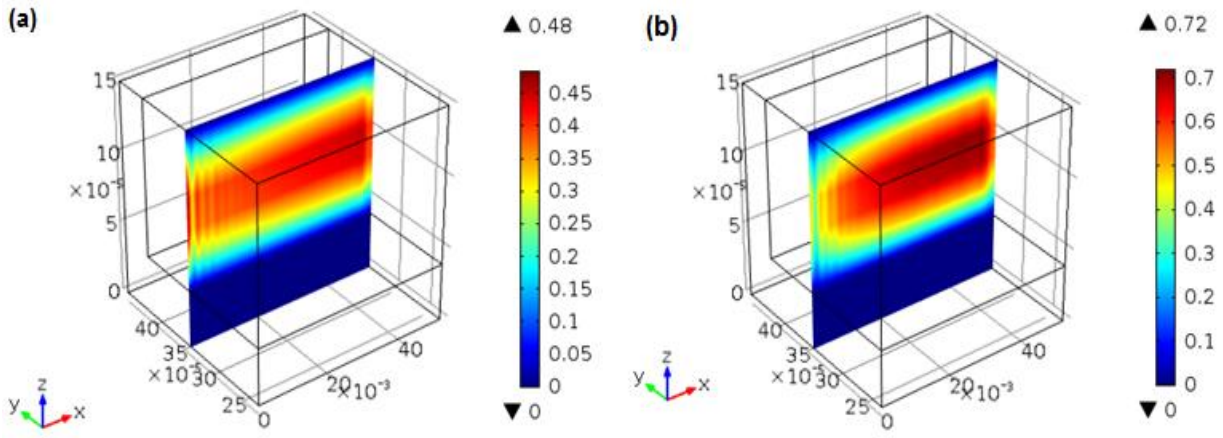

Figure 5. 7 : Axial velocity profile (x-z plane) along the microchannel reactor at an inlet velocity of 0.244 m/s (48 ml/min) and reactor temperatures of (a) 250 ^oC and (b) 350 ^oC.

Overall, the velocity gradients in the microchannel reactor were mainly due to the axial velocity while transverse velocity gradients were found to be negligible (Figure 5.8).

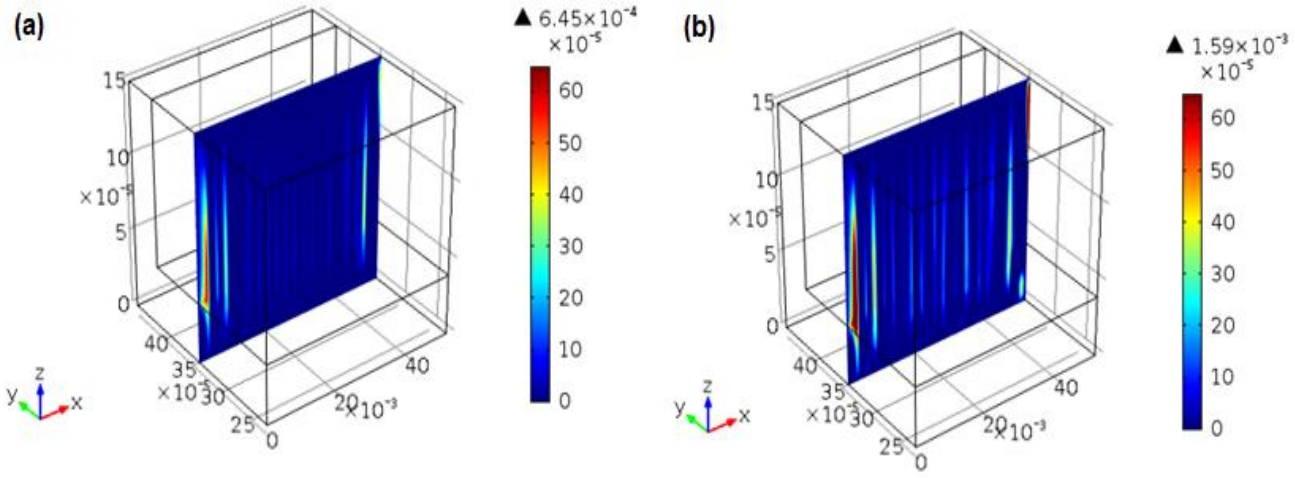

Figure 5. 8: Transverse velocity profiles (x-z plane) along the microchannel reactor at an inlet velocity of 0.244 m/s (48 ml/min) and reactor temperatures of (a) 250 ºC and (b) 350 ºC.

In addition, the velocities were also found to be the lowest in the catalyst region. At the fluid-catalyst interface, the shear rates at these velocities were mostly higher. This trend was evidence of a large change in velocity due to viscous momentum transfer into the catalyst domain (Chiuta, *et al*., 2014). Figure 5.9 shows the shear rate profiles along the channel in the y-z plane.

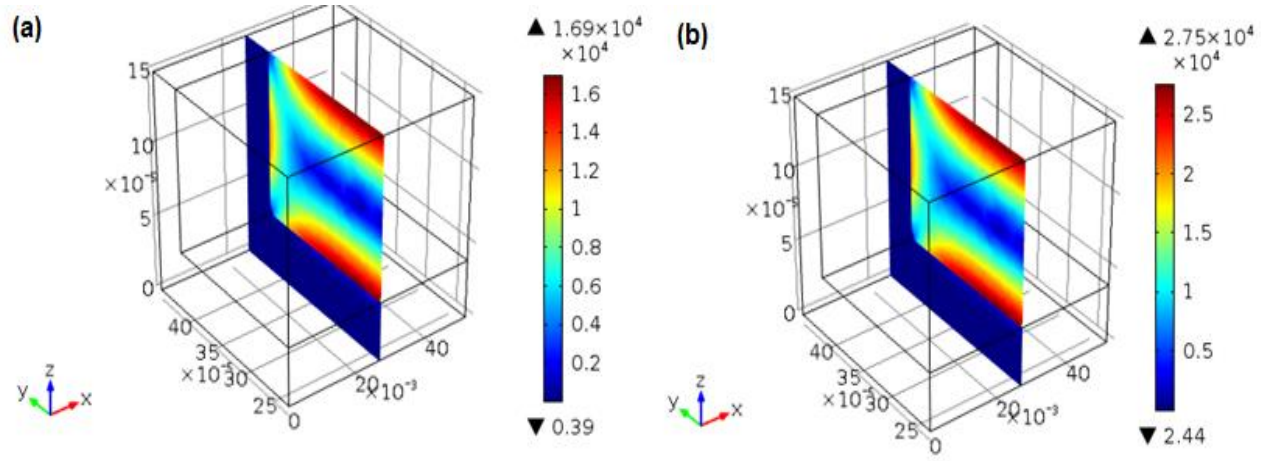

Figure 5. 9: Shear rate profile (y-z plane) at an inlet velocity of 0.244 ms^{-1} (48 ml/min) and reactor operating temperature of (a) 250ºC and (b) 350 ºC .

5.2.3.2 Temperature profile

Figure 5.10 shows the temperature profiles along the microchannel reactor in the x-z plane at an inlet velocity of 0.244 m s^{-1} (48 ml/min) and temperatures of 250 ^{o}C and 350 ^{o}C

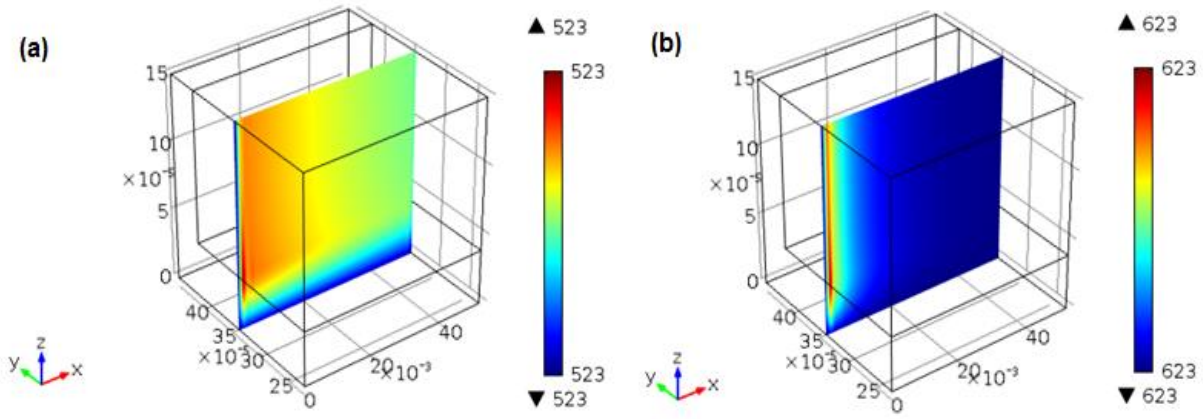

Figure 5. 10 : Temperature profiles (x-z plane) along the microchannel reactor at an inlet velocity of 0.244 m s^{-1} and a reactor temperature of (a) 250 ^{o}C and (b) 350 ^{o}C.

The temperature profiles were found to develop quickly at the channel inlet especially at 350 ^{o}C. At both temperatures, the temperature gradient was generally found to be negligible. This was mainly because both the dehydrogenation and dehydration of FA are only slightly exothermic (-30.88 kJ mol^{-1}) and endothermic (+10.25 kJ mol^{-1}) respectively. In this regard, the temperature gradients show that the endothermic and exothermic effects did not result in any significant change in temperature. It can therefore be concluded from these profiles that the reactor operated under isothermal conditions attributed to the good heat transfer effects of most microchannel reactors.

5.2.3.3 Concentration profile

The component concentration profile along the length of the channel is shown in Figure 5.11 for reactor temperatures of 250 ^{o}C and 350 ^{o}C at an inlet velocity of 0.244 m.s^{-1} (48 ml/min).

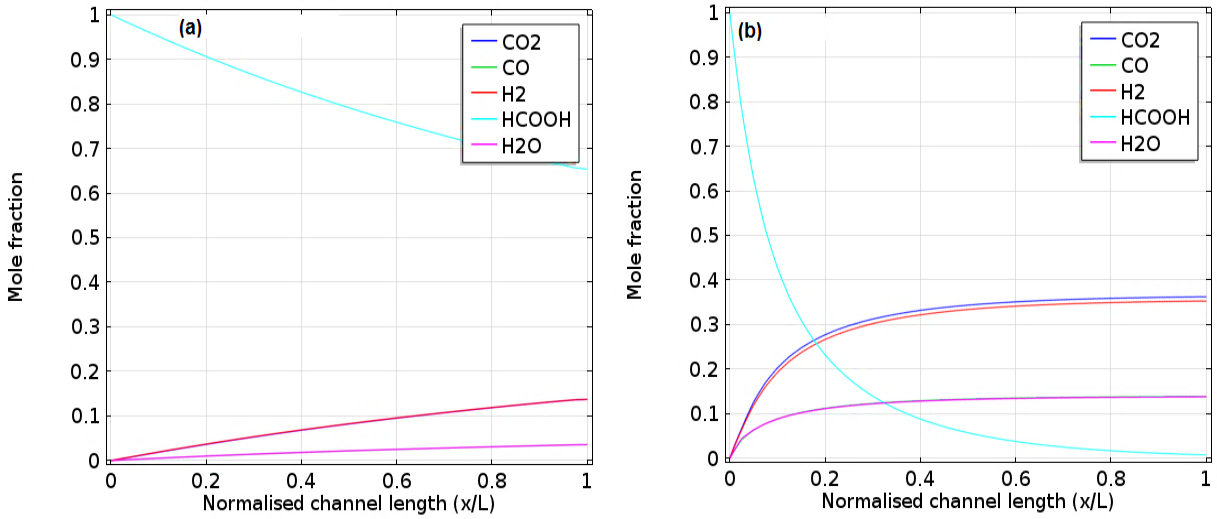

Figure 5. 11: Change in component mole fraction along the reactor channel length for the decomposition at (a) 250 ºC and (b) 350 ºC.

The FA mole fractions decreased along the channel length while CO_2, H_2, CO and H_2O increased simultaneously. The decrease in FA mole fractions shows that conversions increased with an increase in channel length. The FA mole fraction at 350 ºC, however, reached a constant value indicating a point in the reactor where the reaction reached completion. This profile also indicates that the entire reactor channel length was fully utilised in decomposing FA as indicated by the lowest FA product mole fraction achieved close to the channel outlet.

In addition to axial concentration profiles, an analysis of the transverse concentration profiles showed that the reaction mostly occurred in the porous catalyst region (Figure 5.12). As shown in Figure 5.12, large concentration gradients mostly existed in the catalyst region close to the reactor inlet (x=100) while half-way through the reactor length (x=2500)., concentration gradients were smaller. This also indicated that the reaction was more intense at the reactor inlet that it was at the reactor outlet. On the other hand, concentration gradients in the free-fluid and close to the catalyst-fluid interface regions were found to be almost negligible. Overall, the small concentration gradients towards the catalyst –fluid interface shows that the entire 40 µm catalyst layer was used and a thicker catalyst layer will not be required.

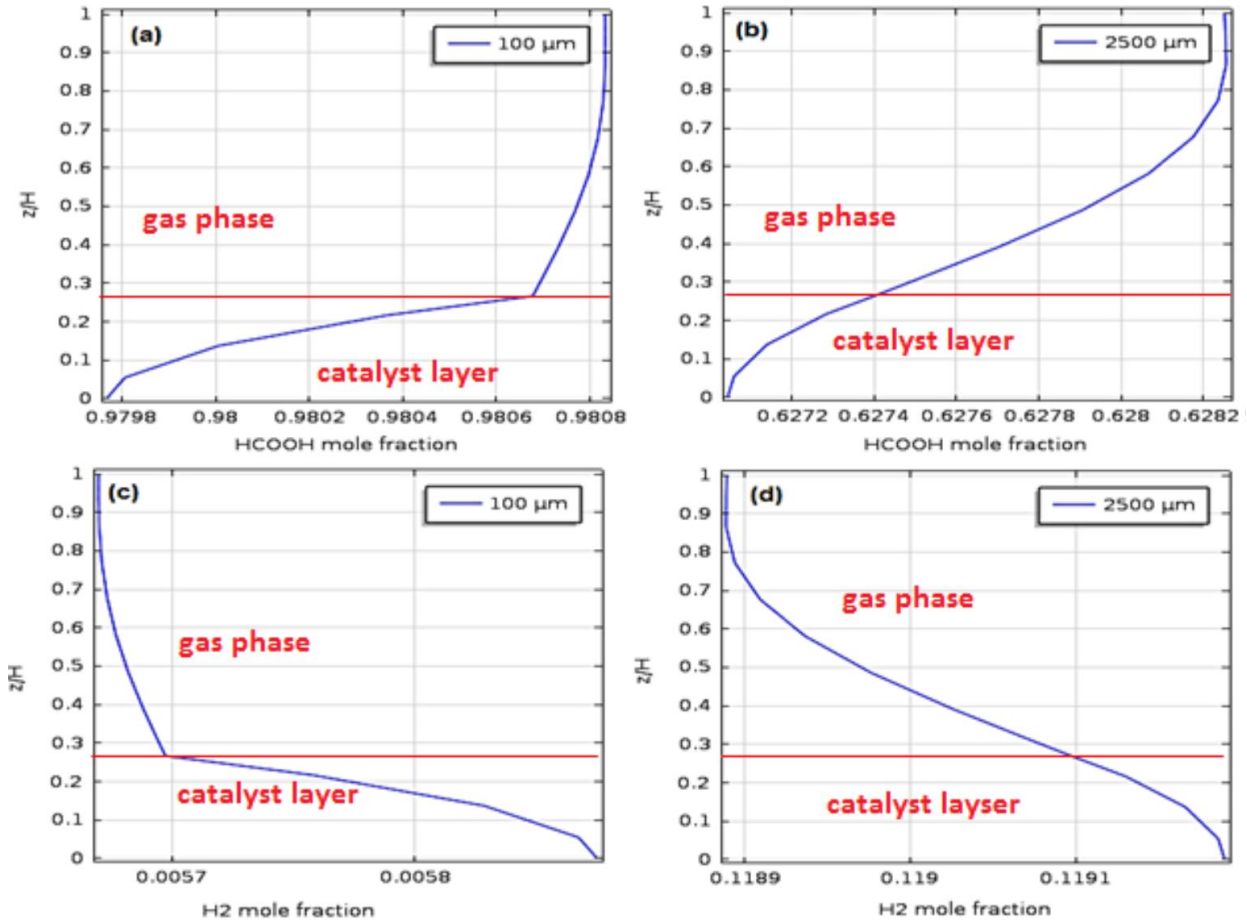

Figure 5. 12 : Transverse HCOOH and H_2 mole concentration profiles at an inlet velocity of 0.244 m.s^{-1}, reactor temperature of 350 ^{o}C and axial locations of (a and c) x= 100 µm and (b and d) x= 2500 µm from the channel inlet.

CHAPTER 6: CONCLUSIONS AND RECOMMENDATIONS.

This chapter presents a summary of the key findings from the experimental and model results of this study. The chapter also presents recommendations for future improvements in advancing the field of FA decomposition for H_2 production. The chapter concludes with a summary of the relevance of the dissertation findings.

6.1 CONCLUSIONS

- A microchannel reactor was successfully characterised and demonstrated for the decomposition of vaporised pure FA (99.99%) and dilute FA (50 vol. %) for the production of H_2 using a 1.15 wt. % Au/Al_2O_3 catalyst at different temperatures of 250 ^oC – 350 ^oC) and flowrates of 12 – 48 ml/min (GHSV of 4.2 – 17.1 $Nml.g_{cat}^{-1}.h^{-1}$).
- It was noted in the first set of the experiments (pure FA) that the microchannel reactor performed well at a reactor temperature of 350 ^oC achieving FA conversions (98 – 99%) close to equilibrium conversions at all vapour FA flowrates of 12 – 48 ml/min (GHSV of 4.2 – 17.1 $Nml.g_{cat}^{-1}.h^{-1}$. At the highest FA throughput (48 ml/min) and highest temperature (350 ^oC), the highest H_2 production rate of 11.8 $NL.g_{cat}^{-1}.h^{-1}$ was achieved.
- Both dehydrogenation and dehydration reactions were, however, observed to occur with CO product concentrations (4 to 15%), increasing with reactor operating temperature. The corresponding H_2 selectivity ranged between 0.69 and 0.88 at the studied reactor temperatures (250 – 350^oC), showing that dehydrogenation was dominant.
- In the second set of the experiments (dilute FA) ,the addition of H_2O (50 vol. %) to FA promoted the occurrence of the WGS reaction resulting in reduced CO concentrations (2 – 7 %) in comparison to those obtained in the decomposition of pure FA (99.99 %). This corresponded to an increase in selectivity towards H_2 production and H_2 yields by approximately 20 % especially at high temperatures (300 to 350 ^oC).
- Overall, for both pure FA (99.99 %) and dilute FA (50 vol.%), the best microchannel reactor performance was achieved at a reactor operating temperature of 350 ^oC and FA vapour flowrate of 48 ml/min (17.1 $Nml.g_{cat}^{-1}.h^{-1}$). At these conditions, H_2 production was maximised with pure FA (99.99 %) while selectivity and H_2 yields were maximised with dilute FA (50 vol.%).

- In addition to the experimental evaluation, a CFD model that described transport profiles within a microchannel reactor was successfully developed on Comsol Multiphysics 4.3 b for the decomposition of pure FA (99.99 %).
- First order kinetic parameters that best fit the experimental results were successfully estimated for both dehydrogenation and dehydration. Validation of the model conversions against the experimental conversions showed that the developed model was an acceptable fit especially at temperatures above 250 ^{o}C with a R^2 value of 0.95.
- Axial velocity profiles were found to be more relevant than transverse profiles. Temperature profiles on the other hand were found to be negligible showing that the microchannel reactor operated under isothermal conditions. Furthermore, axial concentration profiles showed that the reactor length was adequate for the experiments.

6.2 RECOMMENDATION FOR FUTURE WORK

- The catalyst used in this dissertation catalysed both the dehydrogenation and dehydration reactions. For use in PEMFCs however, it is important that the dehydration reaction be suppressed to minimise catalyst poisoning. It is therefore recommended that a more selective catalyst be used for the decomposition process.
- The mathematical performance evaluation of the reactor greatly depended on available kinetics from literature. There is however, currently lack of adequate kinetics for the decomposition of FA for the production of H_2 using Au/Al_2O_3 catalyst. More particularly, the kinetics of the WGS reaction in FA decomposition has to be understood for the modelling of dilute FA experiments. It is therefore recommended that an intensive kinetic study be carried out for better development of a model that would serve as a tool for design and optimisation of the reactor.

6.3 CONTRIBUTION TO CURRENT KNOWLEDGE

- In Chapters 4 of the dissertation, a microchannel reactor for FA decomposition is experimentally evaluated for the first time. This work opens new doors for further advancement in FA-H_2 economy with regard to reactor and process development.
- In Chapter 5, a CFD model is developed, for the first time, for the production of H_2 from FA in a microchannel reactor. This chapter will serve as a guideline in reactor modelling and design for FA decomposition for the production of H_2.

REFERENCES

Aartun, I., Silberova, B., Venvik, H., Pfeifer, P., Gorke, O., Schubert, K., & Holmen, A. (2005). Hydrogen production from propane in Rh-impregnated metallic microchannel reactors and alumina foams. *Catalysis today, 105*, 469-478.

Adam II, T., & Barton, P. (2009). A dynamic two dimensional heterogeneous model for water gas shift reactors. *Internatinal Journal of Hydrogen Energy, 34*(21), 8877-8891.

Agrafiotis, C., & Tsetsekou, A. (2000). The effect of powder characteristics on washcoat quality.Part 1 : Alumina washcoats. *The European ceramic society, 20*, 815-824.

Akiya, N., & Savage, P. E. (1998). Role of water in formic acid decomposition. *AIChE, 44*(2), 405-415.

Al-Akraa, I. M., Mohammad, A. M., El-Deab, M. S., & El-Anadouli, B. E. (2015). Advances in Direct Formic Acid Fuel Cells:Fabrication of Efficient Ir/Pd Nanocatalyst for Formic Acid Electro-Oxidation. *International journal of electrochemical science, 10*, 3282-3290.

Atkinson, D., & McDaniel, J. (2010). *Eptq.com*. Retrieved from

www.eptq.com: http://www.eptq.com/view_article.aspx?intAID=1024

Avinash, P., Logeeswaran, V., & Saif Islam, M. (n.d.). Wet and dry etching. Califonia: University of California,Davis.

AZoM. (2013, March 4). AZO materials : Stainless steel grade 314 (UNS S31400). Retrieved January 15, 2017, from www.azom.com: http://www.azom.com/article.aspx?ArticleID=8259

Baik, S. M., Kim, J., Han, J., & Kwon, Y. (2011). Perfomance improvement in direct formic acid fuel cells (DFAFCs) using metal catalyst prepared by dual mode spraying. *International Journal of Hydrogen Energy, 36*, 12583-12590.

BASF. (2012, December). News and publications : Tradition of ideas : Formic acid. Retrieved December 22, 2016, from basf.com: http://www.intermediates.basf.com/chemicals/topstory/ideen_tradition

References

Benson, E., Kubiak, C., Santhrun, A. J., & Smieja, J. (2009). Electrocatalytic and homogeneous approaches to conversion of CO2 to liquid fuels. *Chemical Society Reviews*, 89-99.

Bird, B. R., Lightfoot, E. N., & Stewart, W. E. (2002). *Transport phenomena* (2nd ed.). New York: John Wiley & Sons,Inc.

Blake, P. G., & Hinshelwood, C. (1960). The homogeneous decomposition reaction of gaseous formic acid. *Proceedings of the royal society A*, 444.

Blake, P. G., Davies, H. H., & Jackson, G. E. (1971). Dehydration mechanisms in the thermal decomposition of gaseous formic acid. *Journal of the chemical society B :Physical organic*, 1923-1925.

Boddien, A., Gartner, F., Jackstell, R., Junge, H., Spannenberg, A., Baumann, W., . . . Beller, M. (2010). ortho-Metalation of Iron (0) Tribenzylphosphine complexes:Homogeneous catalysts for the generation of hydrogen from formic acid. *Angewandte chemie international edition, 49*(47), 8993-8996.

Boddien, A., Gartner , F., Nielsen, M., Losse, S., & Junge, H. (2013). Hydrogen Generation from Formic Acid and Alcohols. *comprehensive inorganic chemistry*.

Boddien, A., Gartner, F., Nielsen, M., Losse, S., & Junge, H. (2013). Hydrogen generation from formic acid and alcohols. *comprehensive inorganic chemistry*, 587-601.

Boddien, A., Loges, B., Gartner, F., Torborg, C., Fumino, K., Junge, H., . . . Beller, M. (2010). Iron catalysed hydrogen production from formic acid. *Journal of the american chemical society , 132*(26), 8924-8934.

Boddien, A., Loges, B., Junge, H., & Beller, M. (2008). Hydrogen generation at ambient conditions: Application in fuel cells. *ChemSusChem, 1*(8-9), 751-758.

Boddien, A., Loges, B., Junge, H., Noyes, J., Felix, G., & Beller, M. (2009). Improved hydrogen generation from formic acid. *Advanced synthetic catalysis, 351*, 2517-2520.

Boddien, A., Mellmann, D., Gartner, F., Jackstell, R., Junge, R., Junge, H., . . . Beller, M. (2011). Efficient dehydrogenation of formic acid using an iron catalyst. *Sciences, 333*(6050), 1733-1736.

Brand , Fedder, Hierold, Korvink, & Tabata. (2006). *Advanced Micro and Nanosystems* (VOLUME 5 ed.). *Weinheim: WILEY-VCH Verlag GmbH & CO.KGaA.*

References

Brandner, J. ,. (2008). Fabrication of microreactors made from metals and ceramics. In T. Wirth (Ed.), *Microreactors in organic synthesis and catalysis.* Weinheim: Wiley-VCH.

Brophy, J. (2004, June). Modular gas to liquids technology. *10th PIN meeting,Heriot -Watt University.* Edinburgh: pinetwork.org. Retrieved from pinetwork.org.

Brown, M., Cohen, M., & Gary, K. (1999). *Fuel cells*. Retrieved February 22, 2015, from www.americanhistory.si.edu/fuelcells/index.htm

Bull, S. (2010). Retrieved June 15, 2016, from gov.uk: https://www.gov.uk/government/uploads/system/uploads/attachment_data/file/317446/hpa_Formic_Acid__General_Information_v1.pdf

Bulushev, D. A., Beloshapkin, S., & Ross, J. R. (2010). Hydrogen from formic acid decompoistion over Pd and Au Catalysts. *Catalysis Today, 154*(1-2), 7-12.

Byron, S. ,., Muruganandam, L., & Murthy, S. (2010). A Review of the Water Gas Shift Reaction Kinetics. *International Journal of Chemical Reactor Engineering, 8*, 1-32.

Cai, W., Liang, L., Zhang, Y., Xing, W., & Liu, C. L. (2013). Real contribution of formic acid in direct formic acid fuel cells:Investigation of origin and guiding for micro structure design. *International Journal of Hydrogen Energy, 38*, 212-218.

Cai, W., Yan, L., Li, C., Liang, L., Xing, W., & Liu, C. (2012). Development of a 30 W class direct formic acid fuel cell stack with high stability and durability. *International Journal of Hydrogen Energy, 37*, 3425-3432.

Chein , R. Y., Chen, Y. C., Chang, C. S., & Chung, J. N. (2010). Numerical modeling of hydrogen production from ammonia decomposition for fuel cell applications. *International journal of hydrogen energy, 35*, 589-597.

CHERIC. (n.d.). *KDB*. Retrieved July 12, 2015, from www.cheric.org/research/kdb/

Chiuta, S., Everson, R. C., Neomagus, H. W., & Bessarabov, D. G. (2014). Experimenatl perfomance evaluation of an ammonia-fuelled microchannel reformer for hydrogen generation. *International journal of Hydrogen Energy, 39*(14), 7225-7235.

Chiuta, S., Everson, R. C., Neomagus, H. W., & Bessarabov, D. G. (2015). Performance evaluation of a high-throughput microchannel reactor for ammonia decomposition over a commercial Ru-based catalyst. *international journal of hydrogen energy, 40*, 2921-2926.

References

Chiuta, S., Everson, R. C., Neomagus, H. W., Le Grange, L. A., & Bessarabov, D. G. (2014). A modelling evaluation of an ammonia-fuelled microchannel reformer for hydrogen generation. *International Journal of Hydrogen Energy, 39*, 11390-11402.

Columbia, M. R., & Thiel, P. A. (1994). The interaction of formic acid with transition metal surfaces ,studied in ultrahigh vacuum. *Electroanalytical Chemistry, 369*, 1-14.

Commenge, J. M., Falk, L., Corriou, J. P., & Matlosz, M. (2002). Optimal design for flow uniformity in microchannel reactors. *AIChE Journal, 48*(2), 345-357.

D'Angelo , N. M., Ordomsky, V., Van der Schaaf, J., & Schouten, J. C. (2014). Continous hydrogen stripping during aqueous phase reforming of sorbitol in a washcoated microchannel reactor with a Pt-Ru bimetallic catalyst. *international journal of hydrogen energy, 39*, 18069-18076.

De Vries, J., & Elsevier, C. J. (2007). The handbook of homogeneous hydrogenation. Netherlands: Wiley VCH.

DeSouza, M., Faria, S., Zanini, G., & Moraes, F. (2013). Production of Hydrogen for Fuel Cell: Microchannel Reactor Modelling for Combustion and Reform of Ethanol in Alternate Channels . *Chemical Engineering Transactions, 32*, 835-840.

Dopkin, D. M. (n.d.). *Silicon processing.* Retrieved March 15, 2015, from enigmatic-consulting.com:http://www.enigmaticconsulting.com/semiconductor_processing/semiconductor_process.html

Du, X., Shen, Y., Yang, L., Shi, Y., & Yang, Y. (2012). Experiments on hydrogen production from methanol steam reforming in the microchannel reactor. *International Journal of Hydrogen Energy, 37*(17), 12271-12280.

Dyosiba, X., Ren, J., Musyoka, N., Langmi, H., Mathe, M., & Onyango, M. (2016). Preparation of value-added metal -organic frameworks(MOFs) using wate PET bottles as sourceof acid linker. *sustainable materials and technologies, 10*, 10-13.

Echave, F., Sanz, O., & Montes, M. (2013). Washcoating of micro-channel reactors with PdZnO catalyst for methanol steam reforming. *Applied Catalysis A:General*, 1-9.

Fellay, C., Dyson, P. J., & Laurenczy, G. (2008). A viable Hydroge-Storage Based On Selective Formic Acid Decomposition with a Ruthenium Catalyst. *Angewandte Chemie, 120*, 4030-4032.

References

Fellay, C., Yan, N., Dyson, P., & Laurenczy, G. (2009). Selectiveformic acid decomposition for high pressure hydrogen generation : A mechanistic study. *Chemistry-European Journal, 15*(15), 3752-3760.

Fukuda, K., Onishi, T., & Tamaru, K. (1969). Decomposition of formic acid on silver catalyst-Adsorption measurement during surface catalysis. *Tran.Faraday Soc, 42*(5), 1192-1196.

Fuller, E., Schettler, P., & Giddings, J. (1966). A new method for prediction of binary gas-phse diffussion coefficients. *Industrial and engineering chemistry, 58*(5), 19-27.

Gad-el-Hak, M. (1999). The fluid mechanics of microdevices -The freeman scholar lecture. *Journal of fluids Engineering, 121*(5).

Gazsi, A., Bansagi, T., & Solymosi, F. (2011). Decomposition and Reforming of Formic Acid on Supported Au Catalysts:Production of CO-Free H2. *Physical Chemistry, 115*(31), 15459-15466.

Guangwen, C., Jun, Y., & Quan, Y. (2008). Gas-liquid microreaction technology:Recent developments and future challenges. *Chinese journal of chemical engineering, 16*(5), 663-669.

Haas-Santo, K., Gorke, O., Pfeifer, P., & Schubert, K. (2002). Catalyst coatings for microstructure reactors. *CHIMIA, 56*(11), 605-610.

Hessel, V., Lowe, H., Muller, A., & Kolb, G. (2005). *Chemical Micro Process Engineering.* Weinheim: Wiley-VCH.

Himeda, Y. (2009). Highly efficient hydrogen evolution by decomposition of formic acid using an iridium catalyst with 4,4'-dihydroxy-2,2'-bipyridine. *Green Chemistry, 11*, 2018-2022.

Hla, S., Park, D., Duffy, G., Edwards, J., Roberts, D., IIyushechkin, A., . . . Nguyen, T. (2009). Kinetics of high-temperature water-gas shift reaction over two iron-based commercial catalysts using simulated coal-derived syngases. *Chemical Engineering, 146*, 148-158.

Holladay, J. D., & Wang, Y. (2015). A review of recent advances in numerical simulations of microscale. *journal of power sources, 282*, 602-621.

Hwang, S.-M., Kwon, O. J., & Kim, J. J. (2007). Method of catalyst coating in micro-reactors for methanol steam reforming. *Applied catalysis A:General, 316*, 83-89.

References

Hyde, J. R., & Poliakoff, M. (2004). Supercritical hydrogenation and acid-catalysed reactions "without gaes". *royal society of chemistry*, 1482-1483.

Iglesia, E., & Boudart, M. (1983). Decomposition of formic acid on copper ,nickel,and copper-nickel alloys:II.Catalytic and temperature-programmed decomposition of formic acid on Cu/SiO2,Cu/Al2O3. *journal of catalysis, 81*(1), 214-223.

Iglesia, E., & Boudart, M. (1983). Decomposition of formic acid on Copper,nickel,and copper-nickel alloys:I.Preparation and characterisation of catalysts. *journal of catalysis, 81*(1), 204-213.

Javaid, R., Kawasaki, S.-i., Ookawara, R., Sato, K., Nishioka, M., Suzuki, A., & Suzuki, T. M. (2013). Continous Dehydrogenation of Aqueous Formic Acid under Sub-Critical Conditions by Use of Hollow Tubular Reactor Coated with Thin Palladium Oxide Layer. *Journal of Chemical Engineering, 46*(11), 751-758.

Jeon, W. S., Yoon, J. W., Baek, C., & Kim, Y. (2013). Minimization of hot spot in a microchannel reactor for steam reforming of methane with the stripe combustion catalyst layer. *International journal of hydrogen energy, 38*, 13982-13990.

Jessop, P., Joo, F., & Tai, C.-C. (2004). Recent advances in the homogeneous hydrogenation of carbon dioxide. *Coordination Chemistry Reviews*, 2425-2442.

Johnson, T., Morris, D., & Wills, M. (2010). Hydrogen generation from formic acid and alcohols using homogeneous catalysts. *Chemical Society Reviews*, 81-88.

Karakaya, M., & Avci, A. K. (2011). Microchannel reactor modelling for combustion driven reforming of iso-octane. *international journal of hydrogen energy, 36*, 6569-6577.

Kari, S., Esko, T., Anti, V., & Marko, L. (1998). *Patent No. US 6429333 B1.*

Kawamura, Y., Ogura, N., Yamamoto, K., & Igarashi, A. (2006). A miniaturized methanol reformer with Si-based microreactor for small PEMFC . *Chemical engiineering science, 61*, 1092-1101.

Khaled, A. R., & Vafai, K. (2003). The role of porous media in modeling flow and heat transfer in biological tissues. *International journal of heat and mass transfer, 46*, 4989-5003.

Klerke, A., Christensen, C. H., Norskov, J. K., & Vegge, T. (2008). Ammonia for hydrogen storage :Challenges and opportunities. *The royal society of chemistry, 18*, 2304-2310.

References

Kolb, G., & Hessel, V. (2004). Micro-structured reactors for gas phase reactions. *chemical engineering journal, 98*(1-2), 1-38.

Kuo, C.-W., Lin, C.-M., Lai, G.-H., Chen, Y.-C., Chang, Y.-T., & Wu, W. (2007). Characterisation and Mechanism of 304 Stainless Steel Vibration Welding. *Materials Transactions, 48*(9), 2319-2323.

Lee, J., Park, J., & Song, H. (2008). A nanoreactor framework of a Au@SiO2 Yolk/Shell Structure for Catalytic Reduction of p-Nitrophenol. *Advanced Materials, 20*, 1523-1528.

Leitner, W. (1995). Carbon Dioxide as a Raw Material: The Synthesis of Formic Acid and Its Derivatives from CO2. *Angewandte Chemie*.

Lerou, J. J., Tonkovich, A. L., Silva, L., Perry, S., & McDaniel, J. (2010). Microchannel reactor architecture enables greener processes. *Chemical Engineering Science, 65*, 380-385.

Lima, D., Zanella, F., Lenzi, M., & Ndiaye, P. (2012). Modelling and Simulation of Water Gas Shift Reactor:An Industrial Case. *Petrochemicals*, 4-74.

Loges, B., Boddien, A., Gartner, F., Junge, H., & Beller, M. (2010). Catalytic Generation of Hydrogen from Formic Acid and its Derivatives :Useful Hydrogen Storage Materials. *Top Catal, 53*, 902-914.

Lycke, D. R., & Blair, S. L. (2009). Formic Acid Fuel Cells. 172-181.

Mars, P., Scholten, J. J., & Zwietering, P. (1963). The catalystic decomposition of formic acid. In *Advances in catalysis and related subjects* (pp. 35-110). *Newyork: Academic press.*

Mei, D., Liang, L., Qian, M., & Feng, Y. (2014). A perfomance study of methanol steam reforming in an A-type microchannel reactor. *International journal of hydrogen energy, 39*, 17690-17701.

Mei, D., Liang, L., Qian, M., & Lou, X. (2013). Modeling and analysis of flow distribution in an A-type microchannel reactor. *International Journal of Hydrogen Energy, 38*, 15488-15499.

Meille, V. (2006). Review on methods to deposit catalysts on structured surfaces . *Applied catalysis, 315*, 1-17.

Mellor, J., Coville, N., Sofianos, A., & Coppertwaite, R. (1997). Raney copper catalysts for the water-gas shift reaction II. Initial catalyst optimisation. *Applied catalysis*, 185-195.

References

MEMS. (n.d.). *mems-exchange.org*. Retrieved June 18, 2016, from www.mems-exchange.org/advantages#fabrication_capabilities

Men, Y., Kolb, G., Zapf, R., Hessel, V., & Lowe, H. (2007). Ethanol steam reforming in a microchannel reactor. *process safety and environmental protection, 85*(5), 413-418.

Millikin, M. (2014). *Green Car Congress*. Retrieved August 27, 2014,

from www.greencarcongress.com

Mitra, B., & Kunzru, D. (2008). Washcoating of different zeolites on cordierite monoliths. *The American ceramic society, 91*(1), 64-70.

Mitsos, A., & Barton, P. I. (2009). *Microfabricated power generation devices.* Weinheim: Wiley-VCH.

Mohammad , M., Jovanovic, G. N., & Sharp, K. V. (2013). Numerical study of flow uniformity and pressure characteristics within a microchannel array with triangular manifolds. *Computers and chemical engineering , 52*, 134-144.

Moreno-Zuria, A., Dector, A., Cuevas-Muniz, F. M., Esquivel, J. P., Sabate, N., Ledesma-Garcia, J., . . . Chavez-Ramirez, A. U. (2014). Direct formic acid microfluidic fuel cell design and perfomance evolution. *Journal of power sources, 269*, 783-788.

Moret, S., Dyson, P., & Laurenczy, G. (2014). Direct synthesis of formic acid from carbon dioxide by hydrogenation in acidic media. *Nature communications*, 1-7.

Nageswara, P., & Kunzru, D. (2007). Fabrication of microchannels on stainless steel by wet chemical etching. *Journal of Micromechanics and Microengineering, 17*, 99-106.

Noto, Y., Fukuda, K., Onishi, T., & Tamaru, K. (1967). Mechanism of formic acid decomposition over dehydrogenation catalysts. *Transaction of the Faraday Society, 63*, 3081-3087.

Ojeda, M., & Iglesia, E. (2009). Formic Acid Dehydrogenation on Au-Based Catalysts at Near-Ambient Temperatures. *Angewandte Chemie International Edition, 48*(26), 4800-4803.

Park, G.-G., Yim, S.-D., Yoon, Y.-G., Lee, W.-Y., Kim, C.-S., Seo, D.-J., & Eguchi, K. (2005). Hydrogen production with intergrated microchannel fuel processor for portable fuel cell systems. *journal of power sources, 145*, 702-706.

References

Patermarakis, G. (2003). The parallel dehydrative and dehydrogenative catalystic action of y-Al2O3 pure and doped by MgO,kinetics,selectivity,time dependence of catalystic behaviour,mechanism and interpretation. *Applied catalysis A:General, 252*, 231-241.

Paunovic, V., Schouten, J. C., & Nijhuis, T. A. (2015). Direct synthesis of hydrogen peroxide in a wall-coated microchannel reactor over Au-Pd catalyst :A perfomance study. *Catalysis Today, 248*, 160-168.

Peela, N. R., Mubayi, A., & Kunzru, D. (2011). Steam reforming of ethanol over Rh/CeO2 catalysts in a microchannel reactor. *chemical engineering journal, 167*, 578-587.

Qin, Y., Wang, J., Meng, F., Wang, L., & Zhang, X. (2013). Efficient PdNi and PdNi@Pd-catalysed hydrogen generation via formic acid decomposition at room temperature. *Chem Commun, 49*(85), 10028-10030.

Quiram, D. J., Jensen, K. F., Schmidt, M. A., Mills, P. L., Ryley, J. F., Wetzel, M. D., & Kraus, D. J. (2007). Intergrated Microreactor System for gas -phase catalystic reactions .1.Scale-up microreactor Design and fabrication. *American chemical society, 46*(25), 8292-8305.

Robert, P. (1997). *Perry's chemical engineers' handbook* (7 ed.). New York: McGraw-Hill.

Robota, H. J., Richard, L., Deshmukh, S., & LeViness, S. (2014). Fischer-Tropsch synthesis in a microchannel reactor:The influence of Co/SiO2 catalyst structure on FTS perfomance. Doha,Qatar: International petroleum technology conference.

Rouge , A., Spoetzl, B., Gebauer, K., Schenk, R., & Renken, A. (2001). Microchannel reactors for fast periodic operation :the catalystic dehydration of isopropanol. *chemical engineering sciences , 56*, 1419-1427.

Ryu, I., Sato, M., Sagae, T., & Hayashi, K. (2013). *USA Patent No. US8,609,034 B2.*

Sebatier, P., & Mailhe, A. (1912). Catalytic Decomposition of Formic Acid. *Comptes rendus Chimie, 6*, 619.

Sigma-Adrich. (2011). *Sigma-aldrich*. Retrieved August 25, 2014,

from www.sigmaaldrich.com/MSD/

Silverwood, I. (2002). *Synthesis and characterisation of Au/Fe2O3 catalysts.* The university of Edinburgh: Athesis submitted for the degree of Master of Science .

References

Sims, J. (2015). *Formic acid decomposition on cobalt surfaces.* Department of Chemical and Biological Engineering,University of Ottawa,Canada: Thesis submitted to the faculty of Graduates and Postdoctoral Studies in Partial fulfillment of the Requirements for the Degree of M.A.Sc in Chemical Engineering.

Soylomosi, F., Koos, A., Liliom, N., & Ugrai, I. (2011). Production of CO-Free H2 from formic acid .A comparative study of ctalytic behaviour of Pt metals on carbon support. *Journal of catalysis, 279*(1), 213-219.

Sun, Y. K., Vajo, J. J., Chan, C. Y., & Weinberg, W. H. (1988). Kinetics and mechanism of formic acid decomposition on Ru(001). *American vacuum society, 6*(3), 854-855.

Tamaru, K. (1958). Adsorption during the catalytic decomposition of formic acid on silver and nickel catalysts. *Transaction of the Faraday Society*, 824-832.

Tan, H., & Pillai, K. M. (2009). Finite element implementation of stress-jump and stress-continuity conditions at porous -medium,clear fluid interface. *Computers and Fluids, 38*, 1118-1131.

Tedsree, K., Chan, C. A., Jones, S., Cuan, Q., Li, W., Gong, X.-Q., & Tsang, S. (2011). NMR guides rational design of nanocatalysts via chemisorption evaluation in liquid phase. *Science*, 224-228.

Wang, Z.-L., Ping, Y., Yan, J.-M., Wang, H.-L., & Jiang, Q. (2014). Hydrogen generation from formic acid decomposition at room temperature using a NiAuPd alloy nanocatalysts. *International jhournal of hydrogen energy, 39*, 4850-4856.

Wenjin Yana, X. J. (2013). Optimization and statistical analysis of Au-ZnO/Al2O3. *Journal of Energy Chemistry, 22*, 498–505.

Wesselbaum, S., Hintermair, U., & Leitner, W. (2012). Continous-Flow Hydrogenation of Carbon Dioxide to Pure Formic Acid using an Intergrated scCO2 Process with Immobilized Catalyst and Base. *Angewandte Chemie International Edition, 51*, 8585-8588.

Wolfel, R., Taccardi, N., Bosmann, A., & Wasserscheid, P. (2011). Selective catalytic conversion of biobased carbohydrates to formic acid using molecular oxygen. *Green Chemistry, 13*(10), 2759-2763.

Worz, O., Jackel, K., Richter, T., & Wolf, A. (2001). Microreactors-A new efficient tool for reactor development. *Chemical Engineering and Technology, 24*(2), 138-142.

Yoo, J. S., Abild-Pedersen, F., Nørskov, J. K., & Studt, F. (2014). Theoretical Analysis of Transition-Metal Catalysts for Formic Acid Decomposition. *ACS Catalysis*, 1226-1233.

Yosaka, Y., Yoshida, K., Wakai, C., Matubayasi, N., & Nakahara , M. (2006). Kinetic and equilibrium study on formic acid decompositionin relation to the water-gas-shift recation. *Journal of physical chemistry, 110*(38), 11082-11090.

Yu, J., & Savage, P. E. (1998). Decomposition of formic acid under hydrothermal conditions . *Kinetics ,catalysis and reaction engineering, 37*, 2-10.

Yu, X., & Pickup, P. G. (2008). Recent advances in direct formic acid fuel cells(DFAFC). *Journal of power sources, 182*(1), 124-132.

Zapf, R., Becker-willinger, C., Berresheim, K., Bolz, H., Gnaser, H., Hessel, V., . . . Ziogas, A. (2003). Detailed characterisation of various porous alumina-based catalyst coating within microchannels and their testing for methanol steam reforming. *Trans IChemE, 81*(PART A), 721-729.

Zapf, R., Kolb, G., Pennemann, H., & Hessel, V. (2006). Basic study of adhesion of several alumina-based washcoats deposited on stainless steel microchannels. *Chemical Engineering and Technology, 29*(12), 1509-1512.

Zeng, Z., & Grigg, R. (2006). A creterion for non-Darcy flow in porous media. *63*, 57-69.

Zhang , S., Metin, O., Su, D., & Sun, S. (2013). Monodisperse AgPd Alloy Nanoparticles and their superior catalysis for the dehydrogenation of formic acid. *Angewandte Chemie, 52*(13), 3681-3684.

Zhang, Y., Zhang, J., Zhao, L., & Sheng, C. (2009). Decomposition of formic acid in supercritical water. *Energy and fuels, 24*, 95-99.

Zhao, H., & Burke, A. (2015). Fuel Cell Powered vehicles. In D. Crolla (Ed.), *Encyclopedia of Automotive engineering.* Wiley.

Zhou, X., Huang, Y., Liu, C., Liao, J., Lu, T., & Xing, W. (2010). Available hydrogen from formic acid decomposed by rare earth elements promoted Pd-Au/C catalysts at low temperature. *ChemSusChem, 3*, 1379-1382.

Zhou, X., Huang, Y., Xing, W., Liu, C., Liao, J., & Lu, T. (2008). High-quality hydrogen from the catalyzed decomposition of formic acid by Pd-Au/C and Pd-Ag/C. *Royal society of chemistry*, 3540-3542.

Zhu, Q., Tsumoria, N., & Xu, Q. (2014). Sodium hydroxide -assisted growth of uniform Pd nanoparticles on nanoporous carbon MSC-30 for efficient and complete dehydrogenation of formic acid under ambient conditions. *5*(195).

APPENDICES

APPENDIX A: PROPERTIES OF FORMIC ACID

Formic acid physical properties

Table A1 shows the general properties of FA as obtained from the Korean physical property data bank

Table A. 1 : General properties of formic acid (CHERIC, n.d.; Sigma-Adrich, 2011)

Basic properties	
Molecular weight	46.03
Normal boiling point	374 K
Freezing point	281 K
Critical temperature	588 K
Critical pressure	7390 kPa
Critical volume	0.124 m^3/kmol
Critical compressibility (ZC)	0.188
Liquid density	1200 kg/m^3
Enthalpy data	
Enthalpy of formation at 25	-378900 kJ/kmol
Gibbs free energy of formation	-351200 kJ/kmol
Heat of vaporization	21924 kJ/kmol
Hazardous data	
Lower flammability limit	18 % in air
Upper flammability limit	57% in air
Flash point	332 K
Auto ignition temperature	874 K
NFPA Rating (health)	3
NFPA Rating (Fire)	2

Formic acid temperature dependent physical properties

- **Vapour viscosity at low pressure**

The temperature dependent viscosity of FA at low pressures was calculated using Reichenberg's correlation for pure organic compounds as obtained from Perry's engineering handbook (Robert, 1997).

$$\mu_{FA} = \frac{AT_r}{[1+0.36T_r(T_r-1)]^{1/6}} \quad \text{.....A1}$$

$$A = \frac{M^{1/2}T_C}{\sum n_i C_i} \quad \text{.....A2}$$

$$T_r = \frac{T}{T_c} \quad \text{.....A3}$$

- **Ideal gas heat capacity**

The ideal heat capacity was calculated as obtained from the Korean website according to a correlation shown below.

$$Cp_{FA} = 1.171000E+01 + 1.358000E-01T - 8.411000E-05T^2 + 2.017E-08T^3 \text{.....A4}$$

- **Low pressure thermal conductivity** (Robert, 1997)

$$k_{FA} = \frac{\mu_{FA}}{M}(1.15C_V + 16903.36) \quad \text{.....} \quad \text{A5}$$

- **Binary diffusivity at low pressures** (Fuller, Schettler, & Giddings, 1966)

$$D_{ij} = \frac{10^{-3}T^{1.75}\left[(M_i+M_j)/M_iM_j\right]^{1/2}}{P\left[(\sum v_i)^{1/3}+(\sum v_i)^{1/3}\right]^2} \quad \text{.....A6}$$

Table for the atomic and structrural diffusion –volume increments

Table A. 2 : Atomic diffusion volumes for use in equation A4

Element	Atomic diffusion volume
C	16.5
H	1.98
O	5.481
N	5.69

Where;

$$\sum v_{FA} = 16.5 + 2(1.98) + 2(5.481)$$

$$= 31.422$$

$$\sum v_{H2} = 2(1.98)$$

$$= 3.96$$

$$\sum v_{CO2} = 16.5 + 2(5.481)$$

$$= 27.462$$

APPENDIX B: CATALYST CHARACTERISATION

In this dissertation, the Au/Al_2O_3 catalyst was coated on manufactured microchannel walls according to the wash coating method (Section 2.3.4.2). In accordance with this procedure, the catalyst pellets as supplied were transformed into three forms namely; the catalyst powder, the catalyst washcoat and the catalyst coated plate. In this section, the original catalyst powder and washcoat catalyst powder are characterised to give a better understanding of the catalyst properties. Characterisation of the catalyst coated microchannel plate was discussed in Chapter 3, Section 3.2 of the dissertation.

X-ray Powder Diffraction

The XRD patterns obtained for the two forms of the catalyst are displayed in Figure B.1.

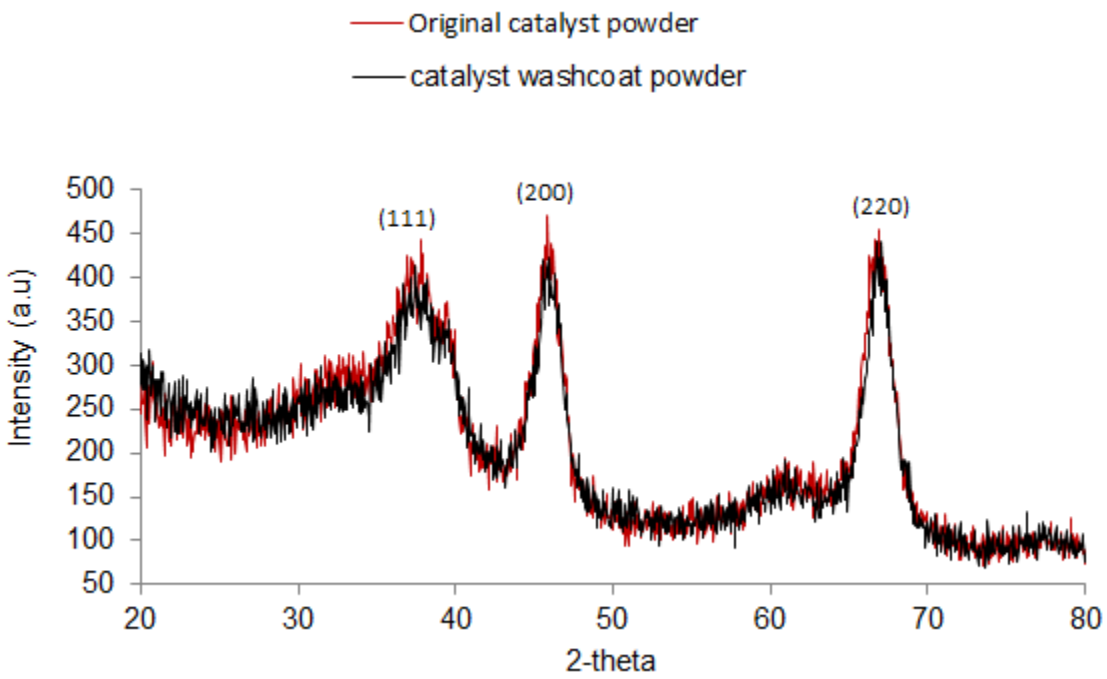

Figure B. 1 : XRD pattern of the original catalyst and wash coat catalyst powder

Figure B.1 shows the presence of Au (111), Au (200) and Au (220) peaks at 2θ = 38.2 °, 42 ° and 64 ° on the original catalyst powder and catalyst washcoat powder. These peaks were indexed in Figure B.1 in accordance with literature (Lee, *et al*., 2008). There was generally no significant difference between the crystalline sizes of the original catalyst and that of the wash coat catalyst.

This is shown by the broadening of the peaks which is similar between the two forms of the catalyst. The broadening of the peaks is generally related to the crystallite sizes according to Scherrer's equation (equation B.1).

$$l = \frac{K_s \lambda}{B cos\theta} \quad \text{.....B.1}$$

The crystallite size therefore varies inversely with the peak width and as such, the broad peaks shown in Figure B.1 indicate that the catalyst had small crystallite sizes. It can therefore be concluded from this XRD pattern that the wash coating process had no significant effect on the crystallinity or active sites of the catalyst.

Surface area measurement.

The catalyst specific surface area was measured by a nitrogen (N_2) adsorption measurement technique in conjunction with the BET (Brunauer, Emmet, and Teller) theory. The measurements were carried out using an ASAP 2020 HD analyser and the BET surface area was obtained from the N_2 isotherms. Table B.1 shows the measured BET surface area and Langmuir surface areas for the different forms of the catalyst.

Table B. 1 : Catalyst surface area obtained from BET analysis.

Parameter	Original catalyst powder	Washcoat catalyst
BET Surface Area	78 $m^2 g^{-1}$	130 $m^2 g^{-1}$
Langmuir surface area	135 g^{-1}	231 $m^2 g^{-1}$
Average particle size	75 nm	46 nm

As shown in Table B.1, the surface area of the wash coat powder catalyst was found to be higher than that of the original catalyst powder. The overall increase in surface area was due to the added additives (PVA) during the wash coating process. The increased surface area can therefore be advantageous during the microchannel reactor coating process as larger surface areas result in better catalyst adhesion to the reactor walls. Most of these additives however tend to decompose during the drying and calcination process and as such, they have no significant effect on the final activity of the catalyst.

Microchannel reactor plate properties

Table B.1: shows the typical elemental composition of the 314 stainless steel material.

Table B. 2 : Stainless steel elemental composition (AZoM, 2013)

Element	Content (%)
Iron, Fe	Balance
Chromium, Cr	23-26
Nickel, Ni	19-22
Manganese, Mn	2
Silicon, Si	1.5-3
Carbon, C	0.25
Sulfur, S	0.03
Phosphorous, P	0.045

APPENDIX C: CALIBRATION OF GAS CHROMATOGRAPHY

The GC was calibrated for H_2, CO_2 and CO using the standard gas mixtures as prepared by Afrox. For all standard mixtures, argon was used as the balance gas. The curves presented in this appendix were obtained at atmospheric pressure and GC oven temperature of 110-220°C. These conditions were maintained during the experimental work.

Hydrogen calibration curve.

A H_2 calibration curve was obtained using three standard mixtures of 9.8, 41.7 and 77.4%. As there was no point during the experiment where H_2 vol % of less than 10 % was obtained, the calibration curve was not forced through the origin.

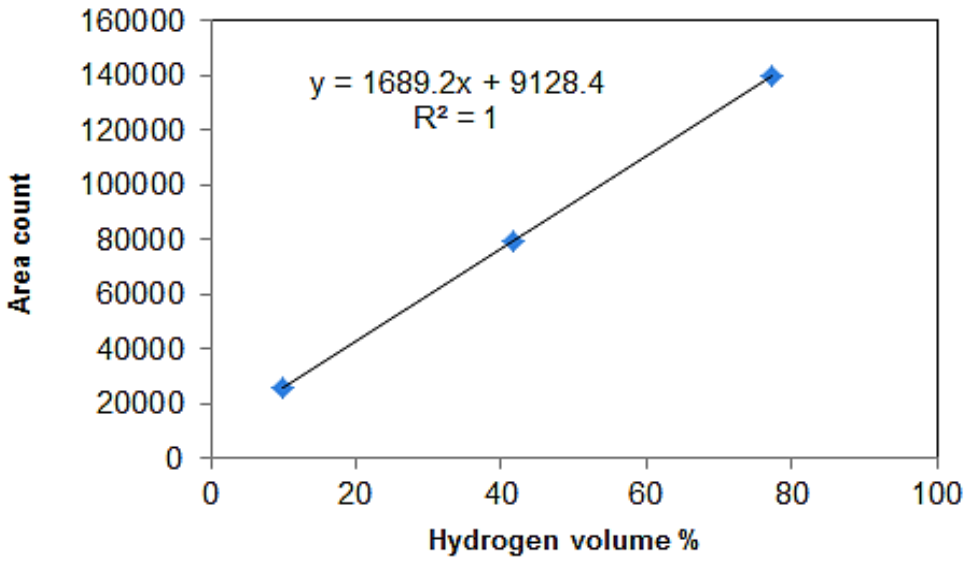

Figure C. 1:H_2 calibration curve

CO_2 calibration curve

Similar to H_2, a CO_2 calibration curve was obtained from three standrad mixtures of 9.5,40.6 and 80 %, as shown in Figure C.2

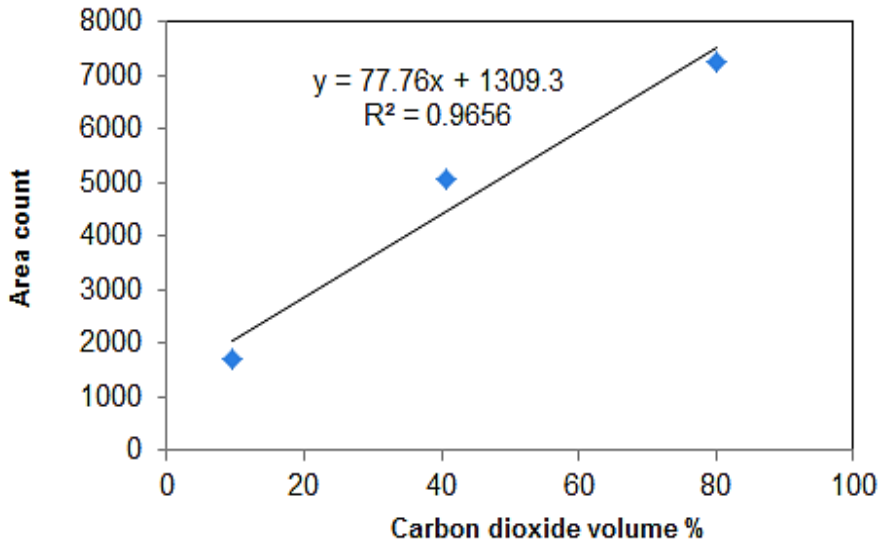

Figure C. 2 : CO_2 calibration curve

FA calibration curve

Figure C.3 shows the FA calibration curve obtained using three standard concentrations (7,20 and 51 %) as obtained from the bubbler. As a 1 % FA concentration could not be obtained from the bubbler,this point was extrapolated, using the other three points. Furthermore, the curve was forced through the origin to cater for traces of FA obtained at high conversions .

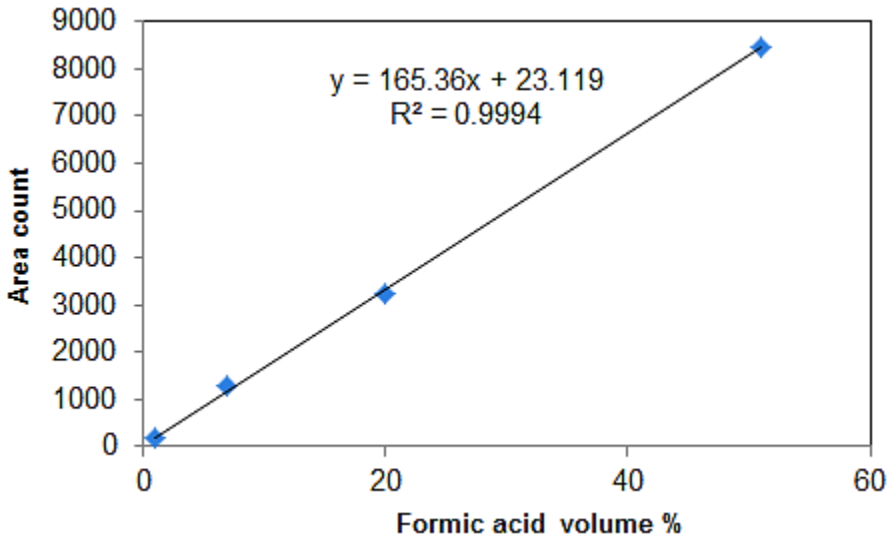

Figure C. 3 : FA calibration curve

CO calibration curve

A CO calibration curve was also obtained from three standard mixtures (0.45, 1 and 10%) while the highest concentration (20%) shown in the graph was extrapolated. Values for CO were further verified by the difference method during the experiment.

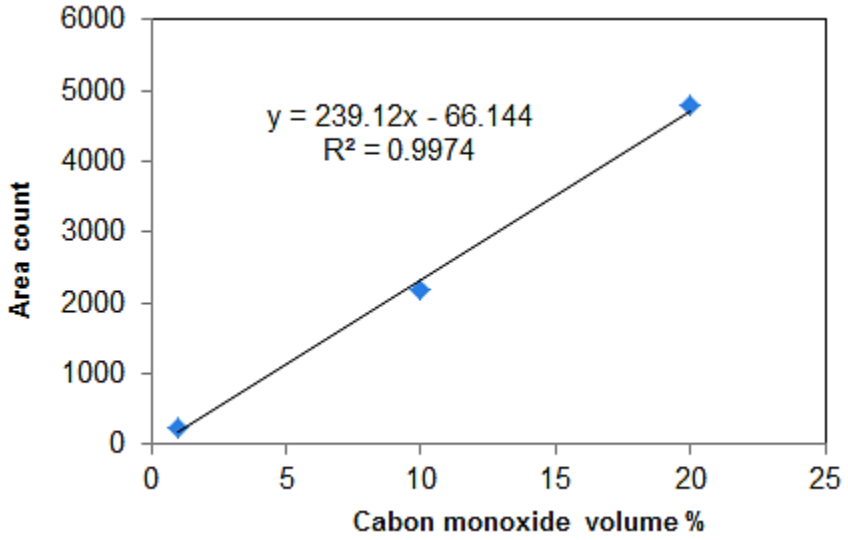

Figure C. 4: CO calibration curve

APPENDIX D: EQUILIBRIUM CALCULATIONS

Appendix D presents the equilibrium results as used in Chapter 4 of the dissertation. The equilibrium calculations were performed considering the occurrence of both the dehydrogenation and dehydration reactions.

Equilibrium conversions for the decomposition of FA

The FA equilibrium calculations shown in Figure D.1 were calculated using thermosolver at the relevant reactor operating temperatures.

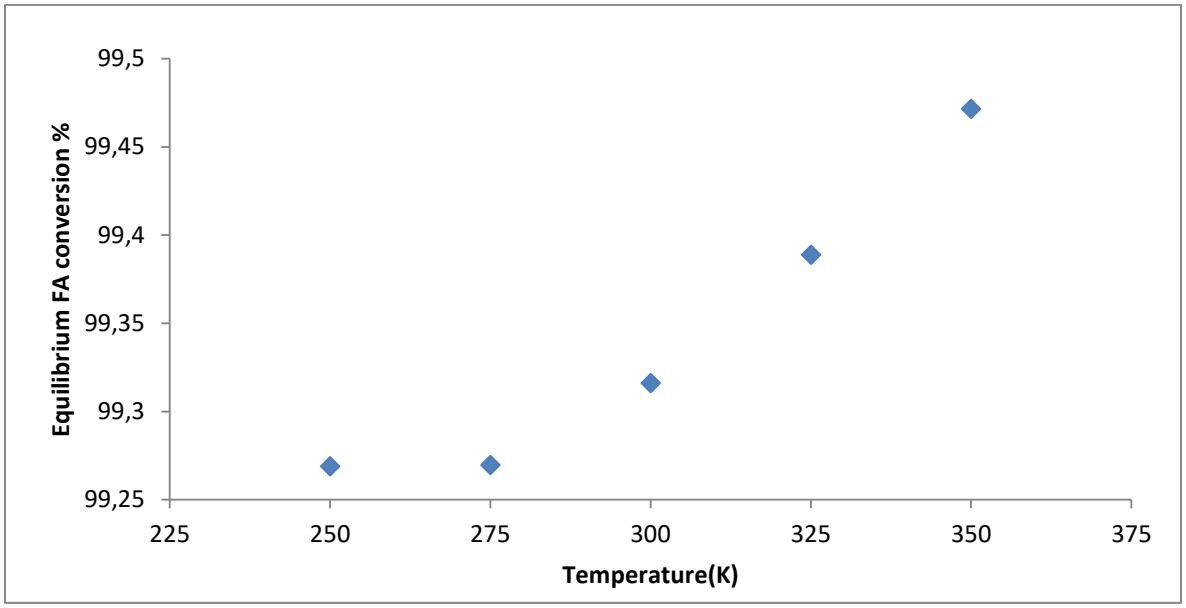

Figure D. 1 : Equilibrium conversions at 250,275,300,325 and 350°C

Equilibrium mole fraction for the decomposition of FA

Figure D.2 shows the equilibrium mole fractions calculated, based on the decomposition of FA according to the dehydrogenation and dehydrations

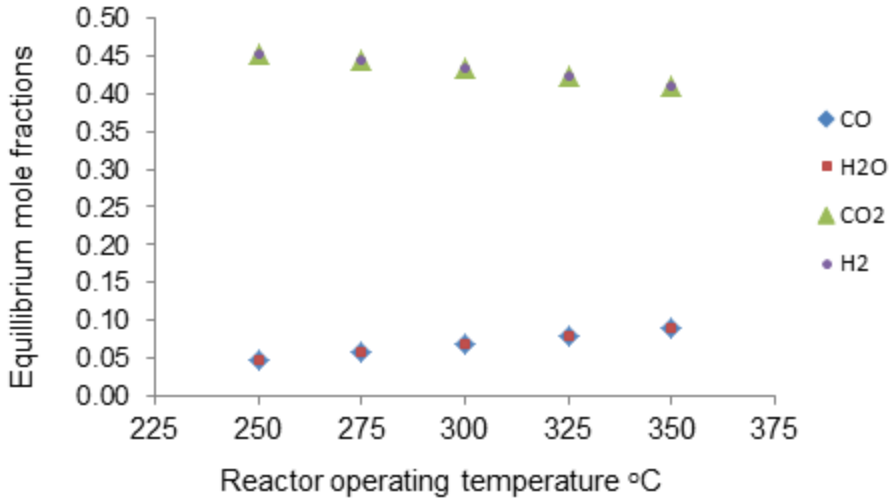

Figure D. 2 : Equilibrium mole fractions at 250,275,300,325 and 350°C.

APPENDIX E: EXPERIMENTAL RESULTS

Appendix E presents results which were not presented in Chapter 4 of the dissertation.

Change in the concentrated FA conversion with time on stream

As shown in Figure E.1 the conversions do not vary significantly with time. This is an indication of steady state reactor operating conditions during the experimental runs.

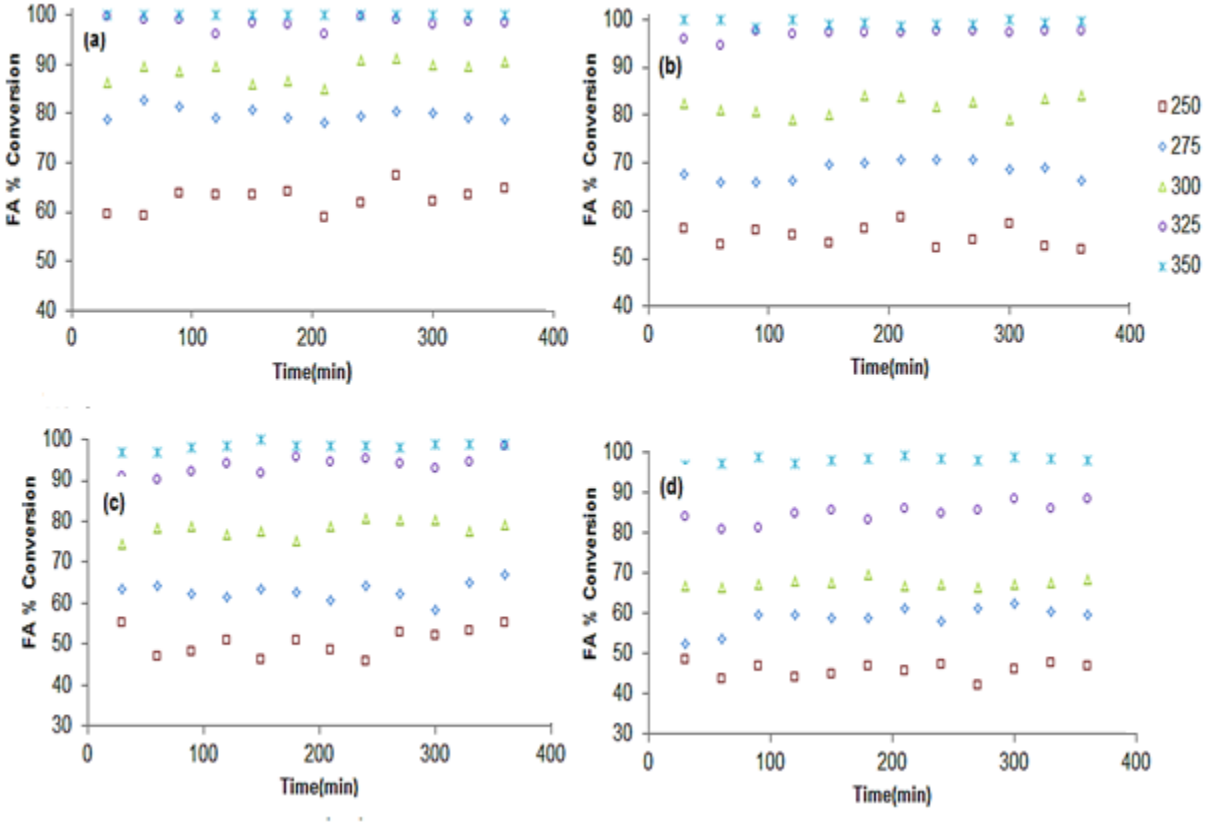

Figure E. 1 : Change in conversion with time on stream at FA flowrates of (a) 12 ml/min, (b) 24 ml/min, (c) 36 ml/min, and (d) 48 ml/min.

Catalyst selectivity with time on stream

The activity of the catalyst throughout the 6 hour runs was also investigated by the change in selectivity with time on stream. Figure E.2 shows this variation for the four flowrates (12 – 48 ml min) investigated in this dissertation.

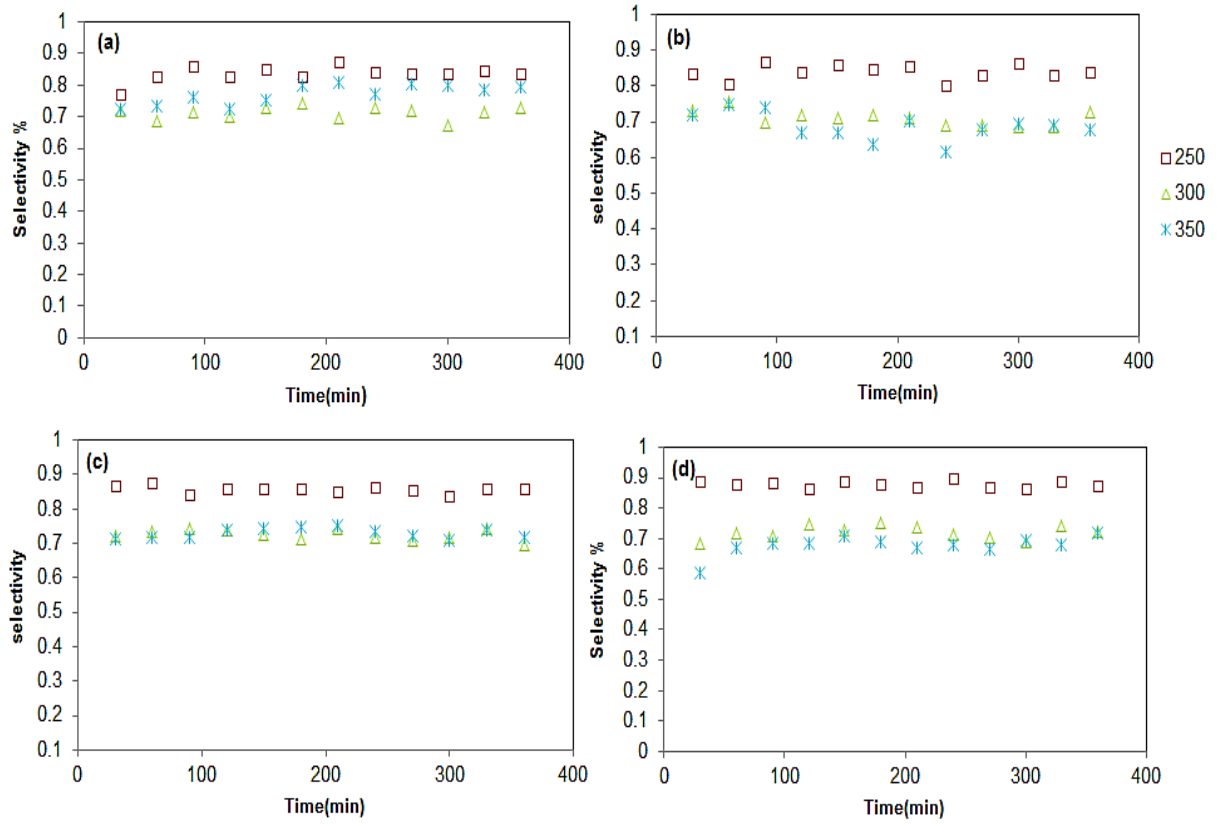

Figure E. 2 : Change in selectivity with time on stream at FA flowrate of (a) 12 ml/min, (b) 24 ml/min, (c) 36 ml/min, and (d) 48 ml/min.